NASA-CR-192025

IN-39-CR
141657
P-211

NASW-4435

PARAS Program:
Phased Array Radio Astronomy from Space

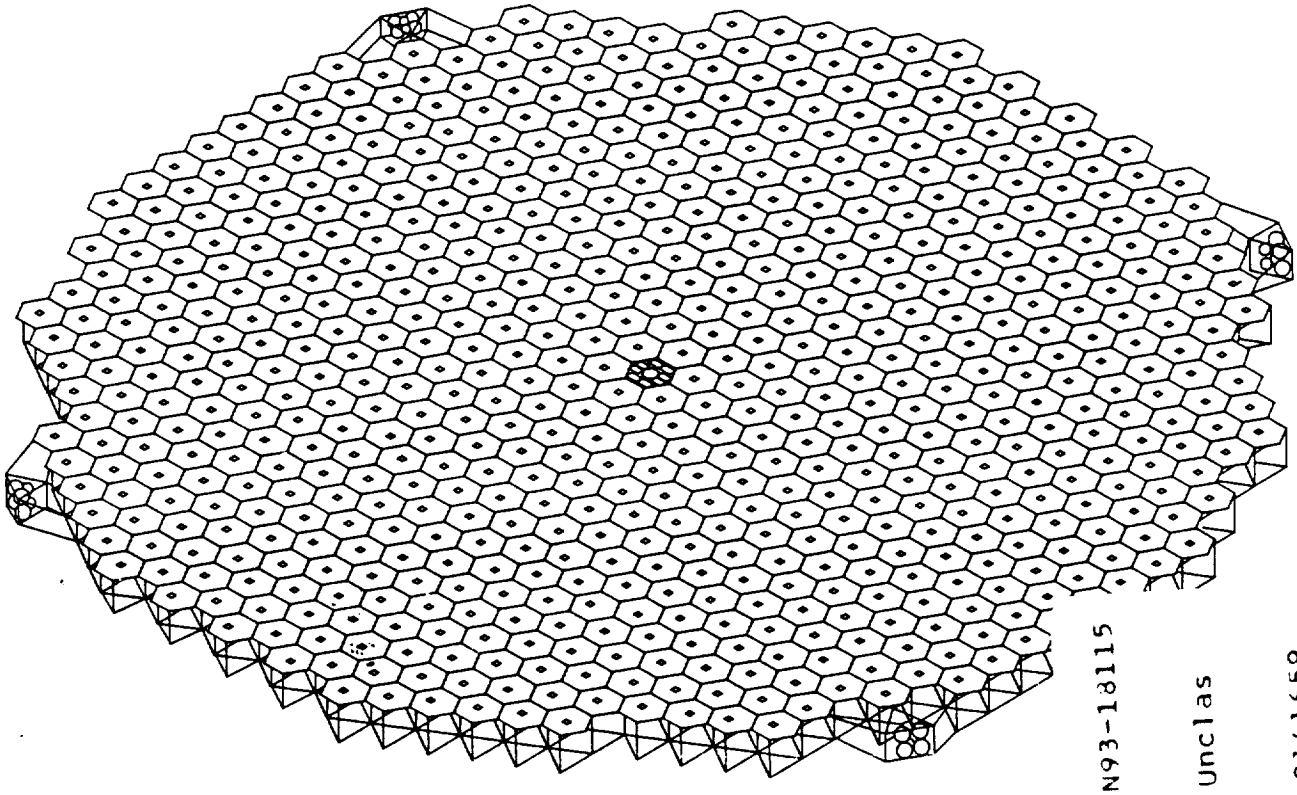

Prof. Antoni K. Jakubowski
David A. Haynes (NASA Langley R.C.)

Ken Nuss
Chris Hoffmann
Michael Madden
Michael Dungan

Department of Aerospace Engineering
Virginia Polytechnic Institute and State University
Blacksburg , Virginia
1992

PARAS Program: Phased Array Radio Astronomy from Space

Prof. Antoni K. Jakubowski
Davy A. Haynes (NASA Langely R.C.)

Ken Nuss
Chris Hoffmann
Michael Dungan
Michael Madden

Department of Aerospace Engineering
Virginia Polytechnic Institute and State University
Blacksburg, Virginia 24060

Abstract

An orbiting radio telescope is proposed which, when operated in a Very Long Baseline Interferometry (VLBLI) scheme, would allow higher (than currently available) angular resolution and dynamic range in the maps, and ability of observing rapidly changing astronomical sources. Using a passive phased array technology, the propesed design consists of 656 hexagonal modules forming a 150 meter diameter dish. Each observatory module is largely autonomous, having its own photovoltaic power supply and low-noise receiver and processor for phase shifting. The signals received by the modules are channeled via fiber optics to the central control computer in the central bus module. After processing and multiplexing, the data is transmitted to telemetry stations on the ground. The truss frame supporting each observatory pane is a novel hybrid structure consisting of a bottom graphite/epoxy tubular triangle and rigidized inflatable Kevlar tubes connecting the top observatory panel and bottom triangle. Attitude control and stationkeeping functions are performed by a system of momentum wheels in the bus and four propulsion modules located at the compass points on the periphery of the observatory dish. Each propulsion module has four monopropellant thrusters and six hydrazine arcjets, the latter supported by a nuclear reactor. The total mass of the spacecraft is 22,060 kg.

TABLE OF CONTENTS

LIST OF FIGURES

LIST OF TABLES

1.0 INTRODUCTION

1.1 Background

Astronomers have long looked to space as the ideal location for observations of celestial objects. Once beyond the interference of the earth's atmosphere and the contamination of terrestrial radiation it is much easier to get clearer and more accurate images. In the past twenty years many different types of observatories have been placed into earth orbit. The infrared, visible, ultra violet, x-ray and gamma ray regions of the electromagnetic spectrum have all been sampled from high altitude vehicles or spacecraft. However, until just recently the only significant radio observations have all been made from the Earth's surface.

There are benefits to be gained by putting a radio observatory into space. Not only are certain radio frequencies filtered out by the atmosphere but there are also terrestrial radio sources that can interfere and complicate the process of interpreting the collected data. In addition, radio astronomy can benefit from telescopes that are far apart yet operate in tandem.

A radio telescope in orbit and a radio telescope on the earth's surface can coordinate the data gathered from a radio source. This technique, called radio interferometry can significantly increase the angular resolution of the observations. This effectively creates a radio telescope with the radiation gathering capability of the two telescopes combined and an aperture equal to the distance that separates them. In addition, the orbital motion of the satellite will increase the u-v baseline plane permitting higher dynamic range in the maps. Since the projected baseline will be changing faster than ground based telescopes rapidly changing radio sources will be more accurately imaged.

At present the international community of radio astronomers is setting up Very Long Baseline Interferometry (VLBI). The maximum aperture for such a system would be the diameter of the Earth which is approximately 12,800 km. A radio telescope placed in a geostationary orbit and operated in conjunction with an earth based telescope on the opposite pole would have an aperture of 48,500 km. This four fold increase in aperture would result in a significant improvement the angular resolution of radio observations.

1.2 Design Requirements

The design request was for a radio telescope of approximately 150 meters in diameter to be placed in geostationary orbit (GEO). The observatory will be launched into low earth orbit (LEO) by the National Launch System (NLS). In LEO it will be robotically assembled. Upon completion the observatory will be boosted up into a geostationary orbit using either on board systems or available Orbital Transfer Vehicles (OTV). The design requirements or summarized in Table 1.1.

TABLE 1.1

DESIGN REQUIREMENTS AND ASSUMPTIONS

* Diameter 150 meters or area of 17,700 m^2.
* Launched by NLS and LEO assembly.
* Lifetime of 10 years in GEO operating environment.
* Photovoltaic power supply.
* Phased-Array radiation collection.
* Observations in centimeter wavelengths.
* Technology projection suitable for year 2010.

The observatory will be designed as a phased array radio receiver. This radio receiver is essentially a collection of panels made of a dielectric surface with a circuit printed onto it. Instead of having to turn a dish to track a radio source, as is done with current parabolic telescopes, this type of receiver can be aimed using electronic phasing. This will allow the observatory to maintain a constant orientation in space. It will face away from the earth at all times but will be able to observe any radio source above the plane of the surface.

There are two advantages to this method of radiation collection. The first is that the observatory does not have to be constructed as a parabola, but can be a simple, planer surface. The second is that since the observatory can be electronically aimed there is little requirement for the telescope to be maneuvered in space. This reduces the loading on the structure, allowing the structure to be very large and very light, and it reduces the requirements for thrusters and propulsion that would be required to maneuver the spacecraft.

The lifetime for the observatory is to be ten years. The power will most probably be supplied by a combination of photovoltaic arrays and batteries. This is an ideal source of energy since a satellite in GEO will only be eclipsed during certain times of the year and only for a maximum period of approximately forty minutes during a twenty four hour solar day. However, different power sources will be

investigated.

Since the satellite will be serving as the platform for an observatory the position and orientation requirements for the spacecraft are precise. To maintain a reasonable level of observational accuracy the orientation of the satellite will not deviate by more than 0.1 degrees. The satellites orbital position will be determinable within 10m, it's velocity within 1 cm/sec and 10^{-5} cm/sec^2 for it's acceleration.

One of the more important considerations in the design of a satellite is the launch mass. The primary source of mass for the telescope is the observatory surface, the support structure, the power system and fuel used for station keeping. The mass of the communication, computing and attitude control systems will be small in comparison.

The actual observatory surface is to be manufactured in discrete panels that will provide a stiff foundation and will allow for assembly into a single contiguous surface. The phased array surface will be bonded to a composite-like sheet which is stiffened by a material such as a honeycomb core and a support composite sheet. This composite sandwich is needed to keep the observatory surface rigid for accurate electronic aiming. Each panel will make observations of its assigned target. The signal will be partially processed by electronics contained within each panel. The observations of these independent panels will then be coordinated by a central computer in the satellite.

The support structure will maintain the rigidity of the entire observatory and will be the foundation upon which the individual composite panels are mounted. The structural stiffness of the observatory is dictated by the operational requirements of the phased array surface. For accurate observations the structure must not deflect more than three centimeters at the perimeter when subjected to probable, operational and environmental loads.

The size and shape of the panels will be determined by the type of structure and the size of the launch container. The mass per unit area of these composite sheets will probably be independent of the design of the support structure. Consequently, it is the support structure where the initial focus of design was.

2.0 PRELIMINARY DESIGNS

2.1 Requirements

The requirements for the structural design of the observatory are many. It is not necessary for the observatory to be circular but it must at least have the area of a 150 meter diameter dish. The structure must be stiff enough to deflect no more than 3 cm from a central reference point under operating conditions. It must also be sufficiently stiff so as not to plastically deform under the accelerations caused by thrusters when performing a orbital transfer or orbital correction.

The structure must be reliable. Materials that deform under variable temperature or complicated mechanisms that can fail must be avoided. The structure must be easy to assemble in LEO. Self deployable technologies or other construction simplifications are ideal. The structure must be light and must be able to fit in an available launch container. The observatory is designed to be launched in a cylindrical container 27 meter long and 6.7 meters in diameter. The launch vehicle will have an estimated launch capacity of 70 metric tons.

Finally, the structure must be able to support the observatory composite panels. The panels do restrict the structure since the individual panel must be in a shape that, when connected, will provide a contiguous surface. The only qualifying shapes are the triangle, rhombus and hexagon. These shapes will be limited in size by the launch

container.

Five preliminary structural designs were considered. The Tetrahedral Truss and the Box Truss which are both entirely self deployable. A Modular Truss which is partially self deployed and then robotically assembled or assembled through Extra Vehicular Activity (EVA). And a composite Rib Design and Inflatable Design which are both completely self deployed.

2.2 Tetrahedral Truss

The tetrahedral truss is a fully collapsible truss design shown in Figure 2-1. When fully deployed the truss is hexagonal and flat in shape and will measure 170 meters on its largest axis. The truss is composed of individual tetrahedral cells. Each cell consists of six face struts with nine support struts made of graphite epoxy tubes. The structure would be self deployable over a period of 1-2 hours.

The deployment process begins as outer restraining devices are severed, followed by the uniform radial expansion of all members with the interior spring joints damped to assure a constant uniform deployment. The face struts are connected by a nodal joint which would lock to ensure no further expansion.

There were two possible configurations for this truss considering the constraints of the launch container. Using 6.7 meter diameter hexagonal face plates the resulting truss

members would also be 6.7 meters in length. Assuming the truss members are graphite epoxy tubes 2.5 cm in diameter and 2 mm thick, the resulting structural mass would be 11,540 kg.

The other configuration was based on using folding equilateral triangles for the observatory face plates. These triangles would be folded and stowed in the launch vehicle as 6.7 meter diameter hexagons. When hinged sections of the panel are unfolded the resulting shape is a equilateral triangle 10.05 meters per side. Using these panels the resulting truss was have members 10.05 meters in length. This would give the structure a mass of 5,650 kg.

However, this is not a fair mass comparison. Assuming a similar loading condition for both truss designs the members in the larger truss would be required to be stronger to give the same structural stiffness as the smaller truss. (i.e. A less dense truss will transfer more load through fewer members than a denser truss and a shorter member is more resistant to buckling than a longer member with the same section modulus.) Consequently, a simple column buckling analysis was performed using Euler's formula as shown in Appendix 2.1. It was determined that for the larger truss to provide the same structural stiffness as the smaller truss the individual graphite epoxy members needed to increased in diameter. This modification to the design of the larger truss increased its mass to 8400 kg. This is still a significant mass savings over the smaller truss

design.

It should be noted that in calculating the structural masses for these designs the mass of the joints and hinges was not included. The mass of these components is inconsequential compared to the mass of the actual structural members.

There are several advantages to the tetrahedral structure. The fact that it is fully deployable will help reduce the amount of the LEO assembly. The truss is a developed technology which has been extensively tested for smaller scale models. The spring deployment replaces the drive motors necessary for other self deployable structures. The configuration offers an excellent stowed configuration in a 2.0 x 2.0 x 10.05 meter package.

However, with a 6.7 meter launch tube, the folded triangle is not the most efficient use of the space available. Other disadvantages would include the possibility of a spring or member failure in the deployment of the structure. Such a failure would be very difficult to repair in space. Although the self deployable factor can reduce workload there is still the individual placement of the panels that must be considered.

2.3 Box Truss

The Box Truss is composed of a large number of cube elements joined in a single layer to form a roughly circular structure as shown in Figure 2-2. Rigid members form each

of the cubes and the cube is stiffened by tension, cross wires on each of its square faces. Since the resulting truss spaces will be square then the observatory panels must also be square. Consequently, this limits the size of the individual cubes to 4.7 x 4.7 x 4.7 meters. The entire structure of the box truss can collapse into a single package. The size of this package is dependent on the thickness of the individual members and the efficiency of the joints. If 2.5 cm diameter graphite epoxy tubes are used then the optimum collapsed dimensions of a 150 meter diameter box truss is 2.5 x 2.5 x 4.7 meters. This can be easily fit within the launch vehicle.

The truss is collapsed by folding the transverse and longitudinal beams. The vertical beams remain at full length. The folding of the beams is accomplished with locking hinges similar to those of the tetrahedral truss. The tension cross-wires will stow easily in the folded truss.

The deployment of the box truss structure begins from the center. A single row of cubes extend out in a beam in both directions from the central hub. As it extends it brings the members for the rest of the truss along. When fully extended the rest of the truss extends from the beam in both directions until the dish is complete.

The mass estimate for the box truss was based on it being constructed with graphite tubes 2.5 cm in diameter and 2 mm thick. The cross wires were estimated at 0.01 kg/m.

The resulting mass estimate for the truss is 9,800 kg.

One of the advantages of the box truss include the fact that it is fully collapsible. However, a box truss of this size would be quite complicated to deploy. The successful coordination of the springs and/or drive motors would be formidable.

2.4 Modular Truss

This is the only design that does not have a self deployable structure. Small sections of truss are unfolded out of the launch vehicle in LEO and then snapped together like building blocks to construct the structure as shown in Figure 2-3.

The honeycomb sandwich observatory panels are used as part of the structure. The panels are formed into hexagons 6.7 meters in diameter. At three corners of the hexagon are graphite epoxy tubes 5.8 meters in length that connect the plate to a triangular truss, directly beneath it, composed of similar tubes.

Cross wires between the honeycomb plate and the triangle complete the structural requirements for the module. The vertical graphite tubes are attached to the honeycomb plate and the triangle with rotating joints. These, and a joint in the middle of the vertical tubes, allow the three tubes to fold beneath the plate, bringing the triangle against the plate's lower surface.

At the apex of the triangle and at the three corners of

the hexagon above the triangle are mechanical connection devices. These connecters will enable the individual modules to be attached together to form a single truss. The modules will be stowed in the launch container in a collapsed form. When in LEO they will be deployed individually and then snapped together into a large truss.

These connectors may also act as electrical connections that could possibly eliminate the need for the running of wires in LEO. Consequently, this design greatly simplifies the assembly job in LEO. The modules will probably be maneuvered into place by assemblers on EVA or a robotic manipulator. But once they are connected there will be no need to do any wiring or lay down the observatory surface since they will already be in place.

Another advantage of this design is the reliability. If the structure in a module is damaged during launch or deployment it can simply be replaced by a spare. Thus eliminating the possibility of repairs in space.

The mass estimate for this design was calculated using only the graphite epoxy tubes and the cross wires. The panels, as in the other designs, were not included. The individual members are graphite epoxy tube 2.5 cm in diameter and 2 mm thick. The cross wires were assumed to have 0.01 kg/m. The resulting mass estimate is 5,130 kg.

2.5 Radial Rib Design

The rib design is a novel use of composite materials and

is shown in Figure 2-4. A radial arrangement of composite beams is joined to a central spool. These beams are joined to each other by a screen mesh and tension wires attached to the spool. The entire assembly can be wound up for stowage and launch into space.

For the PARAS there are 12 ribs each 75 meters in length. Each rib is a series of composite sheets bonded together to form a beam 60 cm deep and 3 cm wide. The rib will have a large vertical moment of inertia, yet a low transverse moment of inertia that can allow the rib to be wound around the hub. The central drum will be 3 meters in diameter. This large size is necessary since the individual ribs can not be coiled around a tighter surface without suffering damage. The ribs will be connected to each other by a fine mesh that will form a surface on which the observatory panels can be attached. Tension wires will run from various points on the ribs to the hub. The coiled structure will be launched into low earth orbit. After the ribs fully extend the electrical wires and the observatory surface will be put in place.

The mass estimate for this structure is 2,500 kg. This is very light but considering the nature of this structure it is reasonable. The advantages of this structure are its light weight and ease of deployment. However, the stiffness of the structure is not very good. The ribs will not act in tandem and will have dynamic motions somewhat independent of each other. This may result in unacceptable motions at the

edge of the observatory. To increase the stiffness the number of ribs could be increased however it would then become impossible for the wound up structure to fit in the 6.7 meter diameter launch container.

2.6 Inflatable Design

This design is based on a relatively new space construction material, rigidized inflatable kevlar. A sheet of kevlar is lined with fibers that remain soft until a chemical process, usually initiated by sunlight, turns the fibers rigid. The prepreged kevlar sheets can be formed into various shapes such as sheets, tubes and spheres. These structures are folded and packed on the ground for launch. When placed into orbit a gas source unfolds and inflates the structure and solar radiation rigidizes the fibers. After a period of hours or days the structure will have cured and the gas can be evacuated leaving a rigid shell.

This design provided a structural foundation for the observatory using inflatable, rigidizing tubes. The tubes are one meter in diameter composed of 140 micrometers of reinforced prepreged kevlar and 26 micrometers of kapton as a gas barrier. The tubes are arranged in two perpendicular layers and are bonded together with an adhesive. The resulting structure is a 150 meter diameter plate similar to an inflatable pool raft as shown in Figure 2-5.

The kevlar tubes are measured out and bonded to each other on the ground and then the entire assembly is folded

and loaded into the launcher. When released from the launcher into LEO an active gas system inflates and unfolds the structure until it is fully deployed. After two days of curing the structure will have rigidized and the gas will be evacuated. Robots or astronauts on EVA will then lay down the observatory surface onto the structure and all wiring and equipment will be attached. After observational testing is performed the observatory will be boosted into GEO.

The structural mass of this design is approximately 3000 kg. This is very light for a structure of this size. However, there are many problems with the implementation of such a design. The structure will require a great deal of pipe to supply the gas required to inflate it. Each separate kevlar tube will need its own gas source. In addition, each tube would have to have many baffles to prevent a flaw in the kapton from deflating an entire tube. This will demand even more pipe to inflate each section. To place the observatory surface, and other equipment onto the structure will require reinforcements to the kevlar to distribute the load. These thicker sections of plastic would have to be bonded to the structure while on the ground to minimize the assembly work required in LEO. These additions to the structure will have a significant impact on the weight estimate. More importantly, it may make it difficult or even impossible to fold the kevlar, without damaging it, into a small enough area to fit into the launch vehicle.

Figure 2-1 Tetrahedral Truss Concept

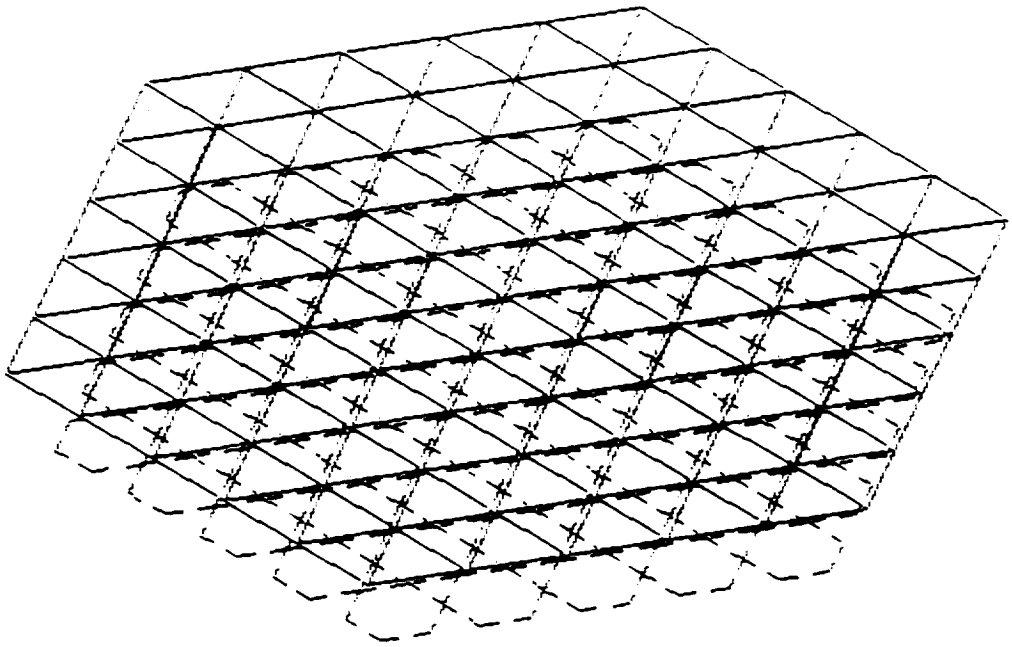

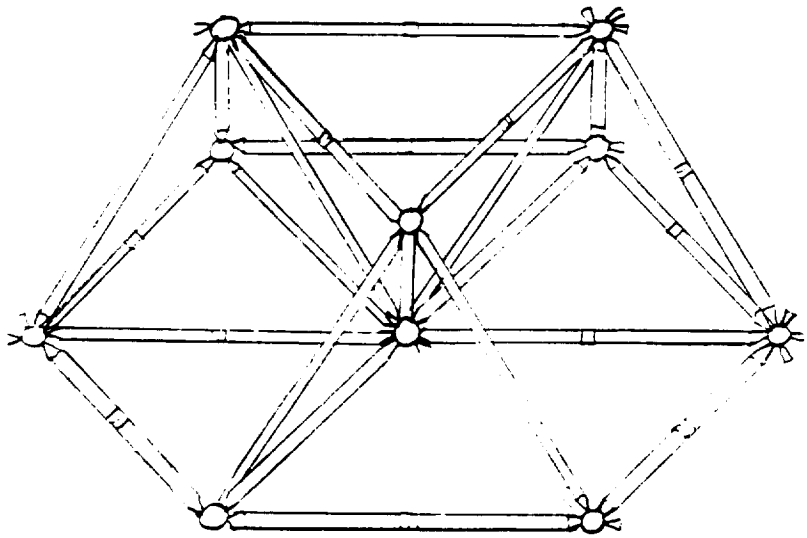

- Self deployable truss using springs and dampers
- Diameter of antenna: 170 meters
- Excellent packaging (2 x 2 x 10 meters)
- Requires additional placement of observatory surface
- Estimated structural mass: 8400 kg

Figure 2-2 **Box Truss Concept**

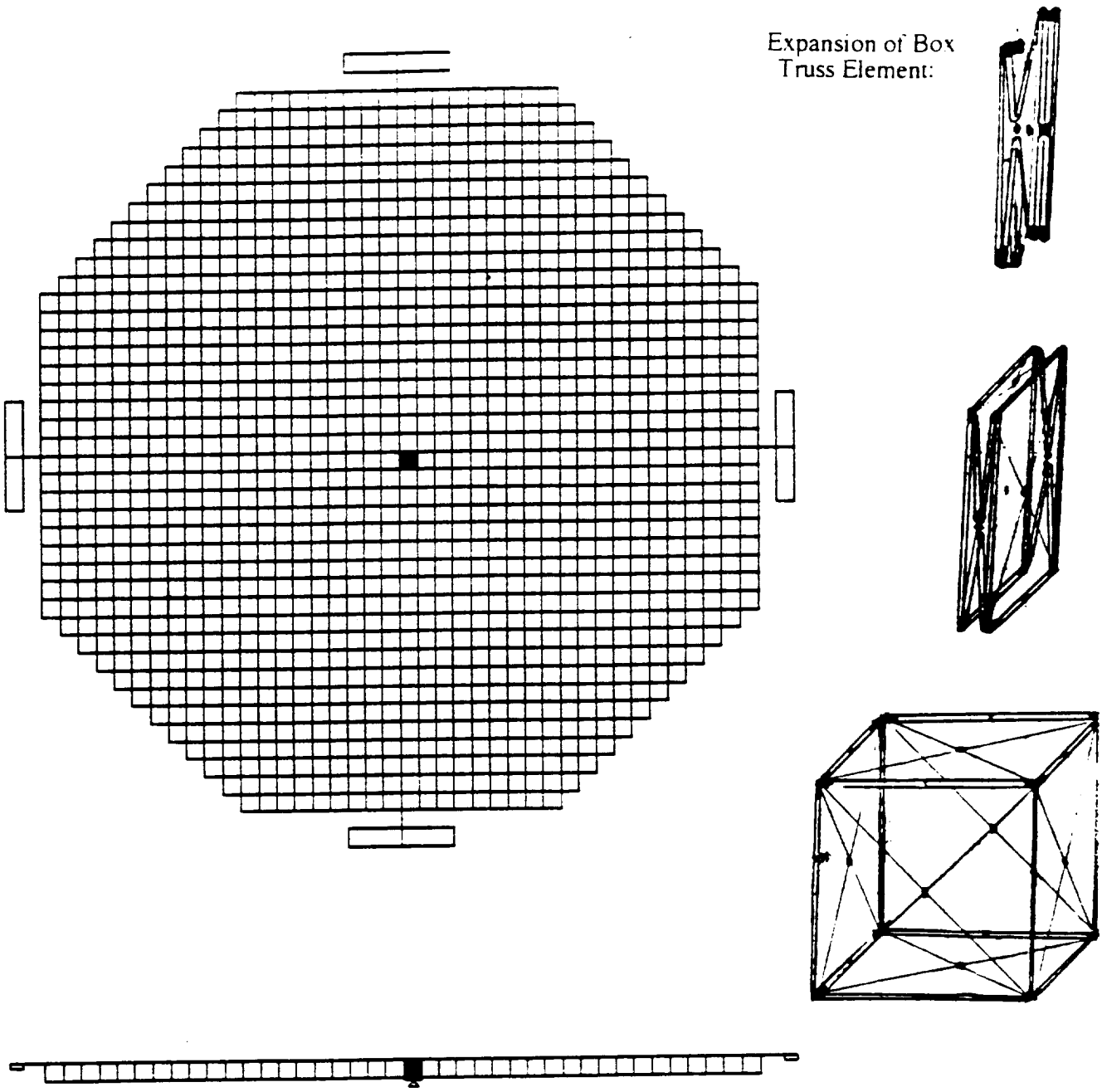

- Self-deployable truss using drive motors
- Excellent packaging (2.5 x 2.5 x 4.7 meters)
- Requires additional placement of observatory surface
- Estimated structural mass: 9800 kg

Figure 2-3 **Modular Design Concept**

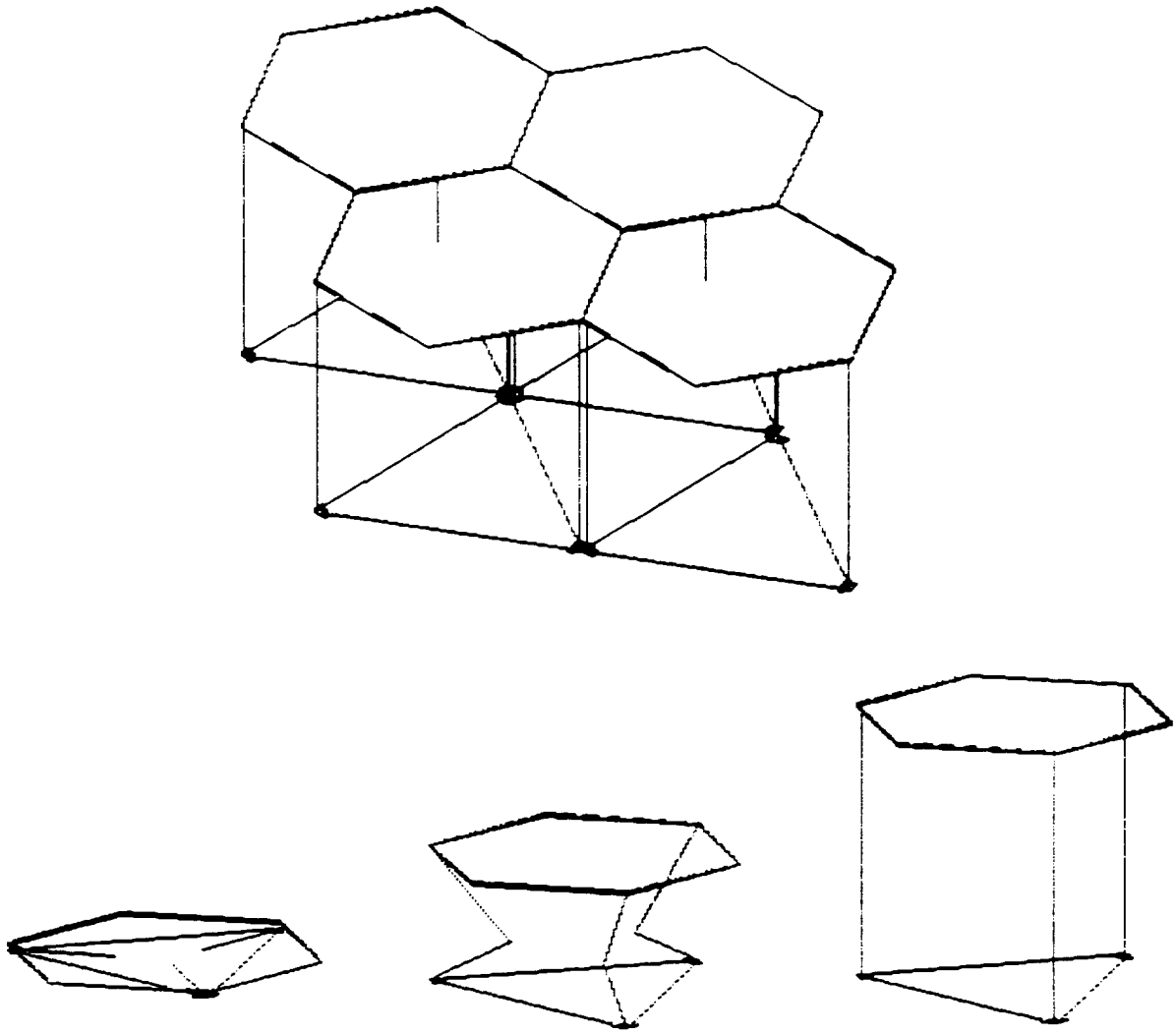

- Collapsible Gr/Ep truss with tension cross wires
- Each module expanded and "snapped" together
- Honeycomb sandwich observatory panels preassembled
- Estimated structural mass: 5130 kg

Figure 2-4 **Wrap Rib Concept**

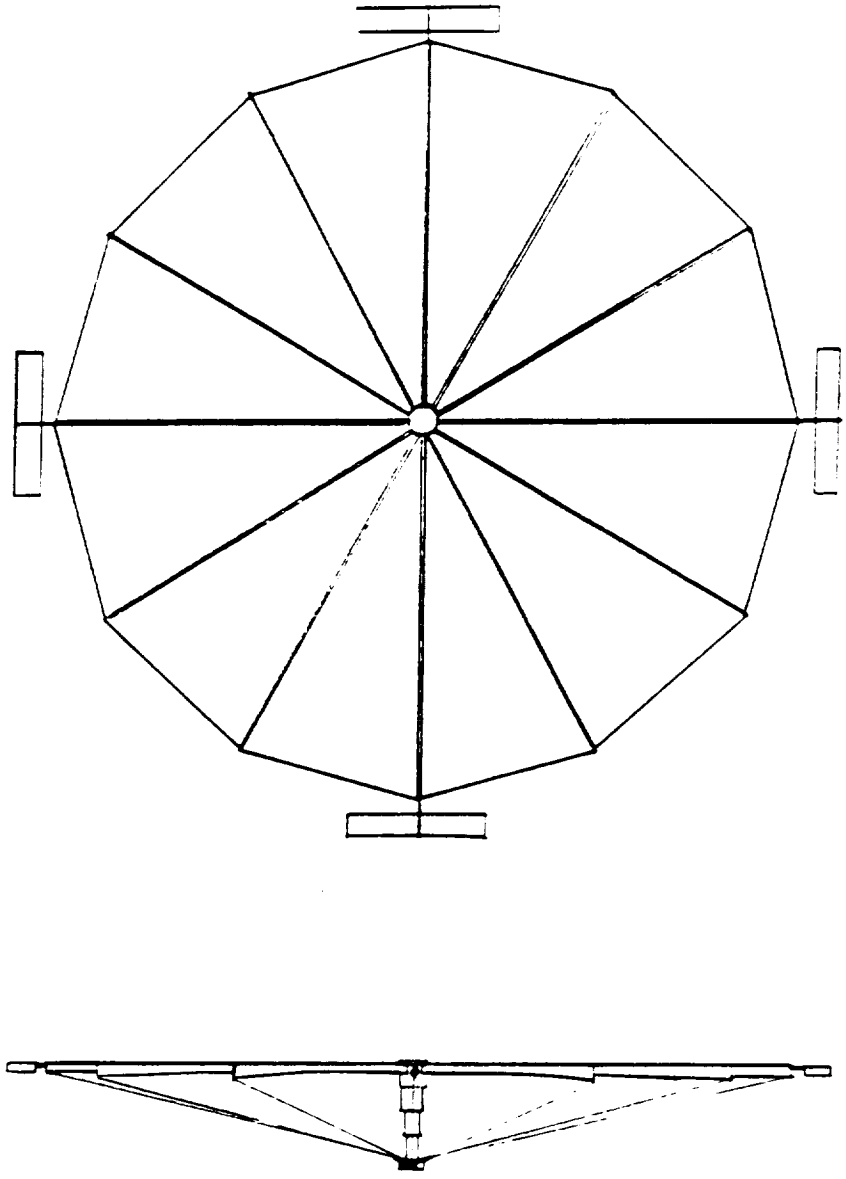

- Ribs wrapped around central bus, unwind for deployment
- Graphite epoxy ribs with tension wires
- Connective mesh
- Requires additional placement of observatory surface
- Estimated structural mass: 2500 kg

Figure 2-5 **Inflatable Raft Concept**

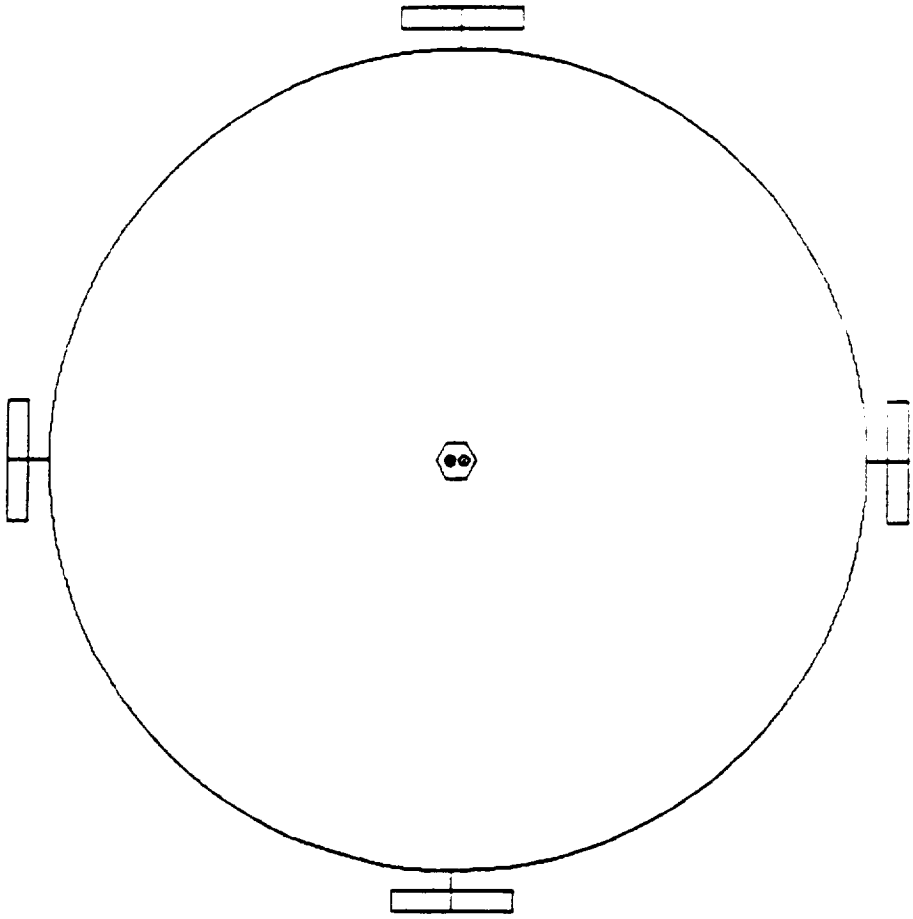

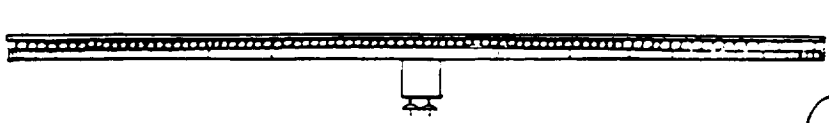

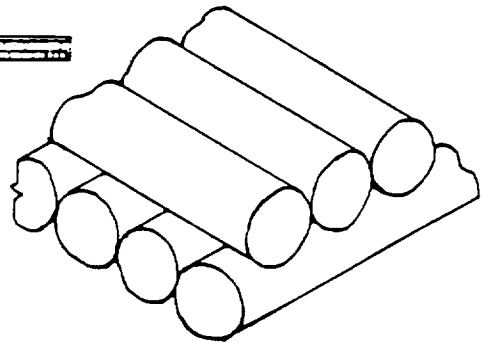

- Self-rigidized inflatable kevlar tubes
- Two orthogonal layers are bonded together
- Deployment by active pressurization
- Requires additional placement of observatory surface
- Estimated structural mass: 3000 kg

3.0 FINAL DESIGN SELECTION

3.1 Selection Criteria

The basis upon which structural design to choose was based on mass, stiffness, reliability, ease of LEO assembly and number of launches that would be required. The mass estimate of each design is determined using the structural mass only. This mass does not include the structural joints, observatory surface or any extraneous equipment. The final mass of the spacecraft could increase by as much as 500% to 1000%. The stiffness is an estimate based on the nature of the structure, the density of the structure, and the number of joints that may have play.

Reliability is an estimate of how dependable the structure is in a faultless deployment and how easy it would be to correct if there was a failure in the structure during construction. This is an important consideration considering the complexity of a structure of this size.

The ease of LEO assembly is based on how many steps are required to construct the observatory in LEO. These steps include construction of the structure, wiring, attachment of the observatory surface, attachment of extraneous equipment, etc.

The number of launches required was determined by the volume consumed in each launch vehicle. The launch vehicles were assumed to have a cargo container of 27 meters in length and 6.7 meters in diameter. The volume consumed was the total volume of the structure, bus, extraneous equipment

and observatory surface. The panels for the observatory surface consume a different volume in the launch vehicle for each design. This is because the panels for each design come in different shapes depending on the form of the structure. The shapes are limited to those geometries that provide a contiguous surface. These include the triangle, square and hexagon. The area ratio of these shapes compared to a circle are respectively 41%, 64% and 83%. These values are referred to as packing efficiencies.

The preliminary designs broke down into three main groups;

1) Self Expanding Truss
   Box Truss
   Tetrahedral Truss
2) Self Expanding Non-Truss
   Inflatable Raft
   Rib Design
3) Modular Truss

3.2 Self Expanding Trusses

The Self Expanding Trusses included the box truss and the tetrahedral truss. The tetrahedral truss has a mass of 8400 kg compared to 9,800 kg for the box truss.

The tetrahedral truss, by benefit of the inherit structural stiffness of the tetrahedral, is assumed to be more stiff than the box truss. Both have an equivalent loss in stiffness resulting from the large number of joints in the graphite epoxy tubes that allow them to fold.

The tetrahedral truss is considered more reliable than the box truss. This is because the tetrahedral truss is completely self deployable. The deployment of the box truss on the other hand is a process that requires various steps to be carried out in a proper sequence. This is a more complicated and more error prone deployment.

Both have a similar ease in LEO construction since there are the same number of steps. Both of these designs, once placed into LEO will have the observatory surface attached to the structure.

The observatory surface for the tetrahedral truss would be in the form of triangle folded into a hexagon. These folded triangles have a packing efficiency of 62%. The observatory surface for the box truss would be in the form of squares with a packing efficiency of 64%. The volume consumed by the actual trusses is approximately the same.

Many characteristics of the two truss designs are equivalent. However, from it's lower mass, higher stiffness and ease of deployment it is clear that the tetrahedral truss is the superior design from the self expanding truss category.

3.3 Self Expanding Non-Truss

This category includes the inflatable raft and the rib design. Both of these designs are very light. The inflatable is only 3000 kg and the rib design is 2500 kg.

The inflatable structure should be quite stiff due to the good bending properties of the 1.0 meter diameter tubes. The rib design is not very stiff. This is because the ribs essentially act independently and can only distribute loads down the rib or through tension wires connected to the central hub.

The reliability of these structures is unknown since both technologies remain relatively untested. Both structures are sure to deploy but whether or not they deploy correctly, without damage is not certain. In addition, the inflatable and the rib design would be difficult to repair if damage was incurred during deployment.

The rib design is easier to assemble than the inflatable. The wiring and observatory surface would need to be put down, and extraneous equipment attached for both. However the rib design would already have the bus attached to the structure and the screen surface of the rib design would be simpler to attach the observatory surface to than the inflatable kevlar.

Both of these designs are not constrained in what shape of observatory panel they use. Therefore, they can use the hexagon which has a packing efficiency of 83%. The packing method for both these structures is uncertain. The rib design must be wound up around the central hub. For an observatory of 150 meters in diameter using the number of ribs required for stiffness it is difficult if not impossible to store a structure of the required stiffness in

a launch volume less than 6.7 meters in diameter. The inflatable design can be folded into a launch vehicle but the number of tubes, valves and hard spots would make folding the structure very difficult. It is doubtful that the kevlar and kapton could be protected from damage in the process. Neither of these designs seems especially promising.

3.4 Modular Truss

The mass and stiffness of this design is similar to that of the tetrahedral truss. The mass estimate for the structure is 5130 kg. The reliability for this structure is very good. The individual modules are easy to deploy, and any damage that the structure sustains can be corrected by simply replacing the affected module with a spare. The ease of assembly is similar to the other trusses. Even though the truss needs to be assembled by hand the observatory panels do not need to be attached since they are already part of the structure. Also there is the potential to incorporate the wiring of the observatory into the connections of the truss which would eliminate another step from the construction process.

The packing ability of modules is also comparable to the other trusses but since the modules are hexoganally shaped they have the advantage of a 83% packing efficiency which is better than both the box or tetrahedral truss.

3.5 Selection

The tetrahedral truss and the modular truss were the two most plausible options for the observatory support structure. The mass of the modular truss is less than that of the tetrahedral by approximately 64%.

The reliability of the modular truss is superior to that of the tetrahedral truss. This is because of the ease of repair for the modular truss. If anything goes wrong with the deployment of the tetrahedral truss it would be very difficult to perform a repair in space if parts demanded replacement. However the modular truss can be constructed step by step with each module being inspected before being attached to the rest of the structure. If a module is bad it can be replaced with a spare.

The modular truss is easier to assemble because the observatory surface is included with the structure and will not need to be attached in an extra step. The modular truss can also have electrical linkages incorporated into the attachment joints that may make it possible to reduce or eliminate any wiring that may have to be performed in LEO.

The packing efficiency of the hexagon on the modular truss is 83%. The packing efficiency of the folded triangle used by the tetrahedral truss is 62%. The tetrahedral truss will require 10.2 meters of launch vehicle and another 28.3 meters for the observatory panels or a total of 38.5 meters. The modular truss with structure and panels will require a total of 36.2 meters. There is no serious advantage here

since both require two separate launches.

However, when all things are taken into account it is clear that the modular truss will provide the best design for this observatory. The modular truss has a low mass, a stiff truss design and is easy to manufacture in space. It will have a reliable manufacturing process that will allow ground testing and easy repair in space.

A qualitative comparison of the various preliminary designs is shown in Figure 3-1.

Figure 3-1 **Comparison Table of Preliminary Designs**

	MASS kg	STIFFNESS	RELIABILITY	ASSEMBLY	NUM. OF LAUNCHES
BOX TRUSS	9,800	HIGH	MED	MED	2
TETRAHEDRAL TRUSS	8,400	HIGH	MED	EASY	2
MODULAR TRUSS	5,130	HIGH	HIGH	EASY	2
RIB DESIGN	2,500	LOW	MED	MED	2
INFLATABLE DESIGN	3,000	HIGH	LOW	MED	2

4.0 STRUCTURAL DESIGN AND MATERIALS

4.1 Overview

To reduce the mass of the modular truss even further inflatable members were incorporated into the design. The vertical graphite epoxy tubes of the module were replaced with self-inflatable, rigidizing kevlar tubes.

These tubes will be folded under the composite panel during launch. When the module is removed from the cargo container and exposed to the sun a chemical within the tube will sublimate and inflate the tube to the desired pressure. After a few hours the kevlar will thermally cure and become rigid and the module can be attached to the truss. Figure 4-1 presents a complete module diagram for reference.

The complete configuration calls for 656 modules assembled radially from a central bus, see figure 4-2. When the modules are joined together to form the complete truss there will be three vertical members arranged in a cluster at each attachment point. This allows the use of the inflatables, since the vertical beams are redundant structural members. If one of the inflatables forms with a dimple or crease, which could make it more susceptible to failure, then there are two other members to back it up.

By using inflatable members the mass of the vertical tubes is reduced dramatically. The simplicity of the design is increased since all the hinges and moving parts required for deployment will no longer be needed. The new mass estimate for the modular truss is 2560 kg.

4.2 Observatory Panels

The design criteria for the selection of the observatory panels included several categories. These panels will comprise most of the mass of the structure and therefore must be light as possible. The surfaces must keep thermal expansion to a minimum so as not to induce bending deformation to the truss below. The panels will be a vital structural component and must be able to withstand the axial, bending and shear stresses it will be subjected to from and thrusting forces.

With these requirements in mind, three comparisons of several facesheets and core materials were investigated and three options for the sandwich configurations were proposed. These include, a rigidized foam core with a polyimide film facesheet, a Nomex fiber core with GR/EP faces, and a kevlar core with kevlar faces. Table 4.1 summarizes these three options.

Table 4.1

Observatory Panel Options

Option:	Rohacell 31IG Upilex S Film	Nomex HRH-10 Gr/Ep T650/ERL-1901	Kevlar HRH-49 Kevlar 49
Modulus E (ksi)	8.07	2200	7600
Shear Mod G (ksi)	2.90	8370	2130
Poisson's Ratio v	0.307	0.314	0.314
Mass (kg)			
Per module	26.5	47.8	42.6
Total surf.	17,390	31,370	27,960

4.2.1 Foam Core / Polyimide Film Surface

The the foam material selected is Rohacell 31 IG manufactured by Rohm Tech, Inc., and the plastic film is an isotropic, polyimide film, Upilex S, manufactured by ICI Films. The foam has a density of 32 kg/m^3 and supplies tensile strength as well as compressive strength; ordinary honeycombs supply very little tensile strength. The film is known for its excellent tensile strength to weight ratio,

low thermal expansion and resistance to radiation. An advantage of the film material is that it has a thickness of 25 micrometers compared to the nominal thickness of 0.127 mm/layer of composite fiber sheets. The facesheets are much greater in mass than the core materials and must be selected carefully.

The sandwich dimensions were first selected due to launch tube packing constraints and is a nominal 2.5 cm for all options. The effective engineering constants E, G, and ν were determined using Composite Laminate Theory for isotropic materials and were found to be E = 8.07E3 psi, G = 2.9E3 psi, and the poisson's ratio of 0.307. These calculations can be found in Appendix 4.1. The total surface mass for this configuration is 17,390 kg and is considerably less than the other options.

4.2.2 Nomex Core / Gr/Ep Facesheets

Option 2 is a Nomex fiber core HRH-10 manufactured by the Hexell Corporation with again Gr/Ep T650/ERL-1901 facesheets. This design is a common one that is being considered in use of smaller orbital reflector antennas. The core density is similar to that of the foam, 28.8kg/m^3. However, it is the facesheets which again comprise most of the mass.

In order to keep thermal expansion to a minimum, Gr/Ep unidirectional fiber tape is applied in layers of various angles, a common selection is the four layer, symmetric,

zero degree, ninety degree fiber configuration or $(0,90)_s$. With a density of 1.6 g/cm^3 and a minimum thickness of 0.127 mm, each face must be 0.508mm thick. This in effect drives up the panel mass significantly. The entire surface mass for this configuration is 31,370 kg. Honeycomb core is a compression bearing frame and does not provide significant tensile strength. The effective tensile properties were assumed to lie in the facesheets and were found to be E = 22E6 psi, G = 8.36E6 psi, and v = 0.314. Although these properties are of the order of 10^3 greater than the film, they may be an overkill for the relatively light loading conditions anticipated for the spacecraft.

4.2.3 Kevlar Core / Kevlar Facesheets

Option 3 is a kevlar core, HRH-49, and facesheets of Kevlar 49, manufactured by Hexell. The advantage to this configuration is its toughness and superiority to damage and thermal cycling. The lamination process is similar to Nomex sandwich with the facesheets again in the $(0,90)_s$ lamination and thicknesses the same. The material properties are E = 7.6E6 psi G = 2.13E6 psi, and v = 0.314. Because of kevlar's low density, 1.38g/cm_3, the entire surface mass is 27,960 kg, a savings of 3410 kg over nomex, but still considerably more massive than the foam option.

4.2.4 Final Selection and Design Optimization

The final selection of the observatory panel was based

on mass, strength and thermal properties. The foam and film option is the best alternative because it cuts the surface mass in half. Figure 4-3 is a schematic of our observatory panel.

The original structural dimensions of the material thicknesses and size were initially estimated based on the expected loads and launch requirements. Following the structural analysis and further investigation into the volume consumed in the launch vehicle it was determined that many of the structural members could have the dimensions reduced.

The thickness of the foam panel was increased because the space was available in the launch vehicle. This additional thickness will improve the panels bending properties. However, this did not result in an increase in mass because the foam inner core was redesigned as a honeycomb structure.

The foam core was increased in thickness from 2.5 cm 3.4 cm. The core was built up from foam honeycomb cells 67 cm across and 2.5 cm deep. The honeycomb was covered by foam face sheets 0.5 cm thick and then layered with the polyimide sheets. The internal walls of the honeycomb structure are 0.5 cm thick. This panel was assumed adequate to withstand the loads determined in the structural analysis. This modification reduced the mass of the observatory panel to 9.279 kg for a total surface mass of 6087 kg.

4.2.5 Phased Array Configuration

In the past, radio telescopes were primarily designed with a parabolic reflector, focusing incoming signals onto one or several feed elements at the center, or focus, of the dish. Of late, the need for lightweight antennas have employed an active phased-array technology where many feed elements are arranged in a planar array. The benefit of this technology is that the sky can be scanned in all directions from an immovable, flat surface. This technology incorporates power amplifiers directly behind a radiating element, phase shifters, attenuators, and integrated circuitry. However, for a 150 m diameter observatory, this technology is too massive. The technology that will employed for this spacecraft is a lightweight, printed circuitry surface, allowing the removal of the bulky phase shifters, attenuators, and other hardware used in current phased arrays.

The printed circuitry is being developed for advanced, lightweight communications satellites at various facilities including the Jet Propulsion Laboratories in California and COMSAT Laboratories in Maryland. A similar circuitry could be developed to act only as a receiver for this telescope.

Figure 4-3 details the phased array surface. The array consists of many patch receiving elements, as shown. The printed, patch element and circuitry are etched onto the polyimide film of the panel surface. An additional 25 um of film would be cover the circuitry, protecting it from radiation damage.

The number of radiating patches that will be used will be directly proportional to the wavelength being observed. Primarily, observations will be at wavelengths between 3 and 21 cm. However, it is possible to observe at millimeter wavelengths if certain panels were to have a denser phased array element surface placed on the panel.

4.2.6 Additional Electronics

Electronics including a central processing unit for phase shifting, amplifiers, power conditioners, and batteries for the module will be located in the center of the panel occupying a cavity in the foam core. A 35.5 x 30.4 x 2.9 cm Nickel Cadmium battery and a 15 x 30.4 x 2.3 cm volume will house the electronics, Figure 4-3. A gallium arsenide solar panel measuring 55 x 43 cm will cover the unit with an additional panel on the back side of the foam panel. Combined, the two panels provide complete observational power for the module. Some type of bracket for these units will be developed to fasten it to the foam panel. Additionally, a hole with diameter of 1 cm will cut through the center of this unit for the module deployment

cable (see section 9 for deployment details).

A network of radiation hardened fiberoptics cables will link each module with the central bus. Such a fiber has been developed by Raychem for military applications and would be suffice for our purposes. The construction, depicted in Figure 4-3, consists of a bare glass fiber housed in successive jackets of silicon buffer, Ethylene-Tetraflouroethylene copolymer, both for radiation protection and heat resistance, and Kevlar for strength. These cables will terminate in the male/female connectors joints located at the three structural corners of the panel. Section 4.7 details more about the joints.

4.3 Graphite Epoxy Truss Members

The base of the module consists of a triangular arrangement of tubes of 2.5 cm diameter, 2 mm thick, and 5.8 m long. Three materials were selected for comparison including two graphite epoxies, T300/934 and T650-35/ERL-1901, and Kevlar 49. Table 4.2 summarizes their comparative properties.

Table 4.2 Tube Materials

	Gr/Ep T300/934	Gr/Ep T650-35/ERL-1901	Kevlar 49
Density (g/cm^3)	1.60	1.59	1.38
Comp. (MPa)	1720	1720	1300
Tensile (MPa)	1530	2100	1378
Modulus E (GPa)	130	150	75
Sp. Stiff. (Nm/kg)	81,300	94,300	54,300
Therm. Exp. (cm/cm/C)	$4.16x10-^6$	$-0.056x10-^6$	$-4x10^{-6}$

Kevlar is known for it superior toughness, low density of $1.38g/cm^3$, and tensile strength. However, it is has a relatively poor compressive strength compared to Gr/Ep and therefore this material is eliminated from consideration in the tubes.

Two graphite epoxies were selected for study, T300/934 which is manufactured by the Fiberite Corporation, and T650-35/ERL-1901 which is manufactured by the Amoco Corporation. Both fibers are manufactured by Thornel. From manufacturer specification, both have identical compressive strengths, 1720 MPa, but T650 has a higher tensile strength and Young's modulus than T300, 2100 MPa and 150 GPa. Both have about the same density of $1.6g/cm^3$. T650 was rated at a lower thermal expansion than T300, -0.056E-6 cm/cm^oC to 0.417E-6 cm/cm^oC, and had a higher specific stiffness of, 5.75GPa/kg, than the T300.

Although T300/934 has been used successfully in many space applications, T600/ERL-1901 has more desirable properties making it the superior choice for the truss members. Each ply has a minimum thickness of 0.127 mm and will be oriented in a configuration similar to that which is being considered for Space Station Freedom, $(45,0_5,45)_s$ and a thickness of about 2mm. Figure 4-4 shows the graphite epoxy tube.

4.4 Inflatable Truss Members

The top panel and the bottom triangle are to be connected with 5.8 meter long inflatable tubes. This technology is known as Rigidized Inflatable Structures (RIS) which is being developed by the European Space Agency for the QUASAT program. The tubes will be 30 cm in diameter and

be composed of 140 micrometers of reinforced prepreged kevlar matrix developed by CIBA-CEIGY for the ESA. A Kapton foil 26 micrometers thick will act as a gas barrier and a metallic aluminum layer 60 nm will act as a thermal control coating for the tube. Figure 4-4 shows the material used.

The tubes will be capped on each end, with no baffles in between. They will be folded in their flexible prepregged state beneath the panel in the launch tube. Each member will contain an exact amount of chemical substance which will under go a sublimation process upon exposure to sunlight. The gas will inflate the tube to the desired pressure for curing in space, forming a rigid truss support.

4.5 Tension Wires

To add torsional stability to the module, graphite fibers impregnated with Teflon and coated with SiO_2 are to be used as cross wires. The cable is manufactured under loading to improve fiber load distribution and toughness.

Table 4.3
Graphite Fibers

Fiber	Tension (MPa)	Modulus (Gpa)	Density g/cm^3	Mass/Length g/1000m
T300	3530	230	1.76	66
M30	3920	294	1.70	53

From manufacturers specifications, T300 and M30 were the least massive of all fibers. The fiber type selected was M30 manufactured by Toyrca for its low mass per length, 53 g/1000m and high tensile strength.

4.6 Joints and Attachment Mechanisms

Each joint will serve many purposes. Primarily it acts as a cap to the inflatable. The bottom connectors will join the graphite epoxy tubes into a triangle and also fasten the graphite tension wires. Figure 4-5 depicts the bottom joint while Figure 4-6 shows the top joint. Since titanium has very high strength and low thermal expansion as compared to aluminum, it was chosen as the material for both joints.

The top connectors will use a male/female port connector for the fiber optics link. Each joint will have a male and female part that will be used to snap the modules together into the truss, as shown in Figure 4-8.

4.7 Material Coatings for Geostationary Environments

4.7.1 Overview

Advanced material coatings are needed to ensure that the materials being considered for the structure remain stable throughout a 10 year lifespan. Three major design areas are being considered: graphite/epoxy tubular truss members, the observatory surface panels, and the vertical inflatable members. Before these materials can be selected, the space environment must be understood.

4.7.2 Environment

Differing environmental conditions exist in low-earth orbit and geo-synchronous orbit. In LEO, the materials will be exposed to temperature ranges of $+93^0$C to -128^0C, UV radiation, high vacuum, and micrometeorites. In GEO, there is an additional flux of high-energy electrons, e^-, and protons, p^+, as the structure passes through the Van-Allen Belts, as well as a temperature range of $+121^0$C to -156^0C. Except for the period during LEO assembly, the spacecraft will be stationed in GEO, therefore this environment will dictate coating requirements.

The optical requirements for GEO include absorptivity, alpha a = 0.20 - 0.35 to reduce the effective temperature, and emissivity, e = 0.15-0.25 to keep the structure from cooling rapidly during solar occult. It is also favorable to produce a coating with low reflectance for assembly procedures. Another area of concern will be the spacecraft

charging due to poor electrical conductivity. It has been estimated that the surface must have a conductivity greater than $1*10^8$ ohm-cm. If not, the surface panels could charge and release electric arcs which could damage the electrical circuitry.

4.7.3 Gr/Ep Truss Members

Several coatings have been studied by the Boeing Corporation for application in LEO which meet the absorptivity and emissivity requirements. First, the application of white paints was quickly ruled out because the large mass that is accompanied with them. Two others are Chromic anodized Al foil and sputtered SiO_2/sputtered Al/Al foil. Both coatings showed no microcracking under thermal cycling, minimal loss in absorptivity due to atomic oxygen over their lifetime; however the anodized foil was superior in adhesion, having a peel strength that exceeded the foil tensile strength.

The study of radiation effects has been a focus of research the past several years. Recent studies by the NASA-Virginia Tech Composites program have yielded some insight into the effects of radiation on Gr/Ep tubes. Specimens have been subjected to radiation up to 10,000 Mrads to represent a 30 year worst case scenario. The results of the experiments show no serious degradation over our expected lifetime of 10 years, only minor degradation at elevated temperatures ($+121^{\circ}F$).

Radiation does, however have a detrimental affect on the absorptivity of the coating. Radiation has been found to darken aluminum surfaces; however, SiO_2 is highly resistant to radiation and will not darken over the spacecraft lifetime. It has been selected as an additional spay coating to the anodized aluminum foil.

The coating selected for these tubes will be the anodized Al foil with a thickness of 0.05 mm and will have a textured surface to decrease reflectivity. The foil will be applied with 0.05 mm (2 mils) of epoxy sheet adhesive. An additional spray of 1 micron of SiO_2 will provide the necessary radiation resistance. The absorptivity of the coating is 0.23 while the emissivity is 0.15. It is estimated that these tubes will see an effective temperature of $27^{o}C$ to $-56^{o}C$. These temperatures do not degrade compressive or tensile strengths of the members or produce any detrimental strains between the foil and tube due to thermal mismatches.

4.7.4 Observatory Panels

Polyimide films have been studied in the past to determine their feasibility in space applications. In the past, the largest problem with these films have been their poor electrical conductivity which allows the craft to build up a static charge. For the PARAS platform, the charge would be released in electric arcs when the face is in darkness. These arcs could be of enough charge to damage

the printed circuitry surface. Estimates show that electrical conductivity must be greater than 10^{-8} $ohm_{-1}cm_{-1}$ in GEO.

The film selected is Upilex S, noted for its resistance to radiation and electrical stability. Listed for Upilex is a conductivity of 10^{-17} $ohm^{-1}cm_{-1}$. This would be acceptable in LEO but not GEO. Solutions to this problem could be the mixture of metallic flakes or ions into the film. A palladium/lithium ion addition should produce adequate conductivity while keeping the mass minimal.

Polyimide film is very stable to radiation because of its highly aromatic chemical structure therefore is not considered a problem. The clear polyimide film would have an absorptivity of 0.20, and be an excellent reflector of sunlight (reflectivity = 0.80) and again the panels would be exposed to an effective temperature range of 27°C to -56°C. Since the panels would most likely be at a room temperature, 25°C, the panels will not expands as much as they will contract. Traditionally, low thermal conductivity has been a characteristic of many foams. Without a dynamic analysis of the temperature cycle that these panels see, accurate contract/expansions cannot be determined. No additional coating is deemed necessary beyond the film.

4.7.5 Inflatable Members

The inflatable kevlar tubes have been manufactured with 60nm of aluminum to shield from oxygen degradation and

control thermal cycling. The aluminum will posses the same properties as the anodized foil used for the Gr/Ep tubes seeing similar effective temperatures and minimal thermal expansions. Additionally, 1 micron of SiO_2 will be sprayed to the inflatables to shield from radiation.

4.7.6 Conclusions

The following materials have been selected for use on the structure:

- Chromic anodized Al foil of 0.05mm for use on the Gr/EP tubes with 1 micron of SiO_2 spray; 0.05mm epoxy sheet adhesive as the bonding agent.
- Upilex S clear polyimide film with palladium/lithium ion addition for observatory panels. No additional coating necessary.
- 60 micrometers of metallized Kapton foil for gas barrier with 60 nanometers of aluminum to shield oxygen degradation and 1 micron SiO_2 for radiation protection.

4.8 Assembly

The truss will be assembled starting with the central bus as shown in Figure 4-9. The modules will be attached one at a time in a spiral pattern. The maximum number of connections for each module will be two. This should be a simple task. Assembly will be conducted using robotic arms or assemblers in EVA. The connectors only need to be pushed together, inserting the male into the female until the

mechanism locks. There is no specific arrangement or orientation for the individual modules since they are interchangeable. Upon completion of the entire truss the extraneous equipment, such as the thruster modules would be attached. The final arrangement of the cells will closely approximate a 150 meter diameter circular disk.

Figure 4-1 **Complete Module**

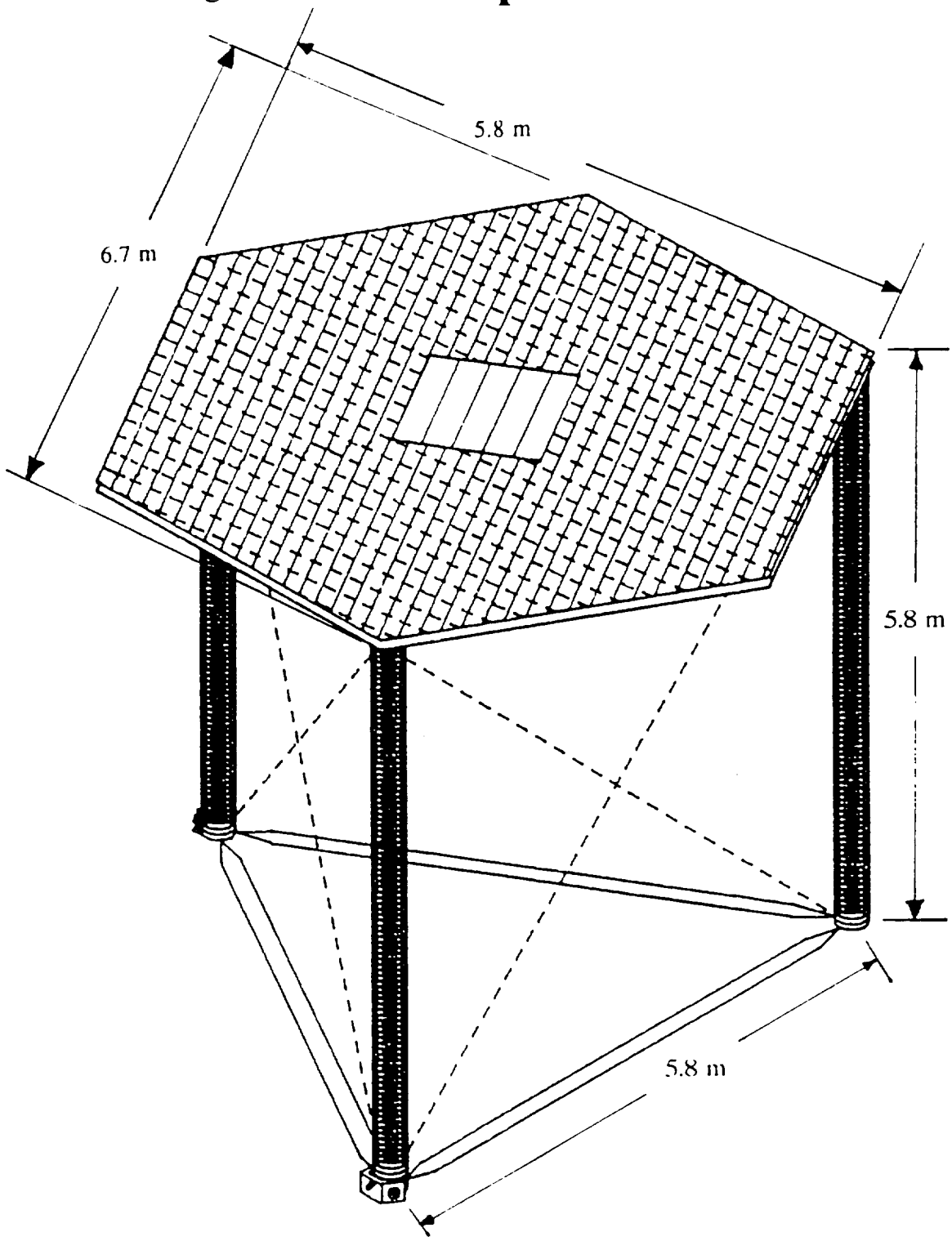

Gr/Ep T650/ERL 1901 triangular truss

Inflatable kevlar vertical struts

Cross wires in tension

Composite foam/polyimide film observatory panels

656 Modules Assembled Radially
from Central Bus

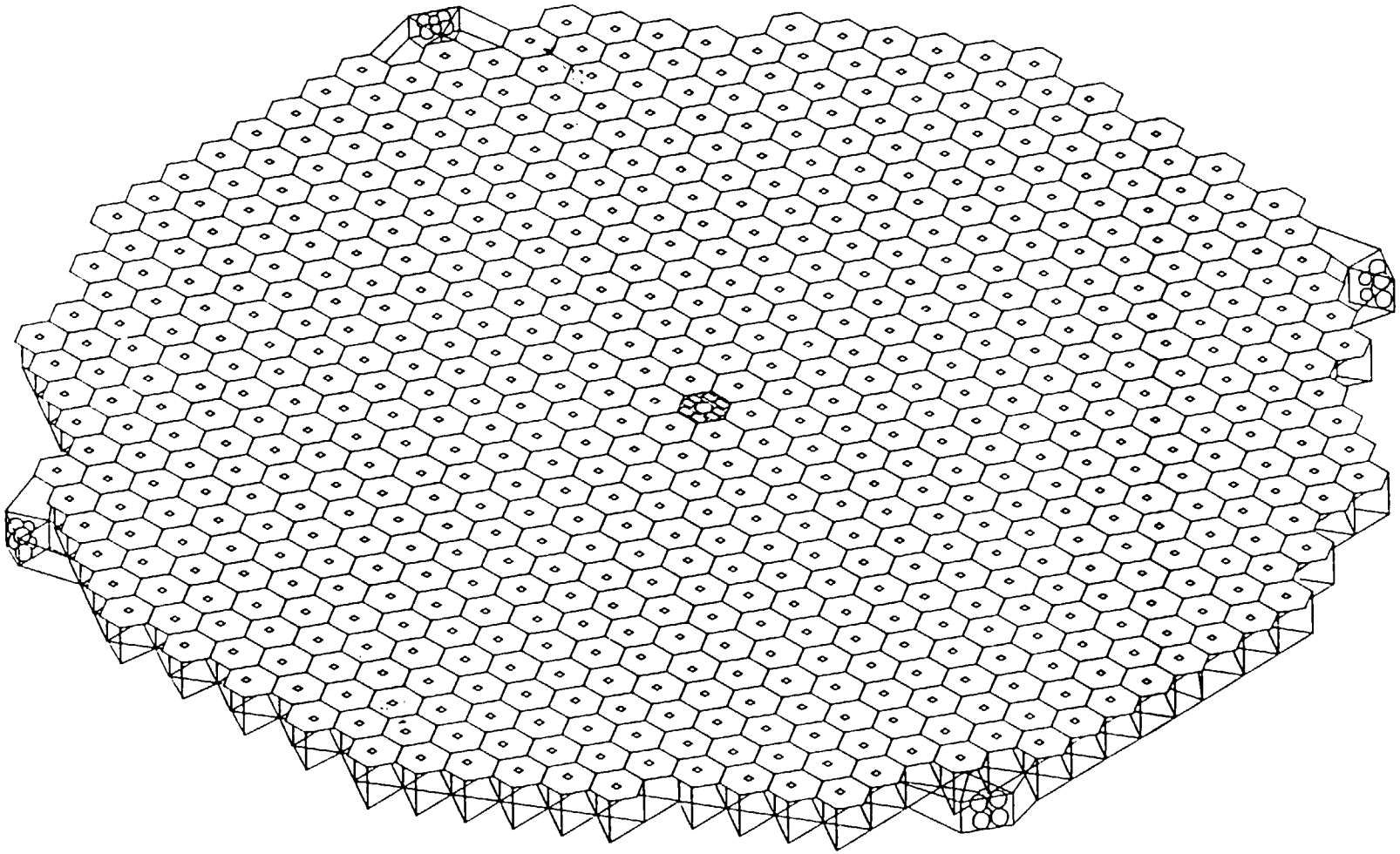

Figure 4-2 **Assembled Configuration**

Figure 4-3 **Observatory Panel**

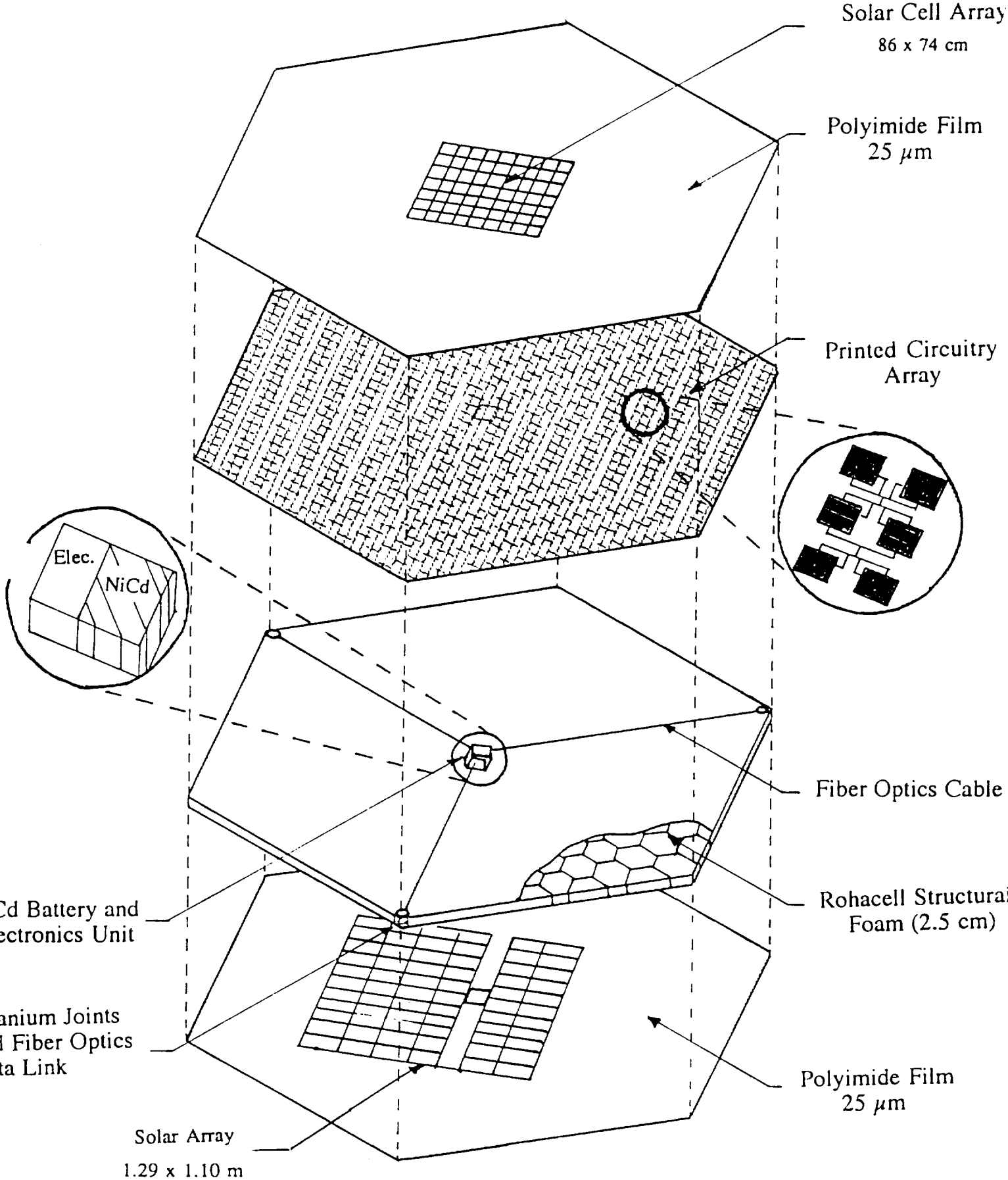

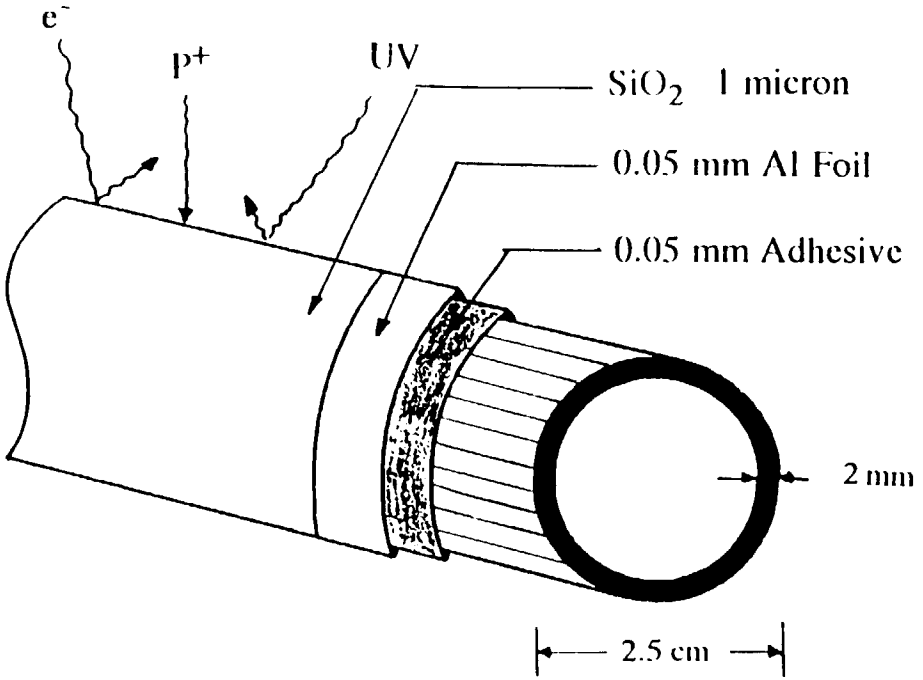

Gr/Ep T650/ERL-1901 Tubes

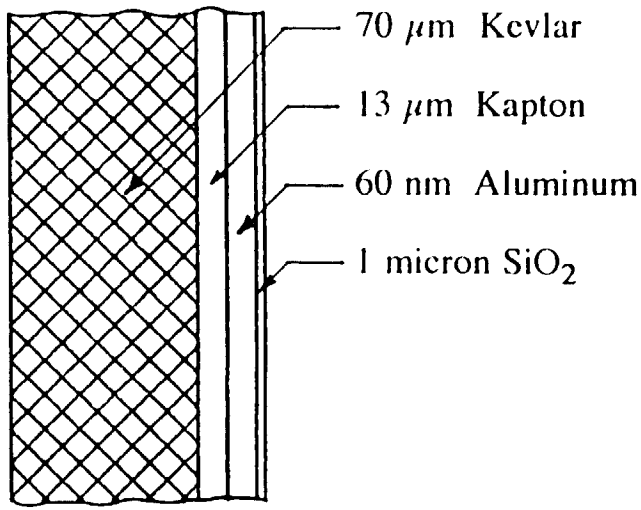

Inflatable Kevlar Tubes

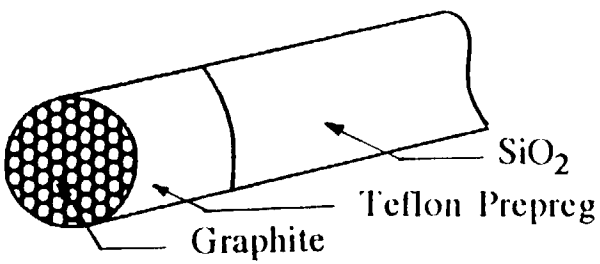

Graphite Tension Wires

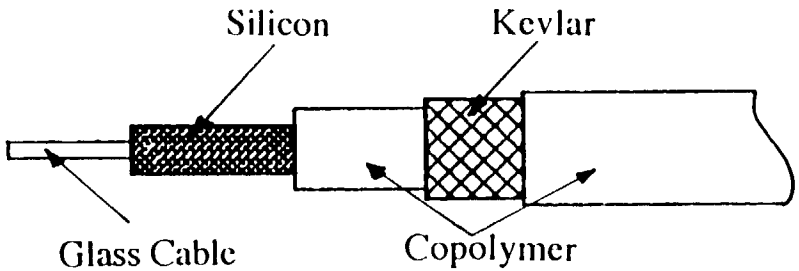

Fiber Optics Cable

Figure 4-4 **Select d Materials**

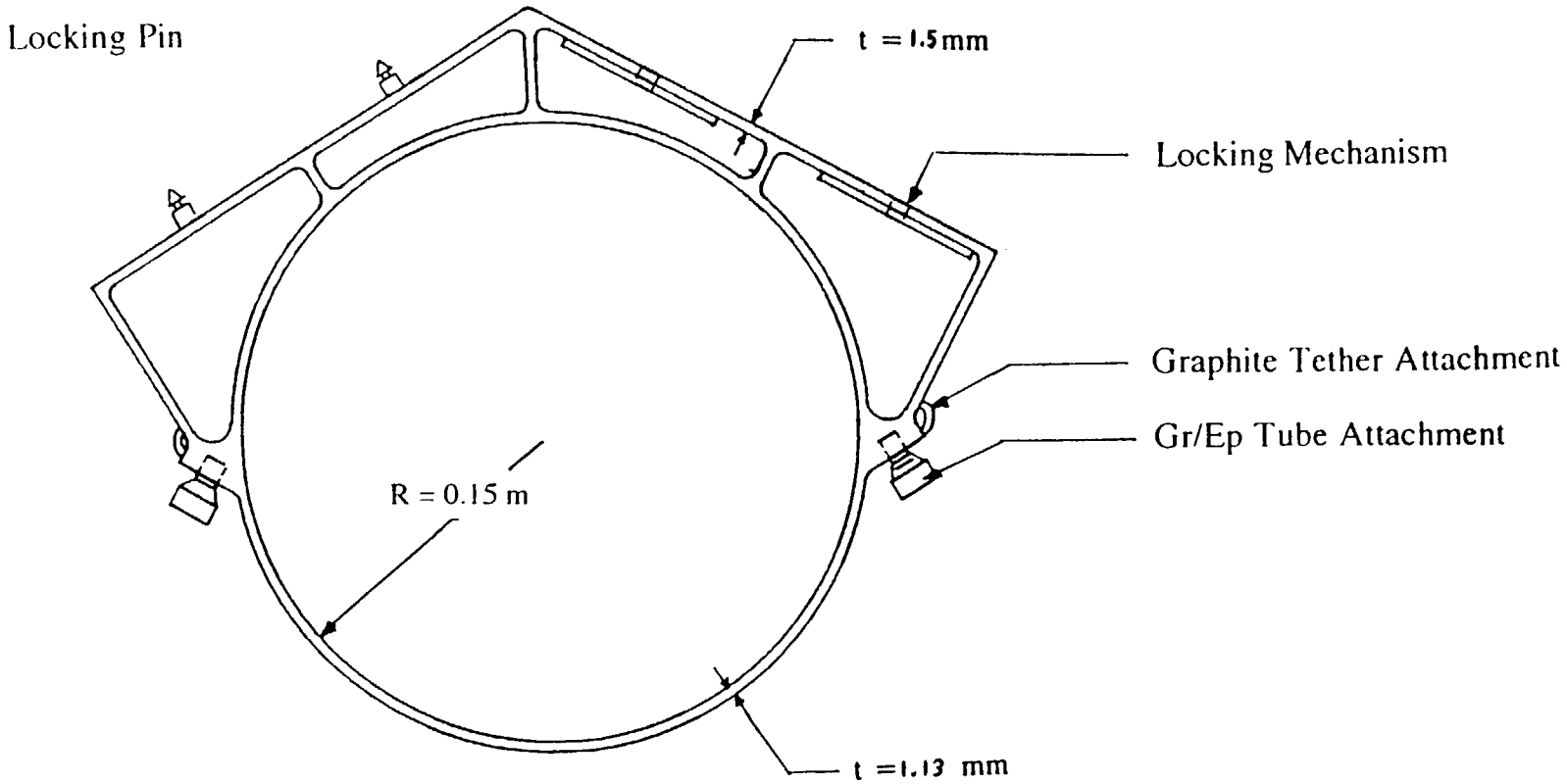

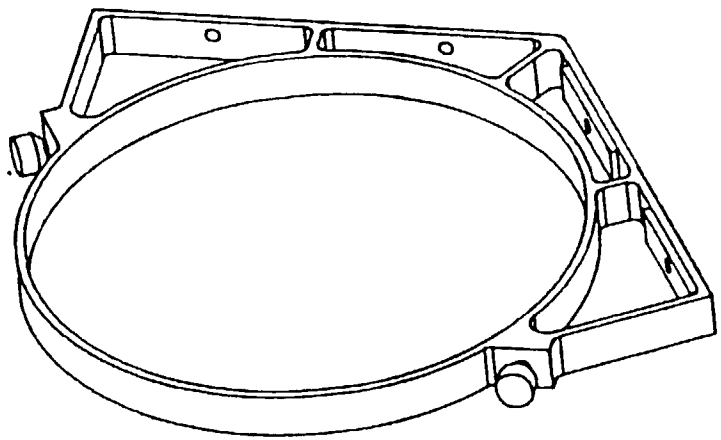

Figure 4-5 **Bottom Connector Joint and Member Attachment**

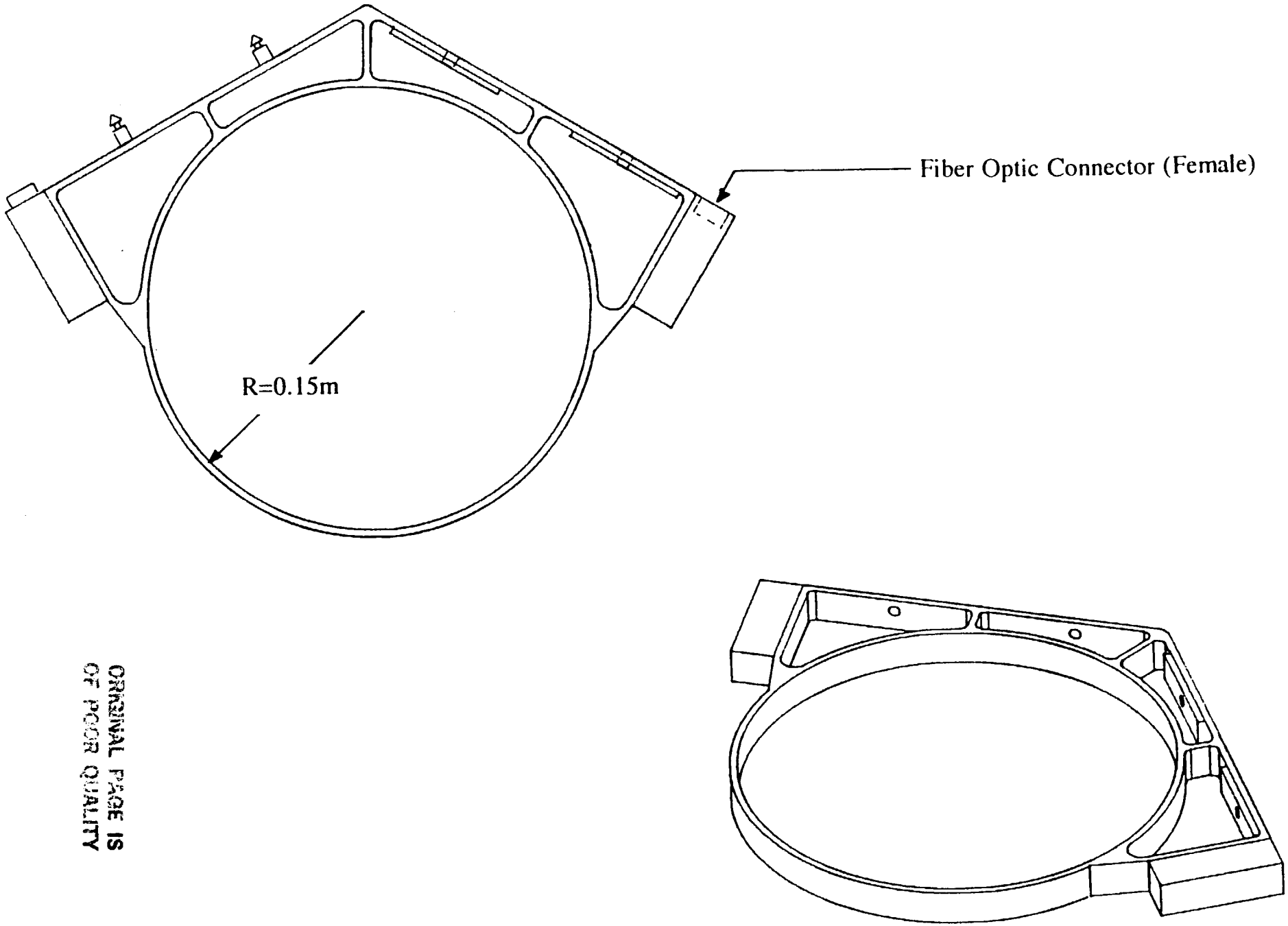

Figure 4-6 **Top Connector Joint and Fiber Optic Connector**

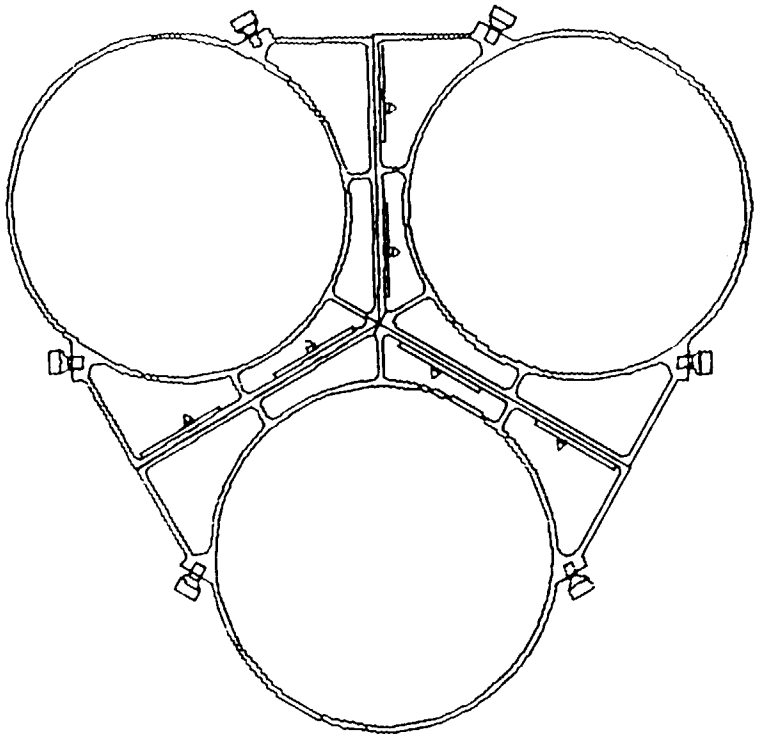

Bottom Connector Joint

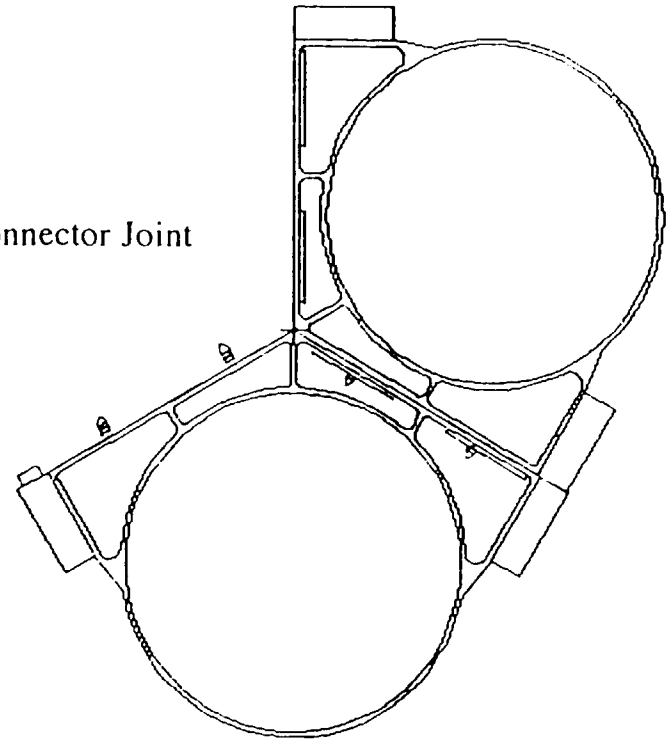

Top Connector Joint

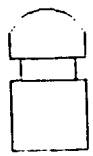

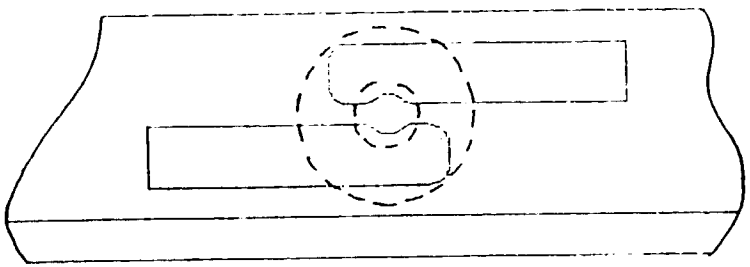

Locking Mechanism

Figure 4-7 **Assembly of Connector Joints and Locking Mechanisms**

Figure 4-8 **Spacecraft Bus and Adjoining Modules**

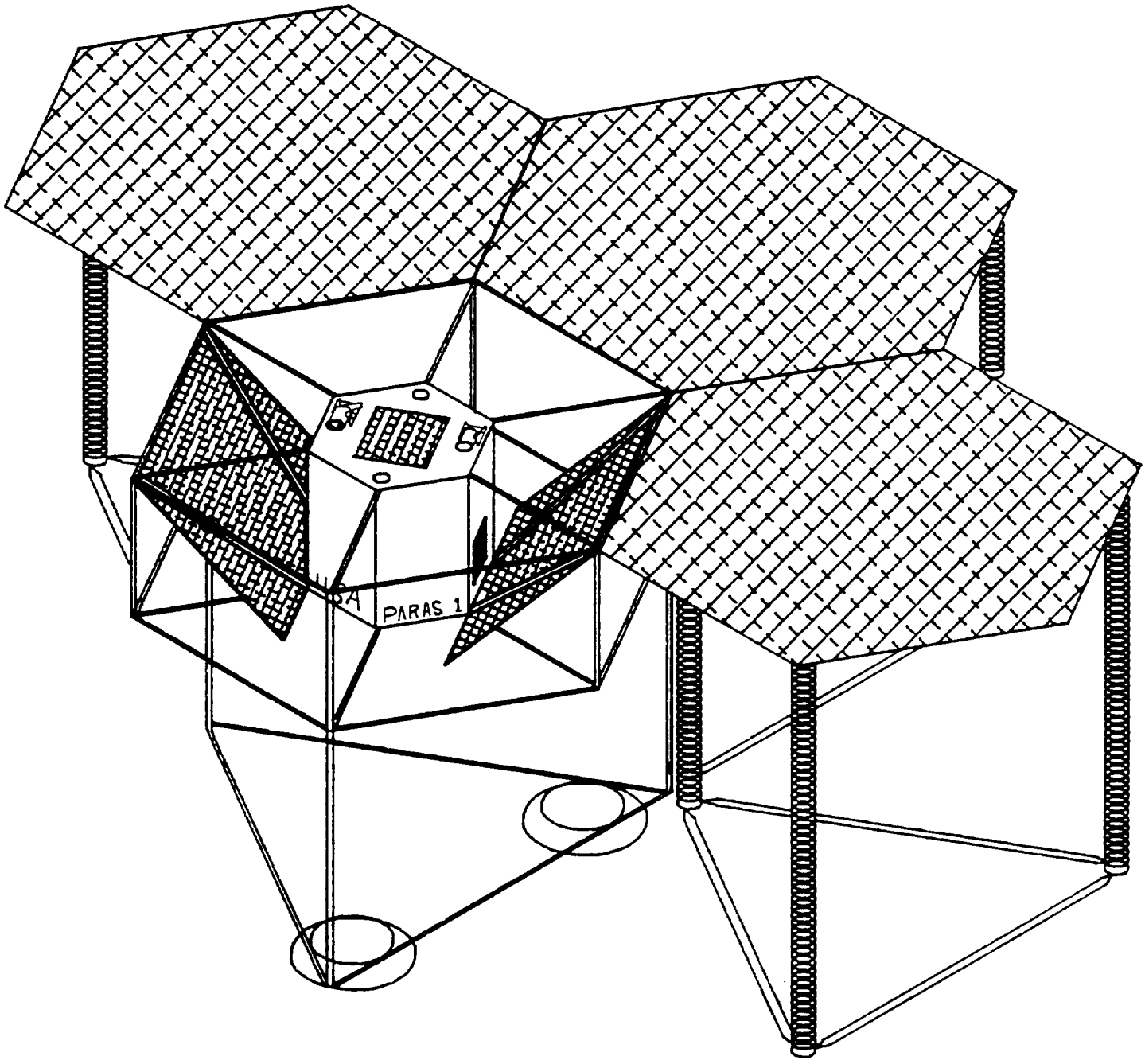

Housing for - Computer
- Communications Hardware
- Power Control
- Attitude Control

5.0 STATIONKEEPING, ATTITUDE DETERMINATION AND CONTROL

5.1 Requirements

The observatory will be subject to several forces that, if left unchecked, will alter the spacecrafts orbit and it's orientation with respect to the earth. Solar radiation pressure and the gravitational influences of the moon, sun and the oblateness of the earth will be the primary forces that the stationkeeping systems must compensate for. And the attitude control system will be needed to maintain the spacecrafts orientation under the torque caused by the solar pressure.

The propulsion system will be required to eliminate orbit perturbations on a periodic basis. The attitude control system must maintain the spacecraft orientation to an accuracy of 0.1 degree and will restrict angular drift about the observatory center of mass to 0.01 degrees/second. The position of the satellite will be maintained to an accuracy of 0.5 degrees in either latitude or longitude. Because thruster firings are likely to cause deformations and vibrations in the structure there can be no radio observations during station keeping operations. Consequently, to insure that the observatory mission is not interfered with the thruster firings must not exceed six hours per day and the number of days required for stationkeeping must be minimized. Such long thrust times are typical for low impulse electric thrusters (i.e. arcjets, resistojets, and ion thrusters.).

5.2 Stationkeeping

Solar and lunar gravity and the solar radiation pressure will increase the spacecrafts orbital inclination by about 0.95 degrees per year. Correcting this deviation, called North-South stationkeeping (NSSK), requires a change in velocity or, delta-v, of 48.4 m/s/yr (See Appendix 5.1.1).

For East-West stationkeeping (EWSK) the oblateness of the Earth and the solar radiation pressure dominate the disturbing forces. These cause the spacecraft to drift east or west of its designed Earth longitude. For traditional geostationary satellites the NSSK requirements are significantly larger than that for the EWSK. However, because the area-to-mass ratio of the PARAS is large (>0.8) the solar radiation pressure will have a much larger contribution to the orbital perturbations. Consequently, the daily EWSK maneuvers require a delta-v of 42.7 m/s/yr, very similar to the delta-v of the NSSK. Desaturation of the momentum wheels used to control spacecraft attitude (see sections 5.3 and 5.4) also adds a minute 1.35 m/s/yr delta-v to the propulsion requirements. These results, as well as the delta-v requirements for attitude control, are summarized in Table 5.1. (The derivation of the EWSK and the NWSK delta-v can be found in Appendix 5.1.1)

TABLE 5.1
Delta-V Requirements for Stationkeeping
10 Year Mission
NSSK -- 483.8 m/s
EWSK -- 427.1 m/s

Momentum Dumping
Roll -- 1.26 m/s
Pitch -- 0.09 m/s
Yaw -- ~0 m/s

The propulsion system was designed to consist of a cluster of thrusters located at each cardinal point of the PARAS satellite as shown in Figure 5-1. Since these points are so far apart they will be independent thruster modules, having their own fuel and power supply. They will be controlled by the computer in the central bus. The North and South thruster modules will control EWSK, roll and yaw, and the East and West thruster modules will control NSSK and pitch.

5.3 Propulsion System Candidates

Attitude control will be maintained by momentum wheels. Monopropellant (hydrazine) thrusters will perform roll and pitch momentum wheel desaturation. Hundreds of flight tests have proven their sturdiness. They are simple in design and inexpensive to fabricate. They generate very low thrust with little loss in Isp. For the small delta-v, they are the lightest system. Table 5.2 details the monopropellant thruster specifications and Figure 5-2 illustrates the tankage and thruster layout at each thruster module.

TABLE 5.2
The Monopropellant Hydrazine Thruster

Thrust= 0.05 N
Isp= 220 sec. (steady state operation)
Chamber Pressure= 100 psia
Mass Flow= 2.273x10-4 kg

The demands for the stationkeeping are more difficult to satisfy than that of the attitude control so several different configurations were considered. These included chemical rockets such as Hydrazine/NTO thruster and resistojets as well as electrical thrusters like the arcjet and the ion engine.

5.3.1 Chemical Rockets

Chemical rockets and resistojets exhibited promise in early evaluations of stationkeeping engines. The resistojet is an augmented catalytic thruster. Future projections indicate that it will achieve an Isp of 320 sec. and a thrust of 0.34 N which will require approximately 0.8 kW of power. A modern chemical rocket is the NTO/Hydrazine bipropellant thruster. It, like the resistojet, allows complete combustion without film cooling do to a iridium/rhenium coating on the chamber walls. A NTO/Hydrazine thruster could generate an Isp similar to the resistojet of 318 seconds. However, bipropellant thruster does not require the added electrical power of the resitojet and it produces a 22 N thrust, almost two orders of magnitude larger than the resistojet. This rocket design dropped the resistojet out of contention. Table 5.3

summarizes the propulsive characteristics of the bipropellant thruster, Table 5.4 details the mass estimate of the bipropellant propulsion system (option 1) and Table 5.5 gives the estimated maneuver schedule. Figures 5-3 and 5-4 illustrate the layout of tankage and thrusters for the Bipropellant design.

TABLE 5.3
The NTO/N2H4 Bipropellant Thruster

Thrust= 22N (5 lbf)
Isp= 318 sec.
Mixture Ratio= 1.1 (oxidizer/fuel)
Nozzle Area Ratio= 150:1
Chamber Pressure= ~120 psia
Mass Flow= 7.0544x10-3 kg

TABLE 5.4
Mass Analysis of Propulsion System, Option 1
Bipropellant Stationkeeping, Monopropellant Attitude Control

Mass (kg):	
Bipropellant Thrusters (16)	11.20
Monopropellant Thrusters (16)	6.00
Gimbals (30% of thruster mass), Bipropellant only	3.36
Support Structure (31% of thruster+gimbal mass)	6.38
Propellant Feed System	90.12
Housing Structure	4.69
Subtotal	121.75
Propellant:	
N2H4	2940.2
NTO	3217.6
Propellant Reserve (6% of propellant mass)	369.5
Subtotal	6527.3
Tankage:	
N2H4 (2.3% of propellant mass)	71.7
NTO (1.6% of propellant mass)	54.6
Subtotal	126.3
Pressurizing Gas (He):	
He	45.2
Tankage (240% He mass)	108.5
Subtotal	153.7
Structure for Tankage (4% of propellants+tanks+He mass)	272.3
TOTAL	7202.0
TOTAL (EQUAL SIZE MODULES)	7240.0

TABLE 5.5
Bipropellant Design (Option 1)
Average Maneuver Schedule

NSSK: One maneuver every 405 days. Rockets will thrust over four days for two hours each day (about apogee).
EWSK: One maneuver every two weeks. Rockets will thrust for fifteen minutes on a single day.
Momentum Dumping: Wheel controlling roll will need desaturation at least 300 times each year. The wheels controlling yaw may need only two or three desaturations over the mission life. The wheel controlling pitch will randomly need desaturation due to error in maintaining an ideal orientation toward earth. It is estimated that no more than 20 desaturations will be needed a year. Each desaturation will take 80 seconds of thrusting time.

5.3.2 Electrical Rocket Systems

All electrical power is generated on the PARAS by fixed solar arrays with batteries to store the energy. (see Section 8.) This design limits the effectiveness of arcjets and ion thrusters. Electric rocket systems, to be compared favorably to the chemical rockets, must generate propulsion module mass savings greater than the additional battery and array mass required to power them. Other power systems besides solar will be considered but the mass of any power generation system must be taken into account. In addition, the attitude control for PARAS is a monopropellant chemical system. Consequently, electrical rocket system will have to have a companion chemical rocket. This could potentially increase the cost and complexity of any electrical rocket configuration.

The candidate arcjet engine is a 5-kW class that generates 0.5 N thrust and 760 sec. Isp. For NSSK, two thrusters will, on average, fire every 405 days for 6 hours daily over a 52 day period. This will demand 10kW of power and 60kW-hr of energy. For EWSK, two engines will thrust for three hours daily over a three day period every two weeks. The maneuvers will require 10kW of power and 30 kW-hr energy. Radiothermal generators and silicon sulfur batteries will supply power for the arcjets (option 2). Overall, this system will save 3108 kgs over the bipropellant design. The characteristics of the arcjet are shown in Table 5.6, the mass analysis is shown in Table 5.7

and the estimated maneuver schedule is shown in Table 5.8. Figures 5-5 and 5-6 illustrate the tankage and thruster layout for this option.

TABLE 5.6
The Hydrazine Arcjet

Input to Power Processing Unit (PPU)= 5kW
Power Processor Efficiency= 95%
Thrust= 0.50 N
Isp= 760 sec
Mass Flow= 1.32x10-4 kg
Thruster Efficiency= 40%

TABLE 5.7
Mass Analysis of Propulsion System, (Option 2)
Arcjet Stationkeeping, Monopropellant Attitude Control

	(kg)
Thruster Package:	
Monopropellant Thrusters (16)	6.0
Arcjet Thrusters (16)	28.0
Gimbals (30% thrusters mass), Arcjet only	8.4
Support Structure (31% of thrusters+gimbals mass)	13.2
Power Processing Units (16)	169.0
Thermal Control (27 kg/KW)	151.2
Interface Modules (4)	47.6
Propellant Distribution System	45.0
Housing Structure	18.8
Subtotal	487.2
Propellant:	
N2H4	2441.2
Propellant Reserve (6% propellant mass)	146.5
Subtotal	2587.7
Tankage:	
N2H4 (2.3% propellant mass)	59.5
Subtotal	59.5
Pressurizing Gas (He):	
He	21.3
Tankage (240% He mass)	51.2
Subtotal	72.5
Structure for Tankage (4% propellants+tanks+He mass)	108.8
TOTAL	3316.0
ESTIMATED MASS FOR EQUAL SIZE TANKAGE:	3332.0
ESTIMATED POWER SYSTEM MASS (RTG w/ Batteries):	800.0
ESTIMATED TOTAL SYSTEM MASS:	4132.0
Mass savings over bipropellant system:	3108.0

TABLE 5.8
Arcjet Design (Option 2)
Average Maneuver Schedule

NSSK: One maneuver every 405 days. Over a 52.4 day period, thrusters will fire for six hours per day (three about apogee and three about perigee on days 379-431).

EWSK: One maneuver every two weeks. Over a three day period, thrusters will fire for three hours per day (ie. days 11-14).

Momentum Dumping: Same as bipropellant system

Because the firing times are enormous compared to the bipropellant design a second arcjet configuration was considered that was powered by a SP-100 nuclear reactor (option 3). This higher power source allows the number of primary thrusters that are firing to double. Although this system is heavier than option 2, it still is 2323 kg lighter than the bipropellant design. The mass analysis for option 3 and the estimated maneuver schedule are given in Tables 5.9 and 5.10 respectively. Figures 5-5 and 5-7 illustrate the tankage and thruster arrangement for this option.

TABLE 5.9

Mass Analysis of Propulsion System, Option 3
Arcjet Stationkeeping, Monopropellant Attitude Control
Overdrive Design -- Half the Thrusting Time of Option 2

	(kg)
Thruster Package:	
Monopropellant Thrusters (16)	6.0
Arcjet Thrusters (24)	42.0
Gimbals (30% thruster mass), Arcjet only	12.6
Support Structure (31% thrusters+gimbals mass)	18.8
Power Processing Units (24)	253.5
Thermal Control (27 kg/KW)	226.8
Interface Modules (4)	71.4
Propellant Distribution System	55.0
Housing Structure	27.5
Subtotal	713.6
Propellant:	
N2H4	2533.2
Propellant Reserve (6% propellant mass)	152.0
Subtotal	2685.2
Tankage:	
N2H4 (2.3% propellant mass)	61.8
Subtotal	61.8
Pressurizing Gas (He):	
He	22.1
Tankage (240% He mass)	53.0
Subtotal	75.1
Structure for Tankage (4% propellants+tanks+He mass)	112.9
TOTAL	3649.0
ESTIMATED MASS FOR EQUAL SIZE TANKAGE:	3667.0
ESTIMATED POWER SYSTEM MASS (10 kW SP-100, 16 W/kg):	1250.0
ESTIMATED TOTAL SYSTEM MASS:	4917.0
Mass savings over bipropellant system:	2323.0

TABLE 5.10

Arcjet Design (Option 3)
Average Maneuver Schedule

NSSK: One maneuver every 405 days. Over a 26.2 day period, thrusters will fire for six hours per day (three about apogee and three about perigee on days 392-418).

EWSK: One maneuver every two weeks. Over a two day period, thrusters will fire for two and a half hours per day (ie. days 13-14).

Momentum Dumping: Same as bipropellant system

Arcjets can share their pressure feed systems with the monopropellant attitude control thrusters maintaining simplicity. Over the satellites expected lifetime the arcjets will have to operate between 1415 and 2830 hours depending on the design. Current arcjets have demonstrated this endurance. Cycling between use of the primary and the redundant thruster could increase propulsion lifetime and will allow for the possibility of mission extension.

The xenon ion engine is a ring cusp design with small-hole-accelerator-grid (SHAG) optics using a two grid scheme. The competitiveness of the xenon ion thruster is handicapped by a low thrust-to-power ratio (~0.04 N/kW) for limited thrusting times. The average daily NSSK correction would require a six hour burn given a thrust of only 1.0 N. This is a thrusting time comparable to the low power arcjet design (option 2). The power and energy required would be 26.6 kW and 160 kW-hr, respectively. The electrical power system to support the ion thruster would require a SP-100 reactor and batteries having a mass of 1612 kg. The overall mass savings over the bipropellant design (option 1) would be 3038kg, 70 kg less than the arcjet design. The Ion Engine thruster specifications are given in Table 5.11 and the mass estimate and maneuver schedule are given in Tables 5.12 and 5.13 respectively. Figure 5-8 illustrates the tankage and thruster layout for this option.

TABLE 5.11
The Xenon Ion Thruster

Employs small-hole-accelerator-grid (SHAG) 2 grid optics
Input power to interface module= 6.653 kW
Power Processor Efficiency = 93%
Total Voltage= 1750 V
Beam Current= 4.623 A
Net-to-Total Voltage Ratio, R= 0.68
Thrust= 0.2501 N
Isp= 3846.5 sec.

TABLE 5.12
Mass Analysis of Propulsion System, (Option 4)
Ion Stationkeeping, Monopropellant Attitude Control

	(kg)
Thruster Package:	
Monopropellant Thrusters (16)	6.0
Ion Thrusters (24)	271.2
Gimbals (30% thruster mass), Ion Only	81.4
Support Structure (31% thrusters+gimbals mass)	111.2
Power Processing Units (24)	850.5
Thermal Control (27 kg/KW)	317.0
Interface Modules (4)	117.4
Propellant Distribution System	88.1
Housing Structure	73.8
Subtotal	1917.4
Propellant:	
N2H4	13.2
Xe	533.6
Propellant Reserve (6% propellant mass)	32.8
Subtotal	579.6
Tankage:	
N2H4 (2.31% propellant, helium mass)	0.4
Xe (4% propellant mass)	21.4
Subtotal	21.8
Pressurizing Gas (He):	
He	0.2
Tankage (blowdown system, no separate helium tank)	0.0
Subtotal	0.2
Structure for Tankage (4% propellants+tanks+He mass)	24.1
TOTAL	2543.0
ESTIMATED MASS FOR EQUAL SIZE TANKAGE:	2592.0
ESTIMATED POWER SYSTEM MASS (13.3 kW SP-100, 16.5 W/kg):	1612.0
ESTIMATED TOTAL SYSTEM MASS:	4204.0
Mass savings over bipropellant system:	3036.0

TABLE 5.13
Ion Design (Option 4)
Average Maneuver Schedule

NSSK: Same as arcjet; Table 5.8
EWSK: Same as arcjet; Table 5.8
Momentum Dumping: Same as bipropellant; Table 5.5

The ion thruster would increase the complexity and cost of the propulsion system because a companion chemical system, using a different propellent, would have to be used for the monopropellant attitude control. To reduce the maneuver time to a level similar to that of option 3 could be done by doubling the number of operating thrusters. However, this would result in a significant mass penalty.

The advantages of the xenon system are that the ion thruster has a much longer life than either the arcjet or the bipropellant thrusters (up to 30,000 hours). And the ion engine design can be modified to allow the capability of performing the orbital transfer to GEO. This can be done by adding a propellant mass of 7000 kg. The other two designs would require between 40,000 kg (arcjet) and 100,000 kg (bipropellant) of extra propellant mass to do the job.

However, it is assumed that by 2010 OTVs of proper size will be available to ferry the spacecraft to its proper orbit. It also seems reasonable that the lifetimes of the bipropellant system and the arcjet should be adequate for this mission.

5.3.3 Propulsion System Selection

A comparison of the masses and the maneuver times of the four contenders indicates that the best choice for the

PARAS propulsion system is the Hydrazine Arcjet design powered by the SP-100 nuclear reactor.

5.4 Propulsion System Support and Configuration

A common regulated pressure feed system employing helium supplies the propellant to the engine, as shown in Figure 5-3. The helium, stored in a carbon overwrapped (Gr/Ep),titanium lined tank at 4000 psia and 264 K, keeps the propellant tanks pressurized at 220 psia utilizing an elastomeric diaphragm. The propellant tanks, carbon overwrapped stainless steel (304L cryofromed), maintain a temperature of 294 K. The tank arrangement is also shown in Figure 5-3. Three isolation valves lie between the pressure feed system and each rocket engine as required by space shuttle safety specifications. A resupply interface, attached to each module, allows for refueling and mission extension. This unit will be a NASA standard part resembling those made under contract by MOOG.

The propulsion system is separated into four modules of equal size to lower the cost of fabrication and launch. Table 5.14 shows the composition of the arcjet system and Figures 5-5, 5-7 and 5-9 show the layout of the system. Each module rests at a compass point on the dish. The packages on the east and west compass points perform NSSK functions and pitch control. The packages on the north and south compass points perform EWSK and roll and yaw control. These assignments are shown in Figure 5-1.

TABLE 5.14
Thruster Module Breakdown
Arcjet/Monopropellant System, Option 3

Dish Compass Point Packages (4)
Each module will have the same size components (Tanks,etc.) but contain different propellant masses.

E-W Compass Points: 4 Arcjet Thrusters (4 firing N-S)
4 Monopropellant Thrusters (firing radially)

* Propellant (Mass of Propellant, Volume of Tank)
  N2H4 (710 kg, 0.710 m3)
  He (5.9 kg, 0.133 m3)
* Total Weight: 955 kg

N-S Compass Points: 4 Arcjet Thrusters (4 firing E-W)
4 Monopropellant Thrusters (firing radially)

* Propellant (Mass of Propellant, Volume of Tank)
  N2H4 (634 kg, 0.710 m3)
  He (5.9 kg, 0.133 m3)
* Total Mass: 879 kg

5.5 Attitude Determination

The observatory must keep its back directed toward the earth to avoid radio interference and must be capable of determining its position in inertial space during an observation. The fixed head star trackers (FHST), the primary sensors, routinely determine the observatories position in inertial space with a high accuracy, 20 arc-seconds. During observations, the FHST's increase the frequency of their measurement to assure stable pointing.

The inertial measurement unit (IMU) assists the FHST in

self tracking. It calibrates itself with data from the star tracker. It then observes the position and velocity of the spacecraft with gyros and accelerometers periodically until receiving new data from the FHST. It then recalibrates itself and continues. The IMU data intake and output become more rapid during maneuvers to check for off-line thrusting, misfirings, and thrust generated torques.

The horizon sensors (acc.= 0.1 degrees) act mostly as back-up. They operate with long periods (@10 min.) between data acquisitions. The CD&H system uses the horizon sensor information to make sure the observatory faces away from the earth and to crudely check the other sensors.

The radio telescope, powered by batteries absorbing the energy of fixed solar arrays, must be able to evaluate the times of eclipse and peak power input. This information does not have to be precise, therefore, coarse sun sensors (acc.= 0.5 deg.) can be used. They will determine the position of the sun and the intensity of its light. Both the horizon and sun sensors will compensate for a failed FHST or IMU.

5.6 ATTITUDE CONTROL

(Appendix 5.2 contains the method of calculating the environmental torques.) The solar radiation torques (pitch and roll torques) dominate the dynamic behavior of the spacecraft. The average moment impulses they impose on the spacecraft (I_{roll}= 490 Nms, I_{pitch}= 475 Nms per half orbit)

loom three orders of magnitude larger than the corresponding gravity gradient imparted moment impulses and the gravity gradient impulse about yaw (I_{yaw}= 1 Nms). Order of magnitude values of the torques reflect this effect (T_{SR}= 0.0124 Nm, T_E= 3.3 x 10^{-4} Nm, T_S= 4.8 x 10^{-6}, T_M= 1.3 x 10^{-5}).

Thus, the sun dictates the actions of the roll and pitch moment impulses. The roll impulse continues growth from orbit to orbit with a period of one half year before reversing direction. However, the pitch impulse changes sign every half orbit and nearly cancels itself out over the whole cycle, retaining a small secular increase of ~5 Nms/orbit. The yaw impulse continually builds upon itself, like the roll, from orbit to orbit but at a very slow pace, ~0.5 Nms/orbit. The yaw moment can be considered a negligible effect with little impact on precision. The residual growth of the pitch can also be ignored. The upper limit of moment impulse the spacecraft will experience in one orbit is 1400 Nms.

Momentum wheels will exercise primary attitude control. The assembly contains four wheels arranged tetrahedrally to offer control on all three axes with a safe degree of redundancy. The assembly can generate a maximum torque of 1.0 N-m (to 3200 rpm) or 0.5 N-m (to 6400 rpm). These values provide a factor of safety that allows counteraction with anomalous magnetic torques caused by violent solar

flare activity. Furthermore, the assembly can store 700 N-m-s of angular momentum.

The roll moment impulse growth will cause the wheels to saturate every one half to two orbits. The chemical thrusters will routinely perform a momentum dump at the completion of an orbit or when saturation occurs. The engines can deliver torques of 3.75 Nm or 7.5 Nm with pulse widths as small as 0.05 seconds; desaturation should require no more than 80 seconds firing time. The thrusters will act as a backup attitude device should the momentum wheels fail or unexpectedly shutdown because of over-speeding or over-heating. Thrusters will perform high angular rate maneuvers generating moments. Table 5.15 enumerates the the attitude determination systems, control systems and thruster assignments..

TABLE 5.15

Attitude Determination and Control Subsystem

Sun Sensors (4)
- Field of View: 64 deg. x 64 deg.
- Accuracy: 0.5 deg.
- Mass: 0.3 kg
- Power: 0 W (Self-Powered)

Fixed Head Star Tracker (2)
- Field of View: 8 deg. x 8 deg.
- Accuracy: 20 arc-sec.
- Brightness Range: +5.7 to +2.0 visual magnitude
- Mass: 8.0 kg
- Power: 18 W

Inertial Measurement Unit
- Gyro Drift Rate: 0.003 deg./hr
- Mass: 16.0 kg
- Power: 63 W

Fixed Head Horizon Sensors (2)
- Field of View: 20 deg. x 20 deg.
- Accuracy: 0.1 deg.
- Mass: 3.5 kg
- Power: 5.0 W

Momentum Wheel Assembly
- 4 Momentum Wheels arranged tetrahedrally
- Maximum torque: 1.0 N-m to 3200 rpm
  0.5 N-m to 6000 rpm
- Maximum Angular Momentum: 600 N-m-s at 6000 rpm
- Mass: 100 kg
- Power: 495 W (peak)

Thrusters
- Pitch control/momentum unloading is performed by thruster banks 1 and 3 on the E-W compass point packages.
- Roll control/momentum unloading is performed by thruster banks 1 and 3 on the N-S compass point packages.
- Yaw control/momentum dumping is performed by thruster banks 2 and 4 on the E-W compass point packages.

5.7 Power System Comparison

Tables 5.16 and 5.17 compare the options for power systems considered for the thruster modules.

TABLE 5.16
Power System Options for Electric Thrusters

Solar Array:
- Gallium Arsenide Cells
- Efficiency= 22%
- Specific Mass= 44 W/kg
- Advantages:
  - High specific mass
  - Proven technology
  - Sizeable for any mission
  - No environmental impact study needed to launch and assemble
- Disadvantages:
  - Solar array may collect energy for only half an orbit and the power the array produces is a sinusoidal function with time. (i.e. Energy= Maximum Power Generation Capability of Solar Array *12 hrs. * 0.663 [root mean square of a sinusoid])
  - Arrays will require a very large surface area
  - Arrays will degrade slightly over the ten year mission
  - Arrays have a moderate resistance to radiation and micrometeoroid impact damage
  - Because power generation is not continuous, the arrays must be coupled with batteries.

Radioisotope Thermoelectric Generators:
- 625 Watt MOD Series (SiGe + GaP Multiple Thermoelectric couples employing radiative coupling)
- Specific mass= 10 W/kg
- Weight per generator= 37.5 kg
- Advantages:
  - Compact (low volume)
  - Reliable continuous power generation for 10+ years without significant degradation
  - Suffers little from radiation or micrometeor impact damage
- Disadvantages:
  - **Only useful for <10 kW missions**
  - Environmental impact study needed for launch and space assembly
  - Very expensive (about $16,000 per watt)
  - Must be placed outside the angular range of the observatory surface (i.e. in the plane of the dish) to eliminate interference from radiation emissions

Nuclear Reactors:
SP-100 series (10kW - 100kW)
Specific mass= 16.0-30.0 W/kg (16.5 at 13kW)
Advantages:
- Compact (low volume)
- Reliable continuous power generation for mission life without significant degradation
- Suffers little from radiation or micrometeor impact damage
- Lowest cost, $800/W

Disadvantages:
- Massive
- Only useful for >10 kW missions
- Environmental impact study needed for launch and space assembly
- Must lie in the plane of the dish pointed away from the spacecraft to eliminate radiation impact on observations. This will increase the moments of inertia more than other systems.

Batteries:
Sodium Sulfur
Specific mass= 210 kW-hr/kg
Depth of Discharge= 80%
Advantages:
- Compact energy storage
- Thermal range eliminates need for radiators
- High specific mass

Disadvantages:
- Under development

TABLE 5.17
Chosen Power Configurations for Electric Engines

Arcjet Engines (option 2):
* Each compass point propulsion package has its own power module
* E-W compass points:
  - 625 W MOD RTG (62.5)
  - 16.4 kW-hr (13.1 kW-hr available) of sodium sulfur battery storage (78.125 kg)
* **N-S compass points:**
  - Two 625 W MOD RTG's (125 kg)
  - 28.1 kW-hr (22.50 kW-hr available) of sodium sulfur battery storage (134.0 kg)
* Total mass of power system: 799.25 kg

Arcjet Engines (Option 3):
* Two 13.1 kW SP-100 Nuclear Reactors. On sits above the North compass point propulsion package and one sits below the South compass point package. 50 A cables link the North reactor to the East compass point

package and the South reactor to the West compass point package. The reactors allow two clusters of two arcjet engines to fire at any one time. During periods when EWSK and NSSK must both be performed, EWSK firings will follow the NSSK firing (i.e. arcjet engines will be firing for a total of nine hours on these days).

* Total mass of power system: 1250 kg.

Ion Engines (Option 4):

* Two 13.1 kW SP-100 Nuclear Reactors. On sits above the North compass point propulsion package and one sits below the South compass point package. 50 A cables link the North reactor to the East compass point package and the South reactor to the West compass point package. The reactors allow two clusters of ion engines (two engines per cluster) to fire at any one time. During periods when EWSK and NSSK must both be performed, EWSK firings will follow the NSSK firing (i.e. ion engines will be firing for a total of nine hours on these days).
* Total mass of power system: 1612 kg.

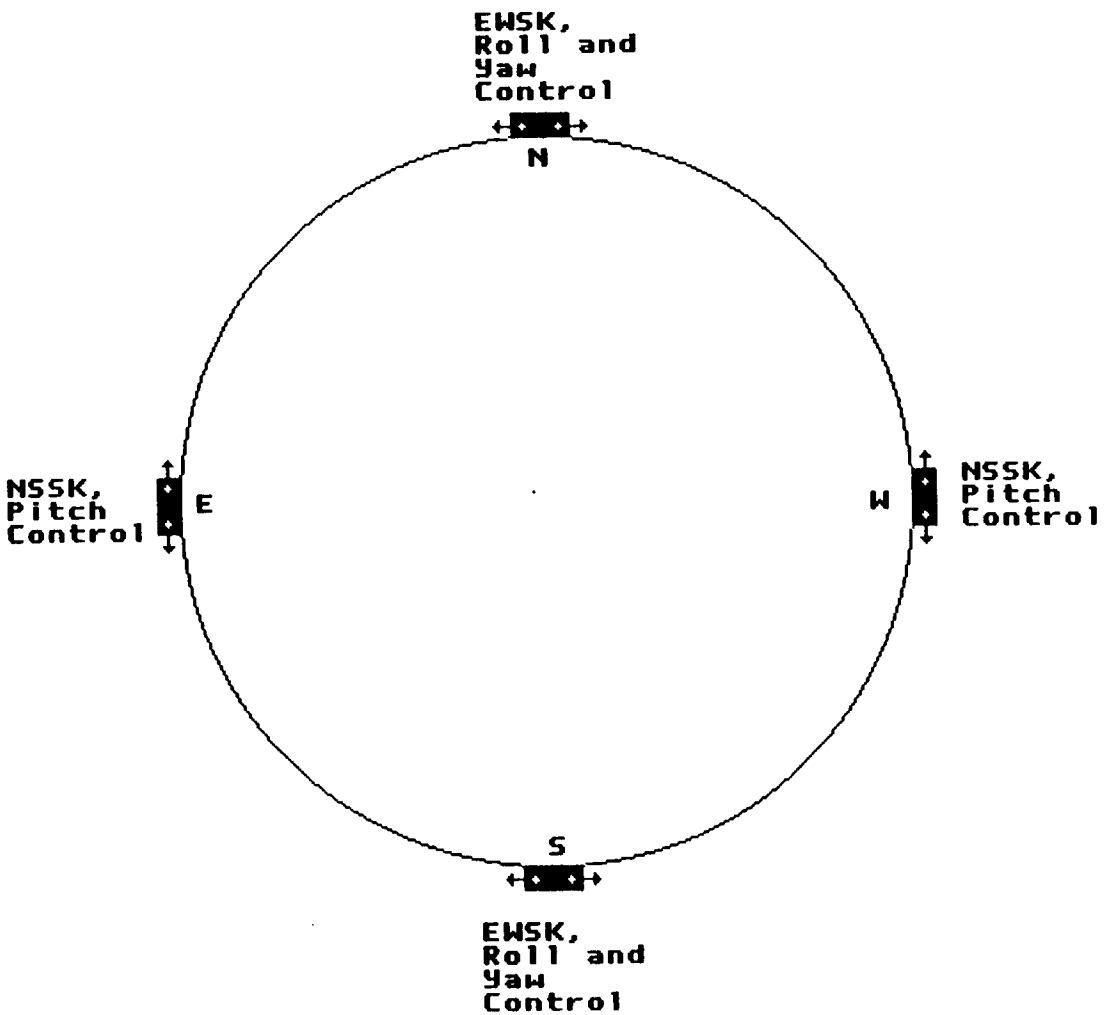

Figure 5-1 **Thruster Assignments**

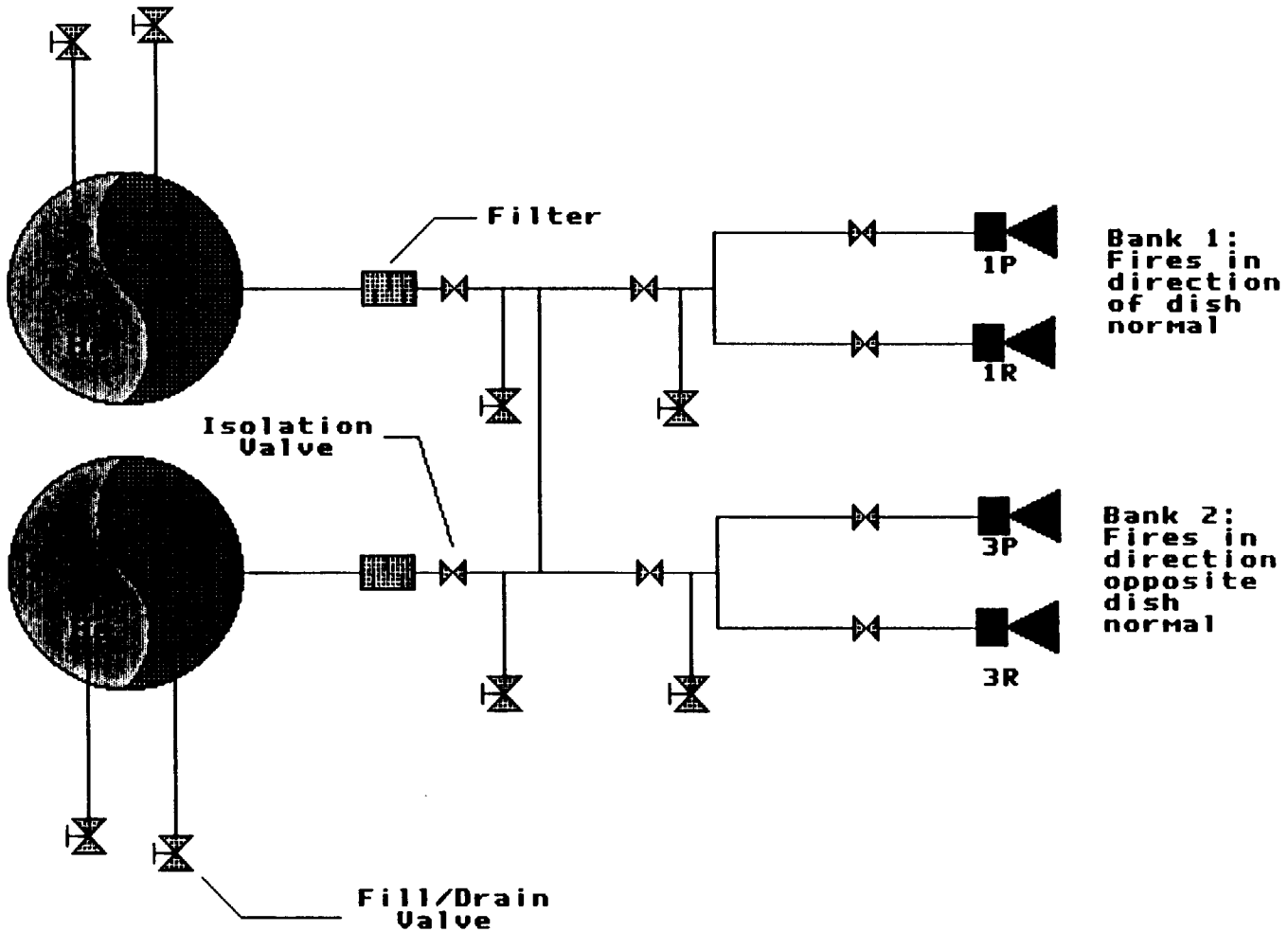

Figure 5-2 **Blowdown Propellant System**

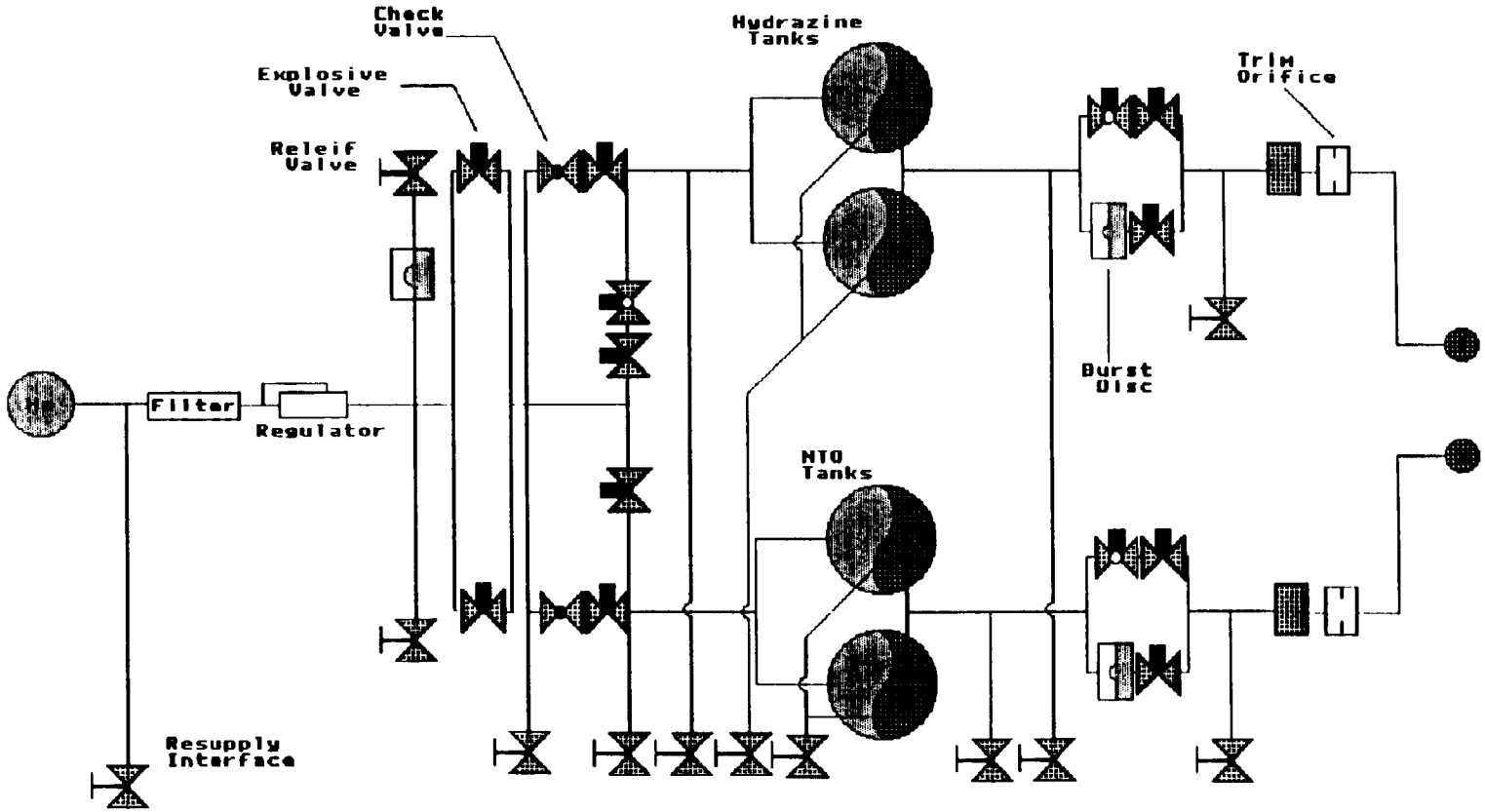

Figure 5-3 **Basic Pressure Feed System and Tankage (Bipropellant Option)**

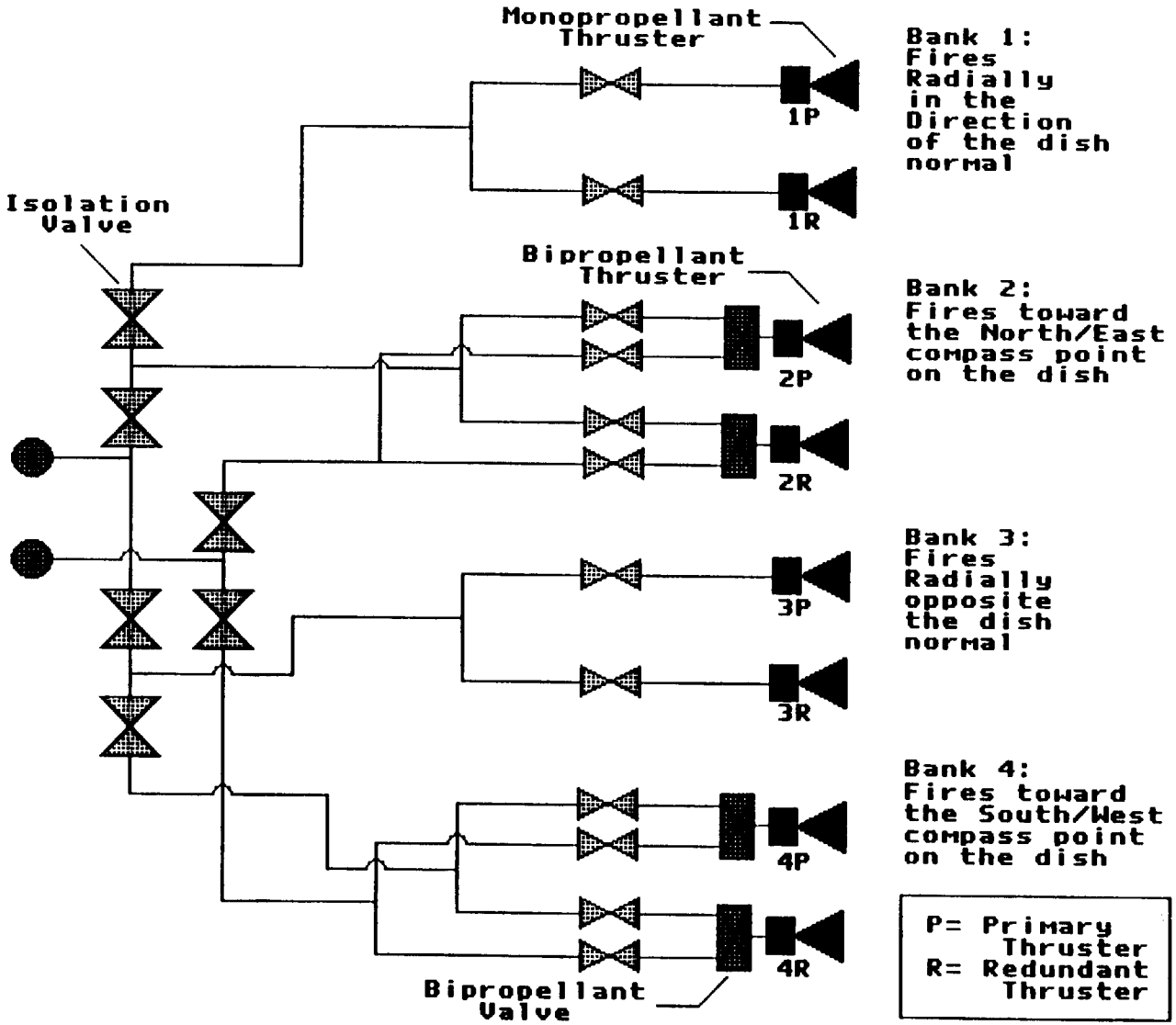

Figure 5-4 **N-S/E-W Compass Point Packages (Bipropellant Option)**

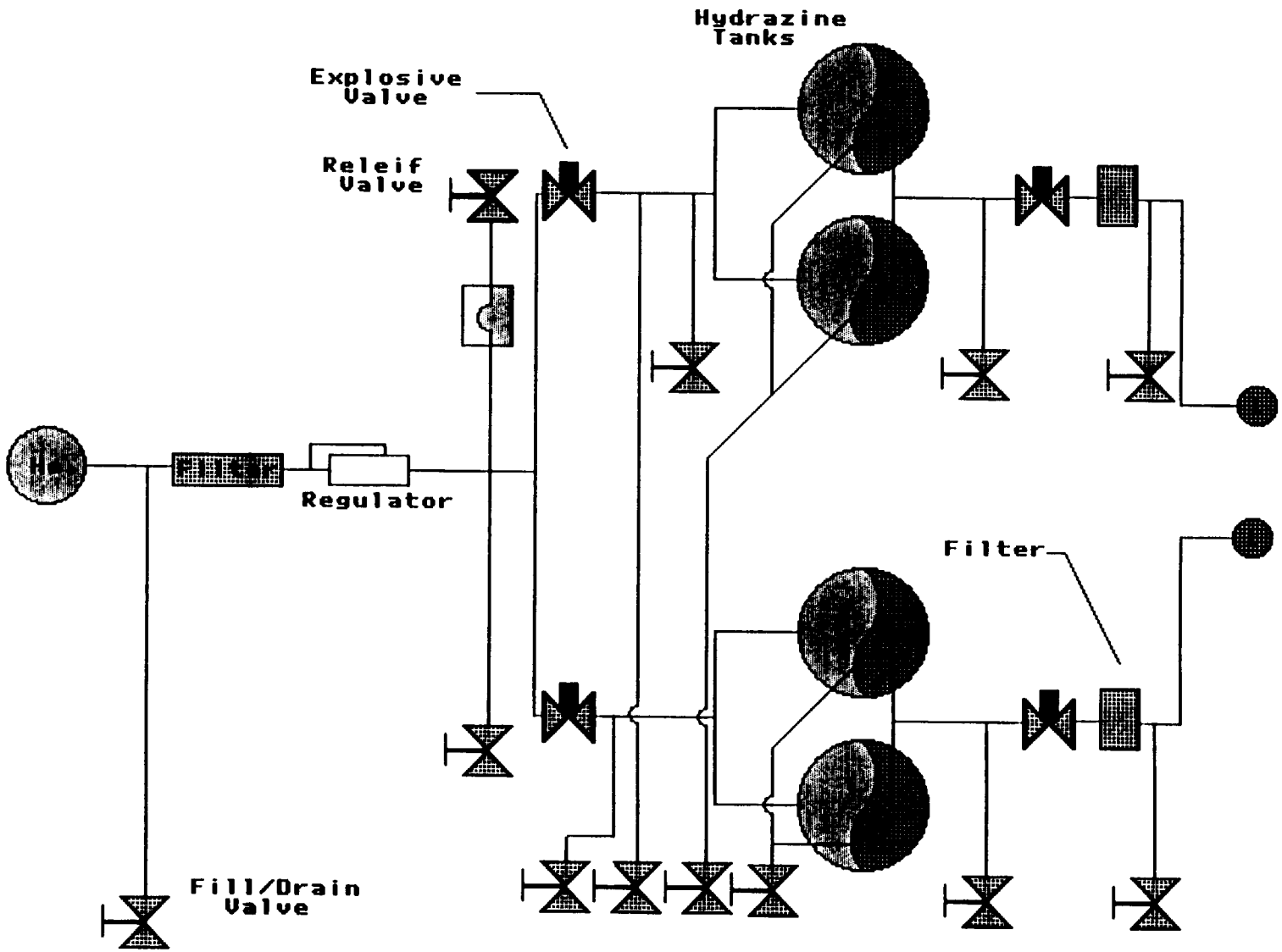

Figure 5-5 **Basic Pressure Feed System and Tankage (Arcjet Option)**

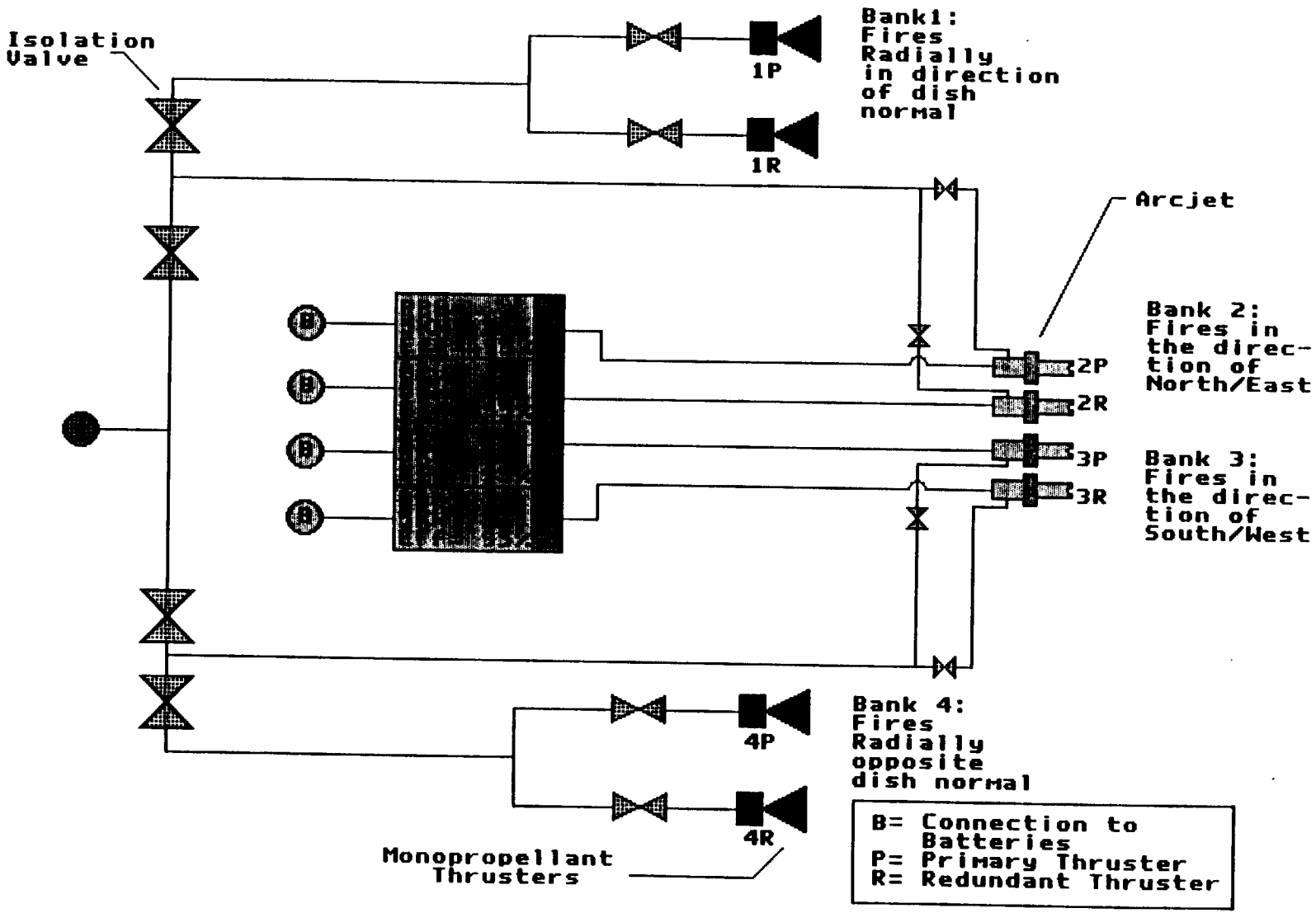

Figure 5-6 **N-S/E-W Compass Point Packages (Option 2)**

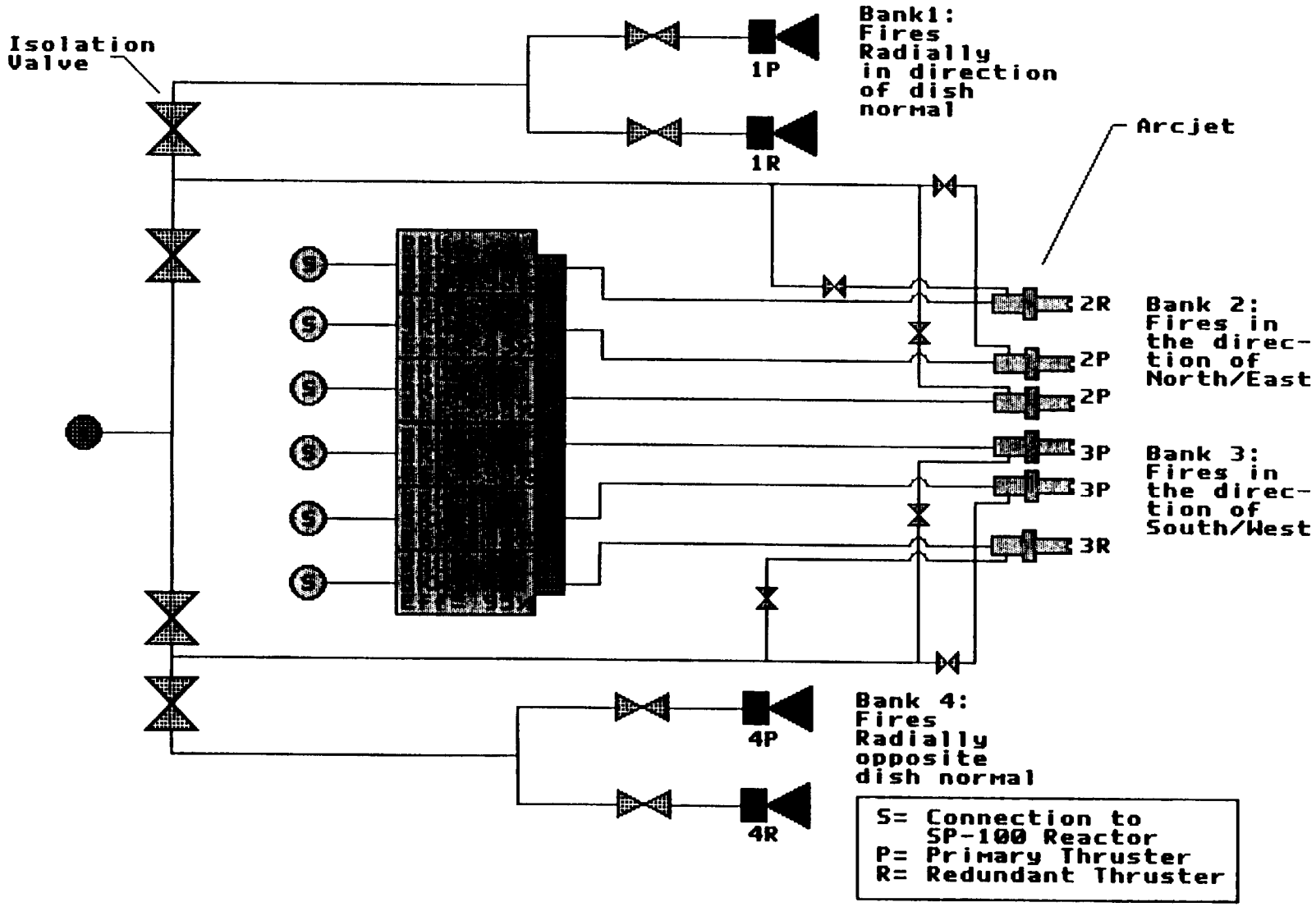

Figure 5-7 **N-S/E-W Compass Point Packages (Option 3)**

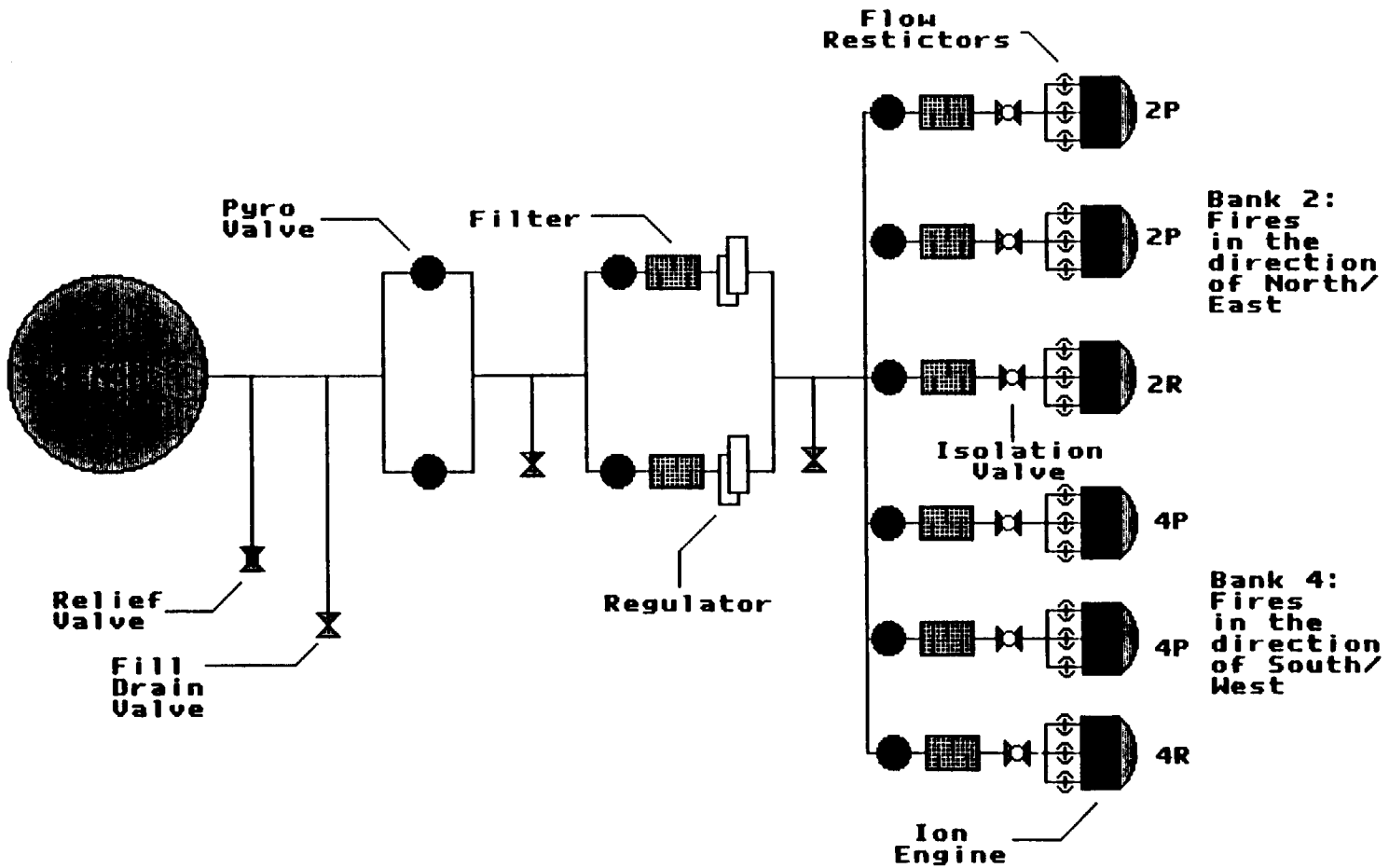

Figure 5-8 **Propellant Feed for Xenon Ion Engines**

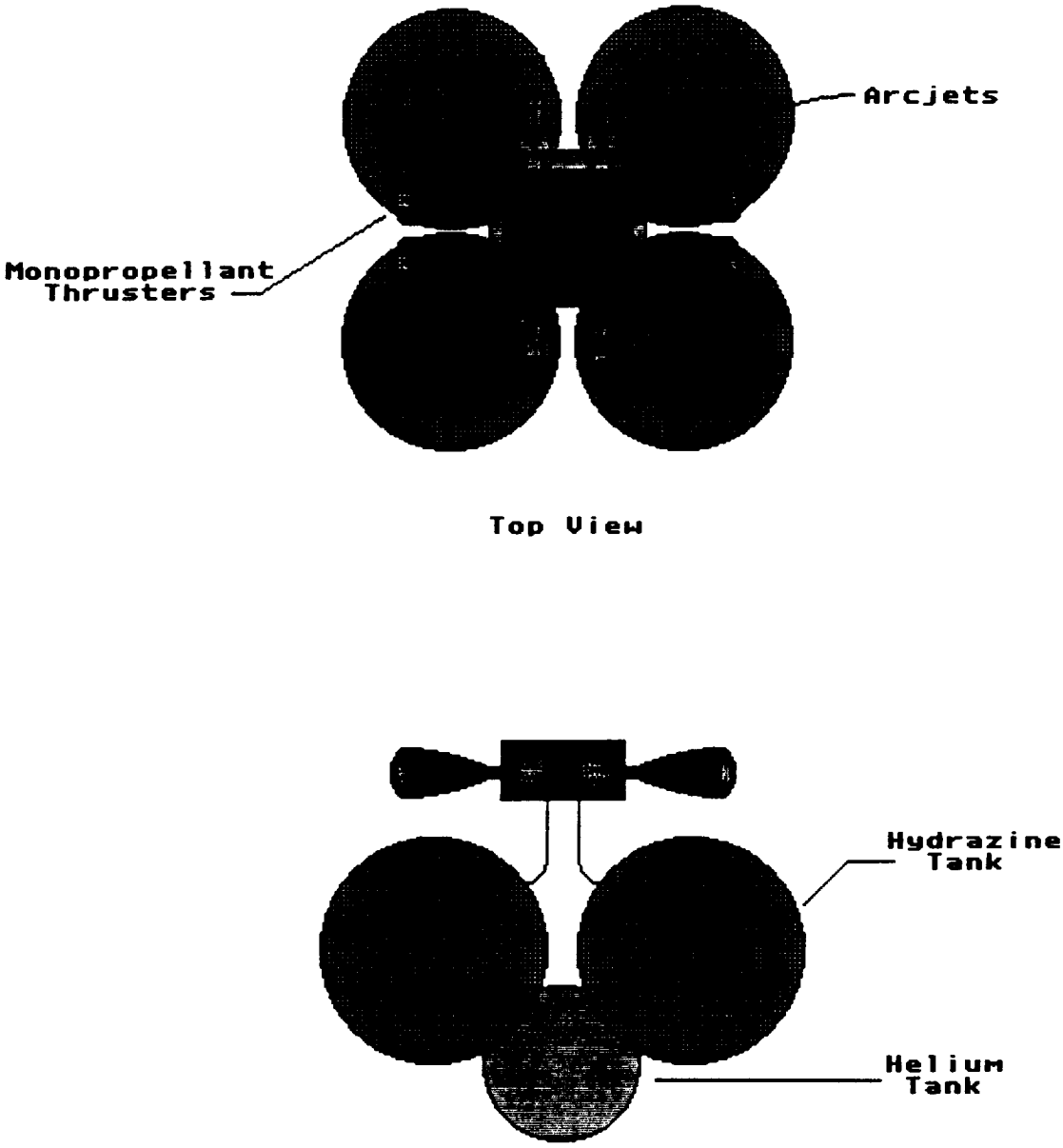

Figure 5-9 **Thruster/Tank Orientation**

6.0 Structural Analysis

To properly size the members that will be used to build the observatory platform there must be a understanding of the largest deflection and the largest stress that will be allowed in the structure. For the observatory the largest deflection permitted at the edge of the dish is 3 cm during periods of operation. The primary source of load during observation periods would be the solar radiation pressure. A larger deflection than 3 cm would degrade the accuracy of the observations. The platform must also be strong enough so that it does not deform plastically when it is subjected to thruster loads or loads resulting from a orbital transfer.

6.1 Preliminary Design

For the early conceptual design a mathematical formula was used. This theoretical formula,shown in appendix 6.1, could give values for moment, shear, deflection and slope for a circular, homogeneous plate under uniform loading, supported in the center. This formula generated values that were used to estimate the maximum levels of stress that the different members of the truss might encounter. A distributed load of 0.01 N/m2 was used in the formula. This was an arbitrary load of an order of magnitude similar to predicted thruster loads. The values generated for this case are shown below in table 6.1.

TABLE 6.1
Maximum Loads For Member Types

Maximum axial load in inflatable tubes = 9.36 N
Maximum axial load in Gr/Ep tubes = 14.7 N
Maximum tensile load in tension wires = 7.68 N

These values were used in addition to the constraint that the maximum allowable deflection at the perimeter was 3 cm. These constraints were used to do the preliminary sizing of the structural members.

6.2 Finite Element Static Analysis

For a more detailed analysis a finite element model was needed. Because of the complex nature of the truss and the high number of members a complete and exact model would have required very large computer calculation times. To reduce this run time it was necessary to simplify the structure and reduce it's size, and at the same time retain the accuracy of the solution.

6.2.1 Model Development

The first way to reduce the model was to take advantage of the symmetry of the structure. Using node restraints to simulate the presence of additional structure it was possible to model only a quarter of the observatory dish. This quarter model is shown in Figure 6-1. The nodes positioned along the X-axis are restrained from motion in the Y direction and from rotation about the X-axis. Similarly the nodes positioned along the Y-axis are restrained from motion in the X direction and from rotation about

the Y-axis. To fix the model the nodes at the position of the bus are restrained in all six modes of motion.

The actual elements of the module were represented using beam, plate and node fastener elements. The three inflatable tubes were combined into a single beam with the moments of inertia and area of the three tubes acting in tandem. Because of the nature of this beam it was assumed to have no torsional stiffness. The graphite/epoxy tubes were modeled as beams and the tension wires were modeled with node fasteners. The observatory panels were represented using a single triangular plate. Because of the difference in shape between the hexagon and the triangle there is likely to be some change in strength between the two representations. To determine the exactly how much the stiffness of the plate was effected two small example models were constructed. The first was a hexagonal plate composed of 88 plate elements. The second was a triangular plate made of a single plate, as used in the full scale model. These two models are shown in Figure 6-2. From the results of the finite element analysis of these two panel representations it was concluded that the single triangular plate had to be reduced in thickness by 20% to accurately represent the stiffness of the hexagonal plate. Consequently, all the triangular panel that make up the modules on the dish are given the thickness of 0.02 meters instead of 0.025 meters.

The stresses of the entire structure were analyzed using a factor of safety of 2.0 However, the graphite epoxy tubes and the inflatable members were deemed more likely to fail in

buckling than in axial yield. Euler's formula was used to determine the maximum axial load each type of member could take. These values were, including a 2.0 factor of safety, 211.9 N for the Gr/Ep tubes and 19,330 N for the inflatable tubes. Axial loads above these values were not acceptable. The panel was also most likely to fail in buckling. Again using Euler's formula and a factor of safety of 2 the maximum value for a compressive axial load on the plate is 816.7 N. All of these values are conservative. Not only because of the factor of safety but also because the assumption that the members were free to rotate at their ends. However, all of the members will have some rotational restraint at their ends that will provide additional protection against buckling. The only remaining structural member is the graphite/Teflon cables. These tethers can only fail in tension and the corresponding maximum load is 3463 N.

6.2.2 Model Load Conditions

With the maximum loads for each member type determined then it was possible to proceed with the various load cases that the observatory may be subjected to. Five load cases were selected as worth investigating. Each load case involves some form of load wether it be environmental or system related. These loads will result in an acceleration of the spacecraft and consequently an opposing inertial force. Example calculation of the inertial loads and the mass distribution used are shown in appendix 6.2.

The first load case is a solar pressure load of 9.6E-6 N/m2. A 80% reflectivity and a 0 angle of incidence is assumed for the

observatory surface. The maximum deflection permitted under this load case is 3 cm at the perimeter. To provide the maximum deflection the worst case scenario is when all the fuel tanks on the perimeter are empty.

The second load case is for a thruster firing in the direction perpendicular to the Y direction, or N-S. At three locations on the observatory there are two 22 N thrusters operating. This results in a total impulse of 132 N. The worst case for this load case would have all the fuel tanks empty for maximum acceleration on the structure. The third load case was similar to the second except now the thrusters were firing perpendicular to the X direction. The difference between these two cases is in the orientation of the truss with respect to the loads. The triangular truss at the bottom surface of the observatory is more capable of handling loads perpendicular to the X direction than the Y.

The fourth load case is for a thruster firing in the direction parallel to the Z direction. Two thrusters are firing at four locations on the perimeter of the observatory. This results in a total impulse of 176 N. The worst case would dictate that the fuel tanks be empty for this load case.

The final load case is for an orbital transfer using 500 N of thrust applied at the bus location. The worst case for this load case is to assume that the fuel tanks are filled. This will result in the maximum bending of the structure.

These separate load cases are shown in table 6.2 and the resulting member loads are shown in table 6.3.

Table 6.2
Load Types In Each Load Case

Load Case #	Distributed Plate Load N/m2	Thruster Point Load East-West N	Thruster Point Load North-South N	Load Direction	Fuel Condition
1	-3.45E-5	3.75E-3	7.11E-4	Z	empty
2	1.303E-2	-21.86	-42.505	X	empty
3	1.303E-2	-21.86	-42.505	Y	empty
4	-1.74E-2	21.81	21.00	Z	empty
5	-4.11E-2	-3.15	-20.64	Z	full

Table 6.3
Maximum Loads In Member Type

Load Case #	Inflatable Axial N	Inflatable Shear N	Gr/Ep Axial N	Gr/Ep Shear N	Panel Axial N	Panel Shear N	Tether Axial N	Deflect. max m
1	0.00325	0.021	0.0434	0.0185	ng	ng	.0054	0.0061
2	0.8299	13.65	24.43	1.730	31.00	10.96	27.04	0.0288
3	1.442	23.71	23.05	3.033	16.52	16.68	33.05	0.2590
4	19.83	12.47	8.29	9.44	9.24	16.58	21.02	0.3907
5	1.60	36.19	78.89	31.08	106.7	69.70	86.72	1.380

The loads shown in table 6.2 are well within the maximum loads determined for the materials. These individual load cases are pictured in Figures 6-3 through 6-7. These plots show greatly exaggerated deformations of the model under the load. The unattached circles in the plots are the undeformed nodes. These are useful in visualizing the deformation.

Load Case 1, shown in Figure 6-3, has a maximum deflection at the perimeter of 6 mm which is well within the maximum permissible for accurate observations. Load Case 2, shown in Figure 6-4, has a 3 cm deflection. For Load Case 2 and the following loadcases a 3 cm deflection is allowed since there will be no observations taking place during the maneuver. The largest loads occur immediately around the position of the thruster modules. Load Case 4, shown in Figure 6-6, has a large deformation of 0.39 meters in the region of the thruster modules. The entire dish is bending upward around the central mass of the observatory dish. In Load Case 5, shown in Figure 6-7, the deflection is 1.38 meters as the observatory dish sags under the g-load of the orbital transfer vehicle (OTV). Although this is a significant deflection all of the member loads are well within allowable values.

6.3 Thruster Foundation Design

For many of the load cases the maximum loads occur immediately adjacent to the thruster modules. These high loads occur either from the inertial load caused by the high mass of the fuel or from loads generated by the thrusters themselves. In any case, these loads must be efficiently transferred to the structure of the dish in the most efficient manner possible to distribute the load and reduce stresses in the members.

In designing a module for the thrusters there were many primary concerns. A sound structural foundation would need to be provided to give support to the fuel tanks and insure that little

deformation would occur under loading from thruster operation. Because of possible damage to the observatory truss due to thruster exhaust the thruster nozzles would need to be held away from the truss and canted at an angle. The modules had to be of a similar design to minimize design and construction costs. And the modules had to be designed in such a way that they would efficiently be stored in the launch vehicle.

6.3.1 Thruster Module

The thruster module was design as a triangular structure composed of Gr/Ep tubes of the same design as used in the observatory dish. The entire module, as shown in Figure 6-8, is a triangle 4.73 meters at the base by 2.37 meters high. The depth of the structure is 2.8 meters.

The module contains two hydrazine and two NTO tanks of a maximum volume of 1.37 cubic meters. In addition there is a Helium tank of volume 0.493 cubic meters. The thrusters are located on a package on the large face of the module.

The modules are stowed in a 6.7 meter diameter launch shroud as shown in Figure 6-9. All four of the modules will be placed adjacent to each other in the launch vehicle. They will only consume a total length of 2.8 meters. When removed from the launch vehicle a deployable truss will need to be unfolded. Each of the modules has a unique truss arrangement due to the dissimilar structural arrangements on the perimeter of the observatory surface. A typical truss arrangement is also shown in Figure 6-9. The truss will unfold using no slip, locking

hinges. At the ends of the truss members will be attachment joints to link it with the observatory truss. There will also be graphite tethers for additional stiffness.

6.3.2 Thruster Module Arrangement

Because the bottom structure of the observatory dish is a triangular truss there are differences in the way the truss is arranged at the North, South, East and West compass points of the satellite. This means that each thruster module must have a unique attachment arrangement so that it can secure itself to the structural members of the observatory truss available to it at its assigned location.

The truss for the East Thruster Module is shown in Figure 6-10. This is the most simple arrangement. It is attached to the two adjacent attachment joints on the two nearest module. Note how the thruster module is elevated above the level of the observatory panels. This is to put the thruster cluster at the same level as the satellite center of mass (C.M.) (0.83 meters below the panel surface). Since the C.M. of the fuel tanks is also at the same position it will insure that the C.M. of the observatory does not change as the fuel in the tanks is expended.

The truss for the West Thruster Module is shown in Figure 6-11. This truss has longer member than the East module since it must span a larger distance to reach available attachment joints. The truss for the South Thruster Module is shown in Figure 6-12. This is an asymmetric arrangement necessitated by the availability of attachment joints. The North Thruster Module is

of a mirror image design as the South.

6.3.3 Thruster Module Truss Analysis

The North and South Thrusters both have extremely long members. These are prone to buckle, especially under the high loads that they would be subjected to during thruster operation. Eulers equation and a small finite element model were used to determine the appropriate size of the graphite epoxy tubes. From the analysis it was determined that a 4 cm diameter tube of a thickness of 2 mm would be sufficient. The graphite tethers of 1.5 mm diameter would also be used.

The average mass of the resulting module and truss, including attachment joints is 75.7 kg.

6.4 Connector Joint Design

The connecting mechanisms that are used to attach the modules to each other contribute a significant mass to the spacecraft. To minimize their weight a detailed structural analysis was performed. These joints are shown in Figures 4-5, 4-6 and 4-7.

The maximum loads for the attachment joints were taken from the finite element model of the observatory platform and from the Thruster Module Analysis. The Connectors were compared for both an aluminum and a titanium design. The primary places on the joint looked into were axial and shear stress in the locking pin and plate. Stress due to bending in the metal behind the pin and the metal surrounding the inflatable tube and the Gr/Ep attachment point.

Using a factor of safety of 2 the resulting thickness of the metal could be decided. The metal hoop that holds the inflatable member is 1.5 mm thick and the other metal supports are 2.25 mm thick. the locking pin is 8 mm in diameter with a 5 mm diameter neck that is used by the locking plate.. The locking plate is 2 mm thick.

These dimensions result in a mass per joint of 0.4395 kg for the lower joint and 0.4148 kg for the upper joint.

6.5 Launch Considerations

Although the spacecraft is well suited for the loads encountered in space it must also be able to survive a g-load for launch into LEO. The observatory modules are especially prone to damage under a launch load.

The observatory modules were designed to be stacked on top of each other in a launch container They would be supported in the vertical direction where the connection joints meet the launch container walls. However, the battery and electronic mass at the center of the foam panel would have no support.

A small finite element model was developed for a panel under launch conditions. It is a symmetrical half panel with a mass load at its center from the battery and electronic, support at its corners and support from Gr/Ep tubes beneath it. This is shown in Figure 6-13. From this analysis it was concluded that the foam would fail under launch conditions at the battery-electronics package would tear from the panel.

The solution to this problem is simple. A tension wire will

be attached to the top of the launch container that will pass through a hole in the center of each module. A locking mechanism in each module will grip the wire providing support to the panel at its center.

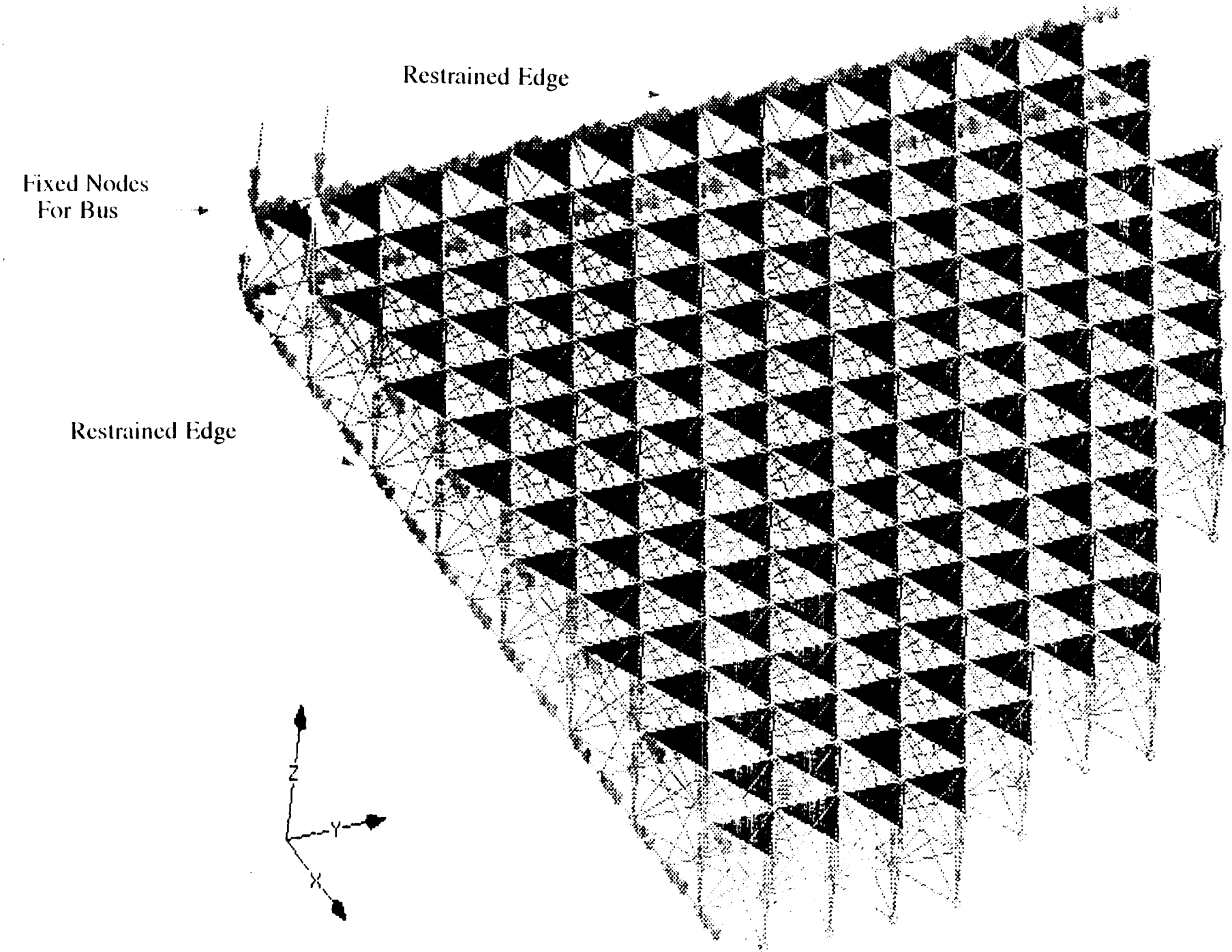

Figure 6-1 **Quarter Model**

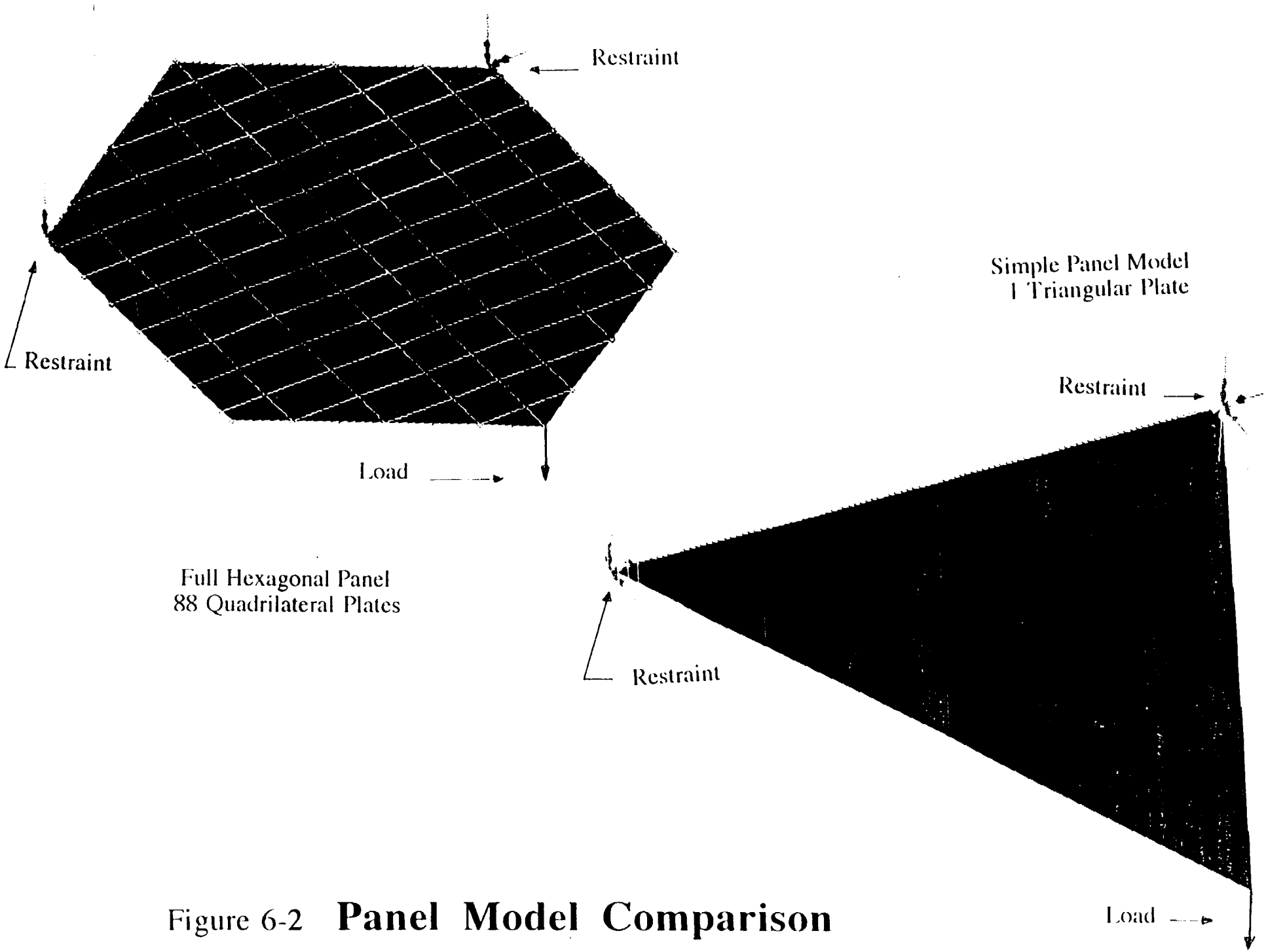

Figure 6-2 **Panel Model Comparison**

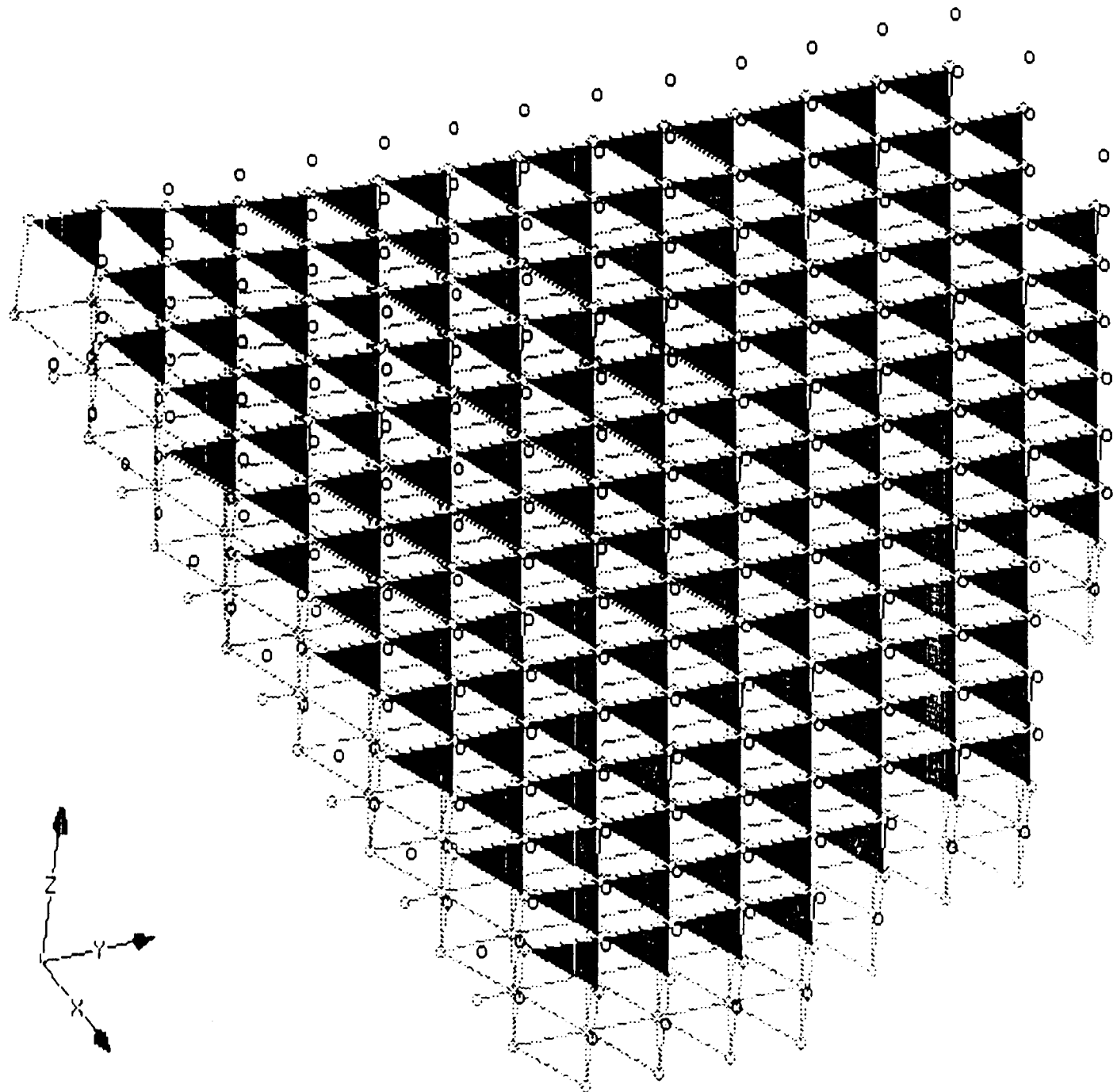

Figure 6-3 **Load Case 1: Solar Pressure**

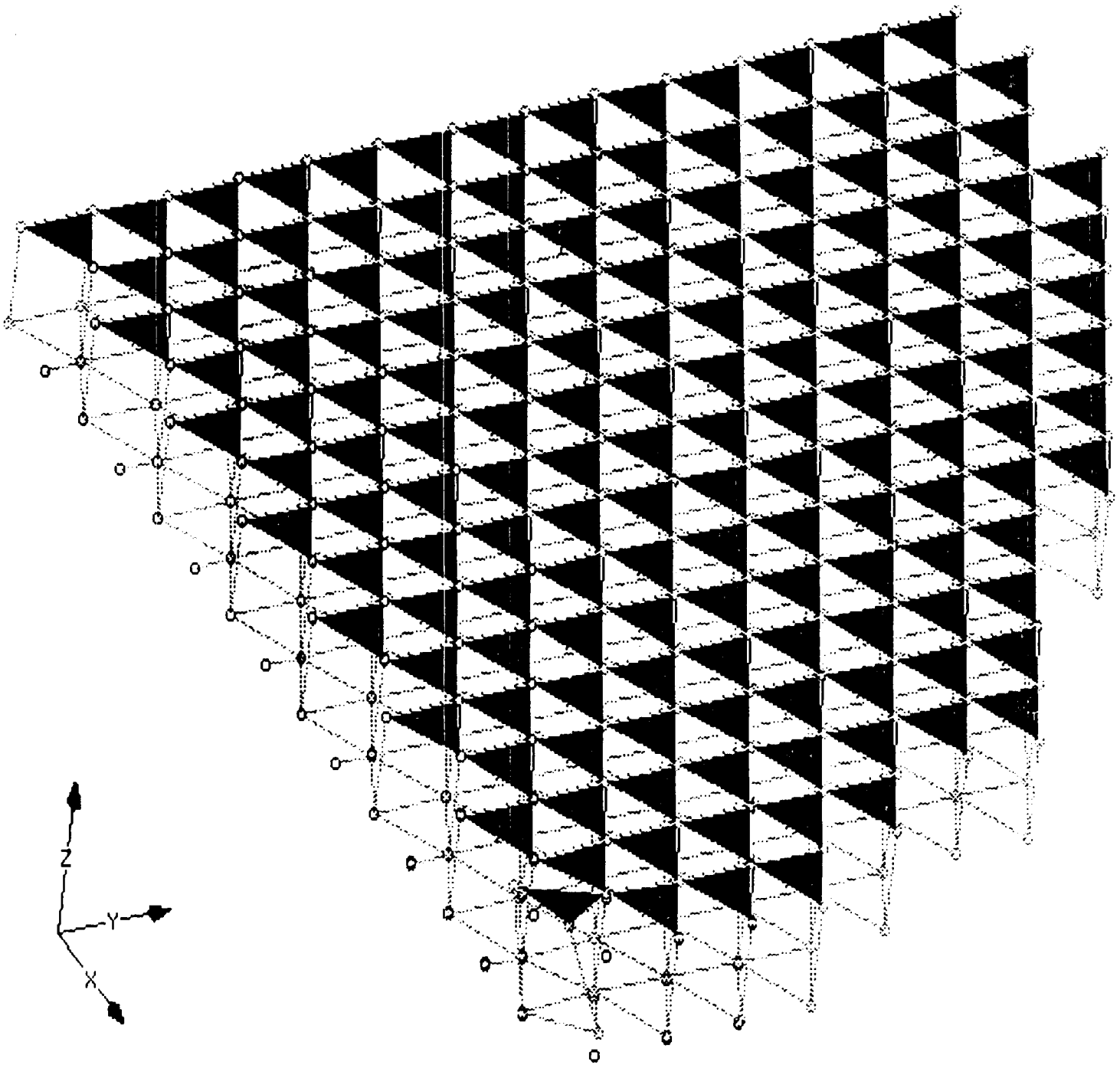

Figure 6-4 **Load Case 2: Y Thruster**

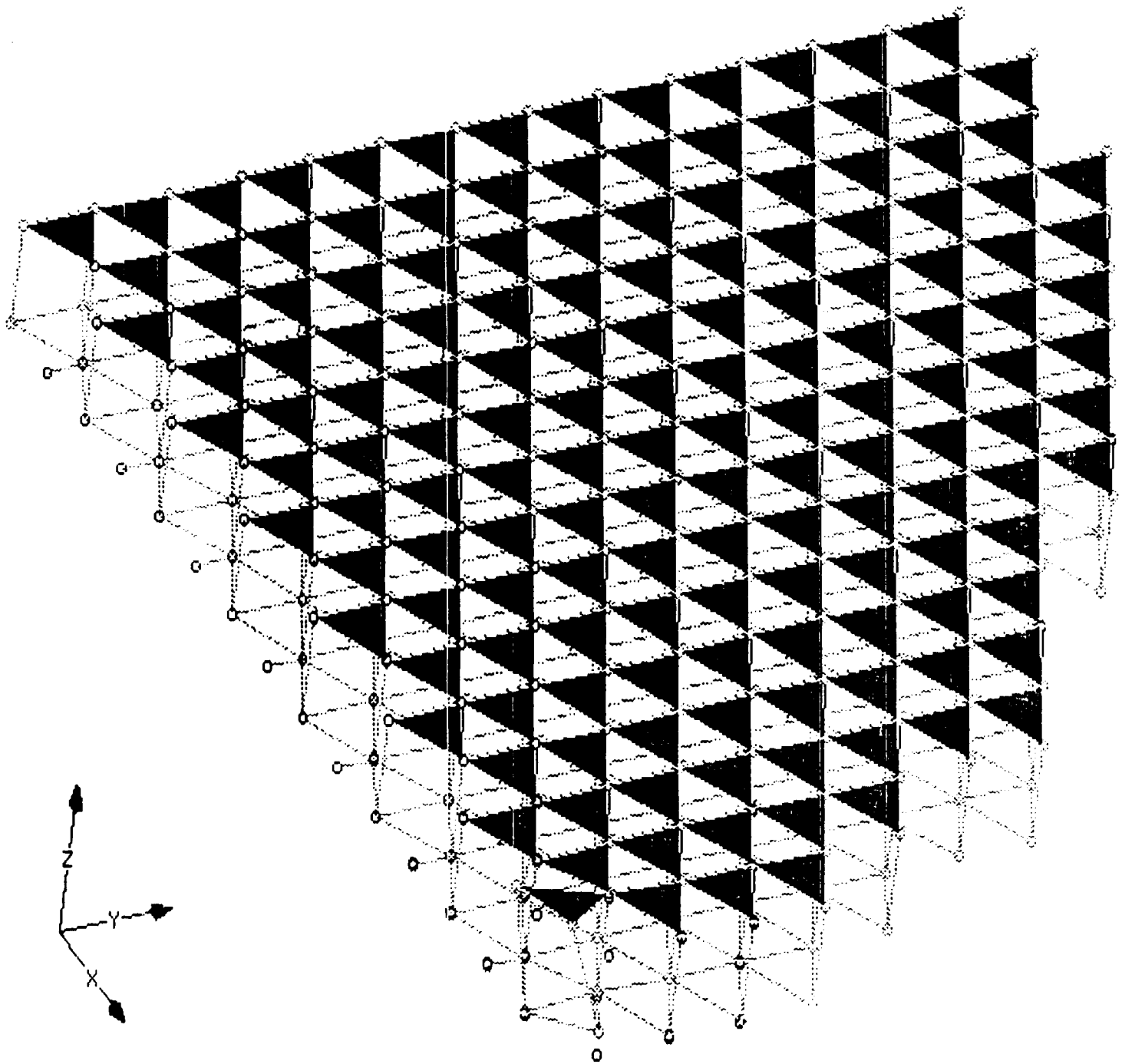

Figure 6-5 **Load Case 3: X Thruster**

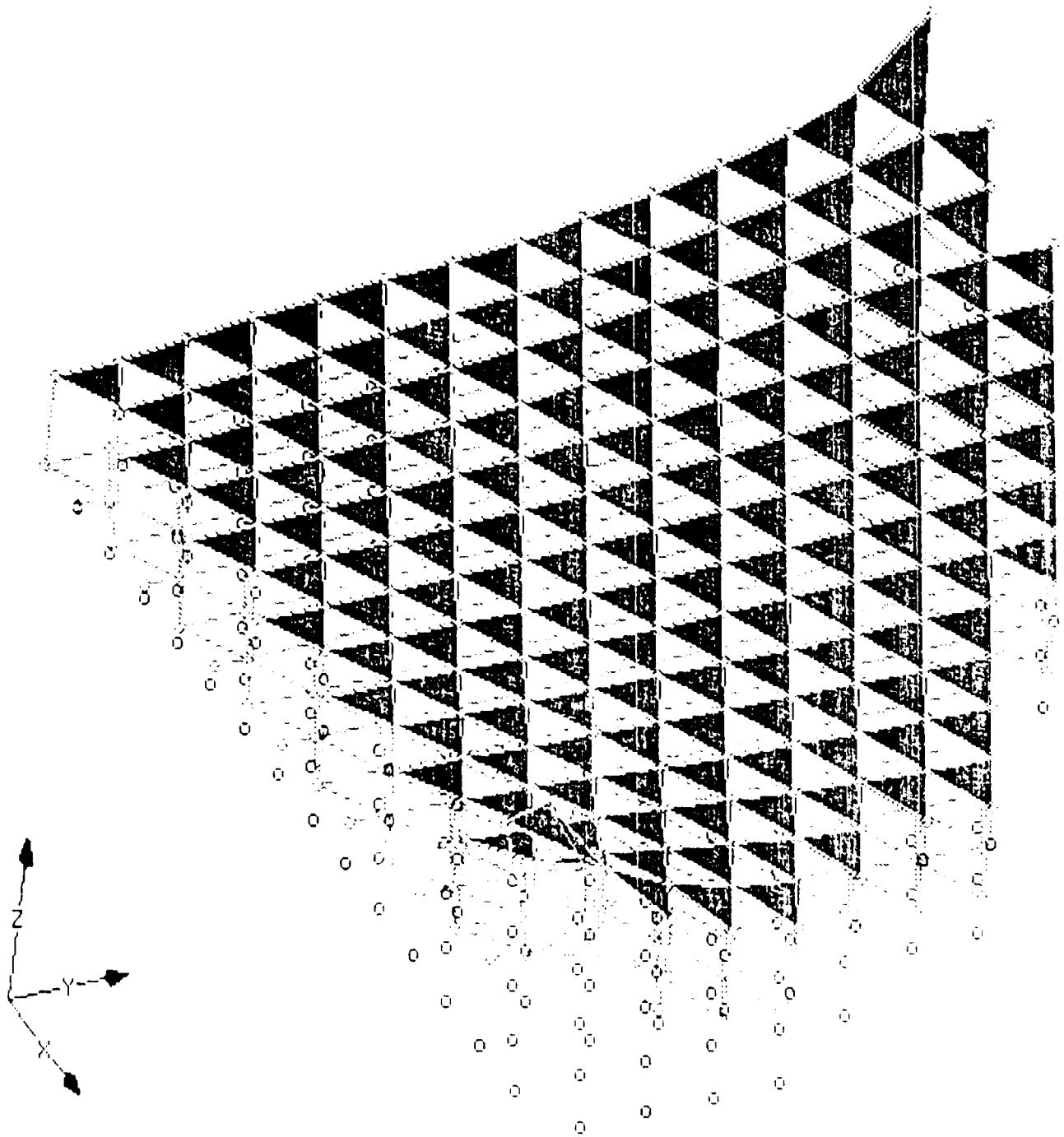

Figure 6.6 **Load Case 4: Z Thruster**

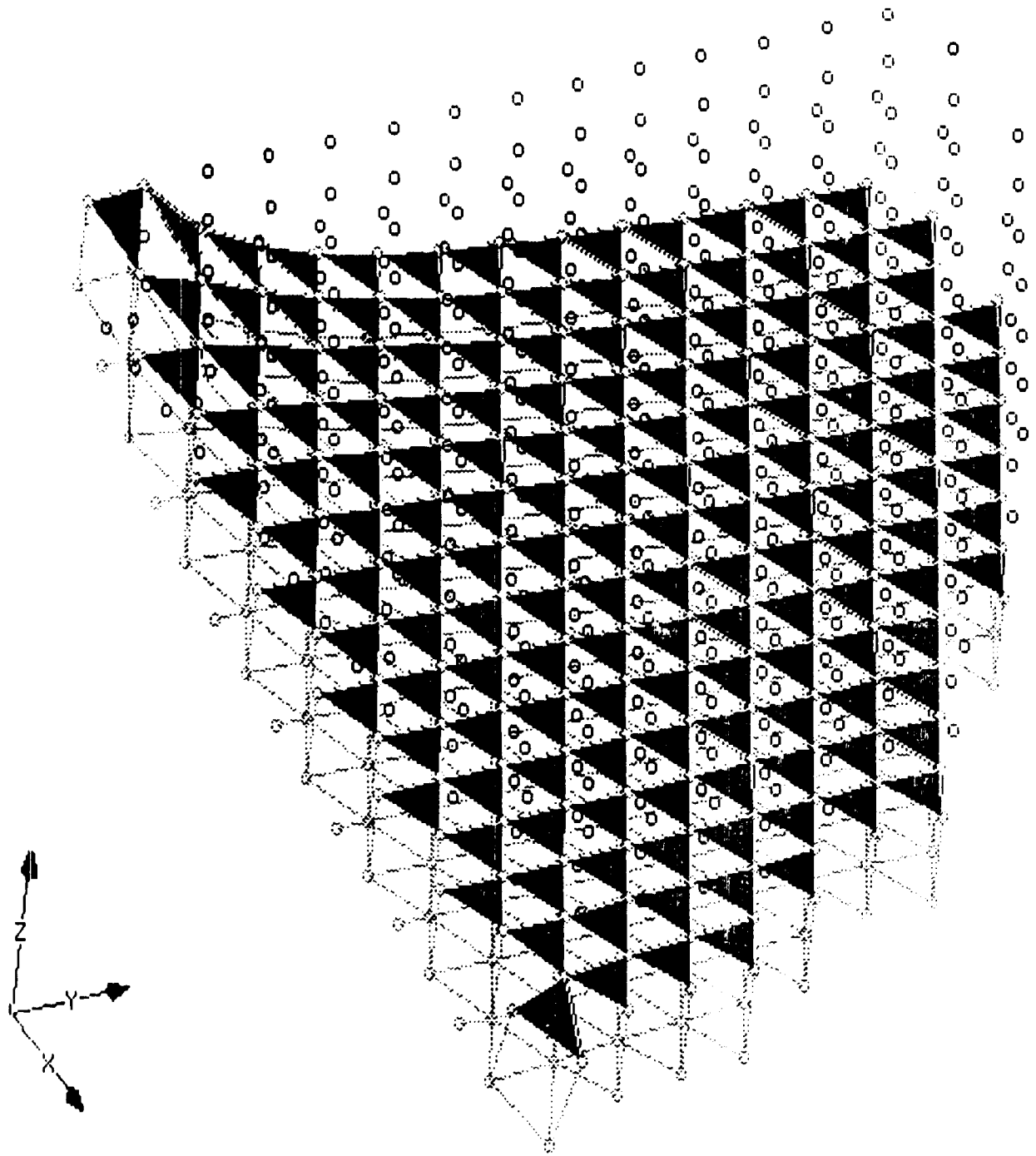

Figure 6-7 **Load Case 5: OTV**

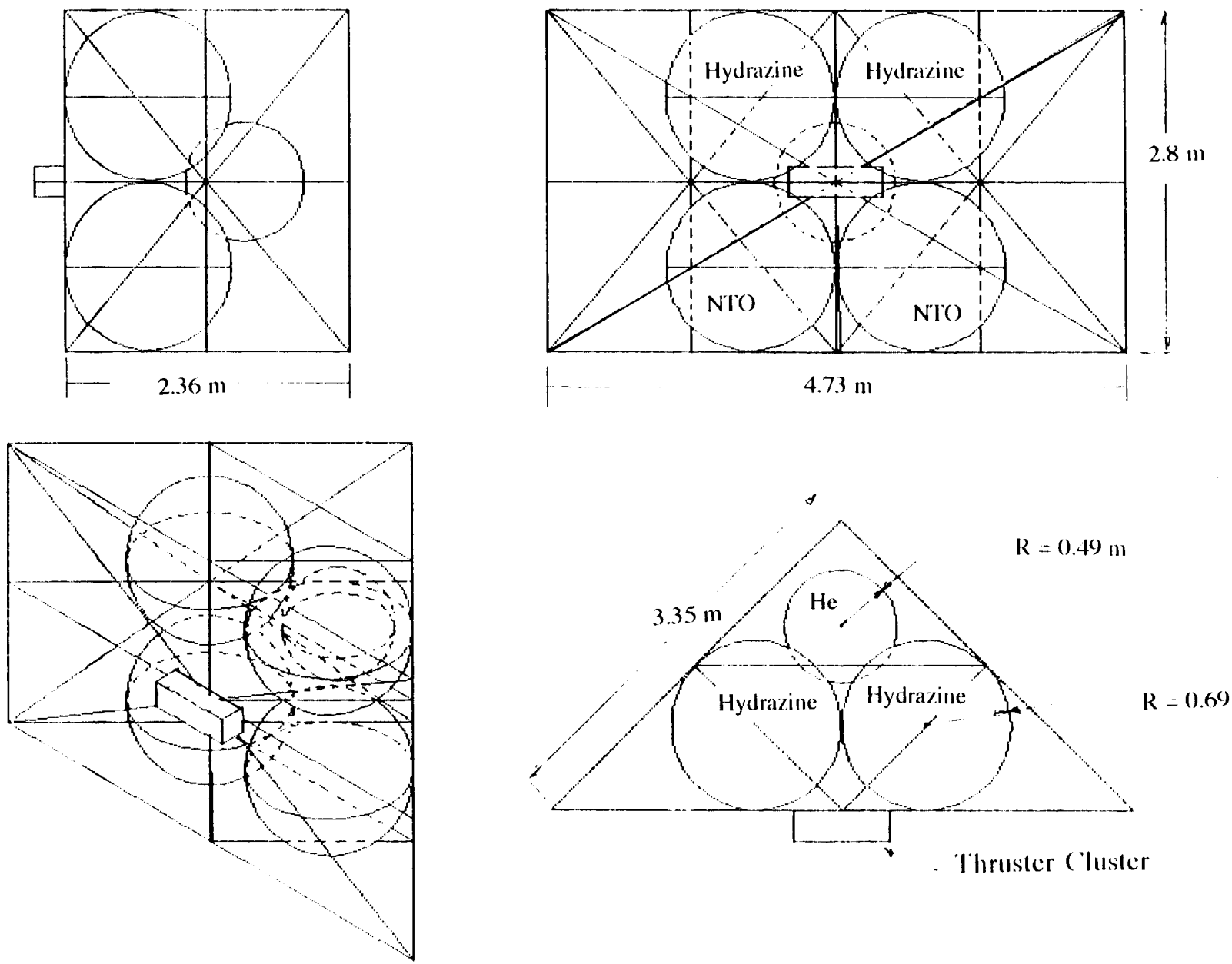

Figure 6-8 **Thruster Module**

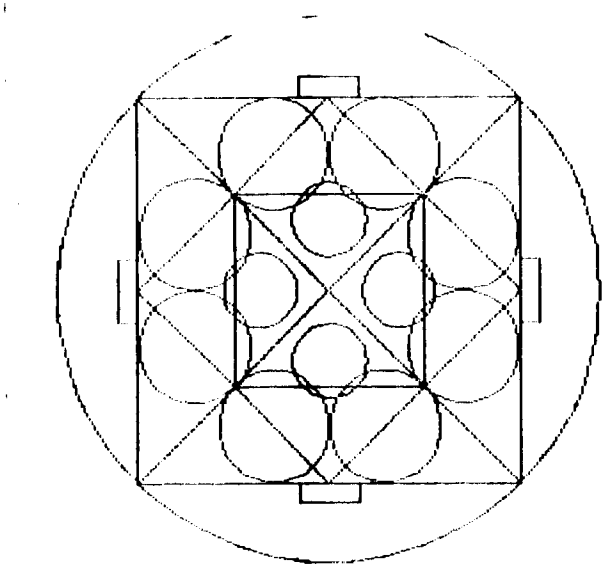

Stowage in 6.7m Diameter

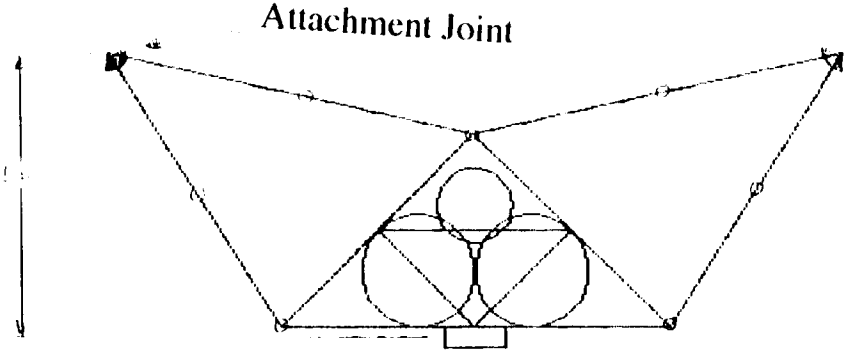

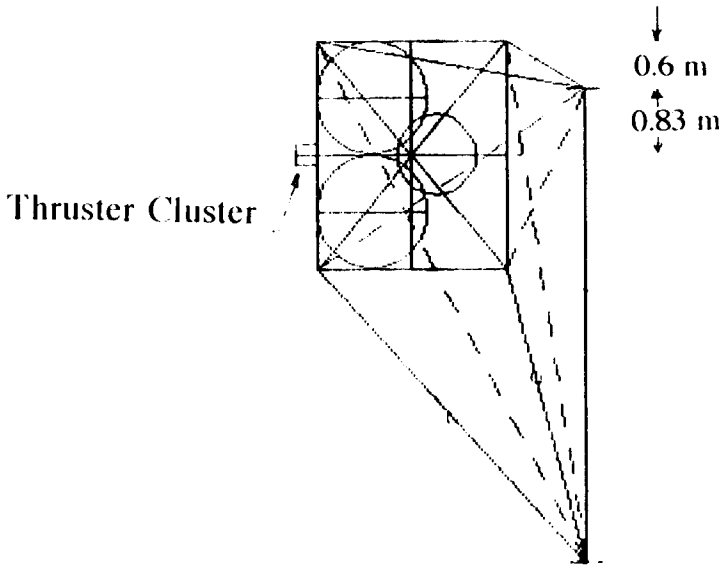

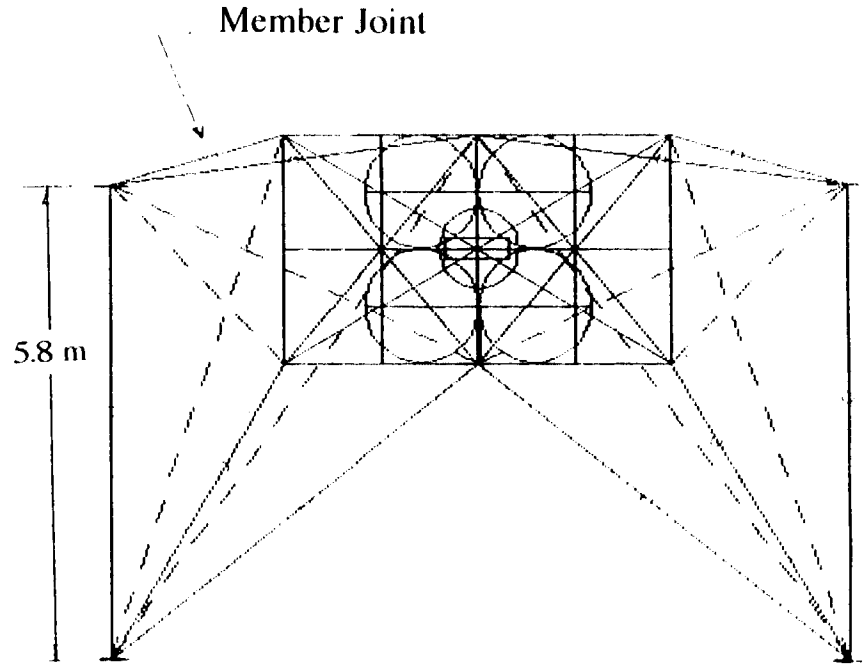

Figure 6-9 **Thruster Module Deployment & Stowage**

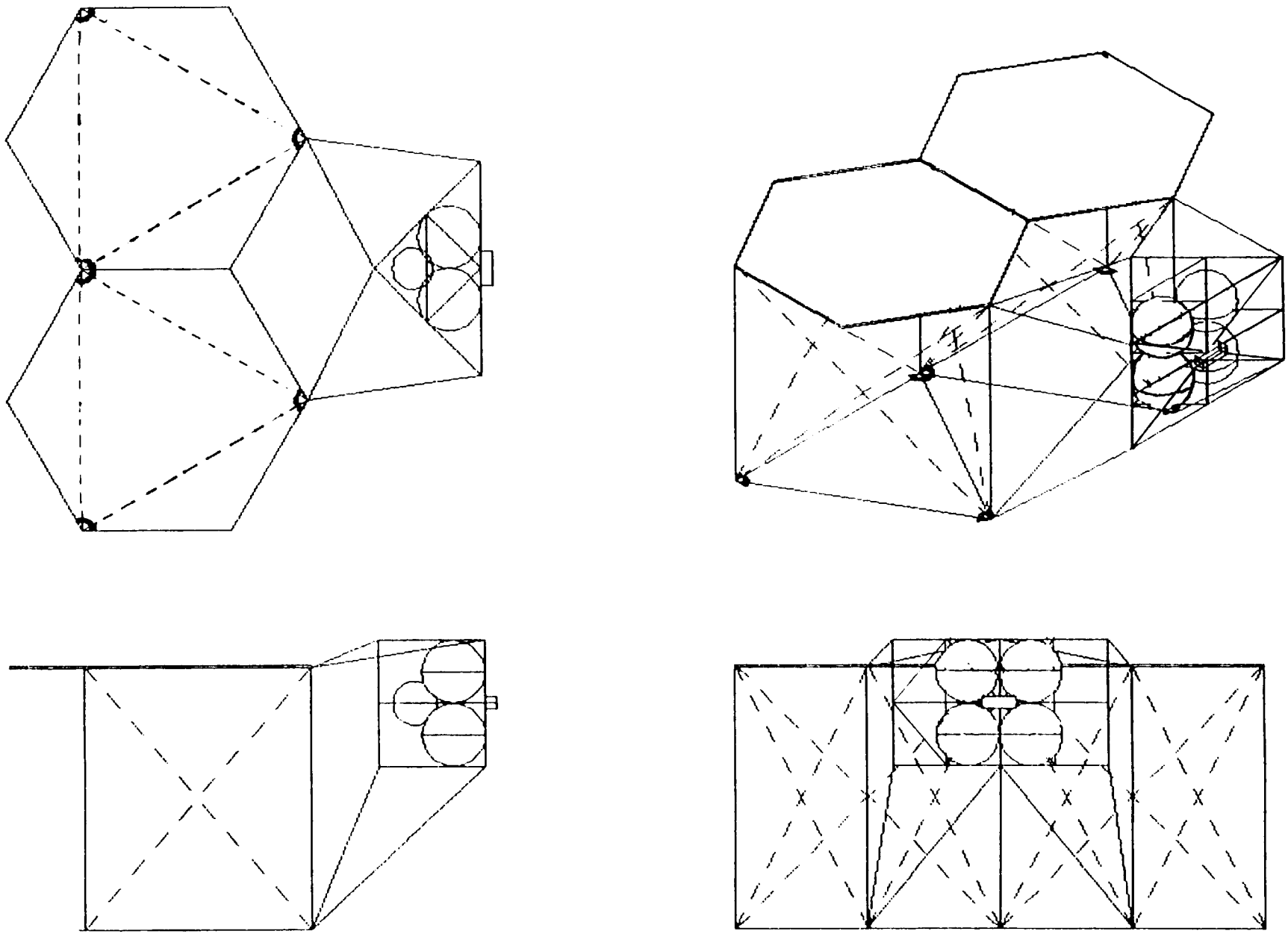

Figure 6-10 **East Thruster Configuration**

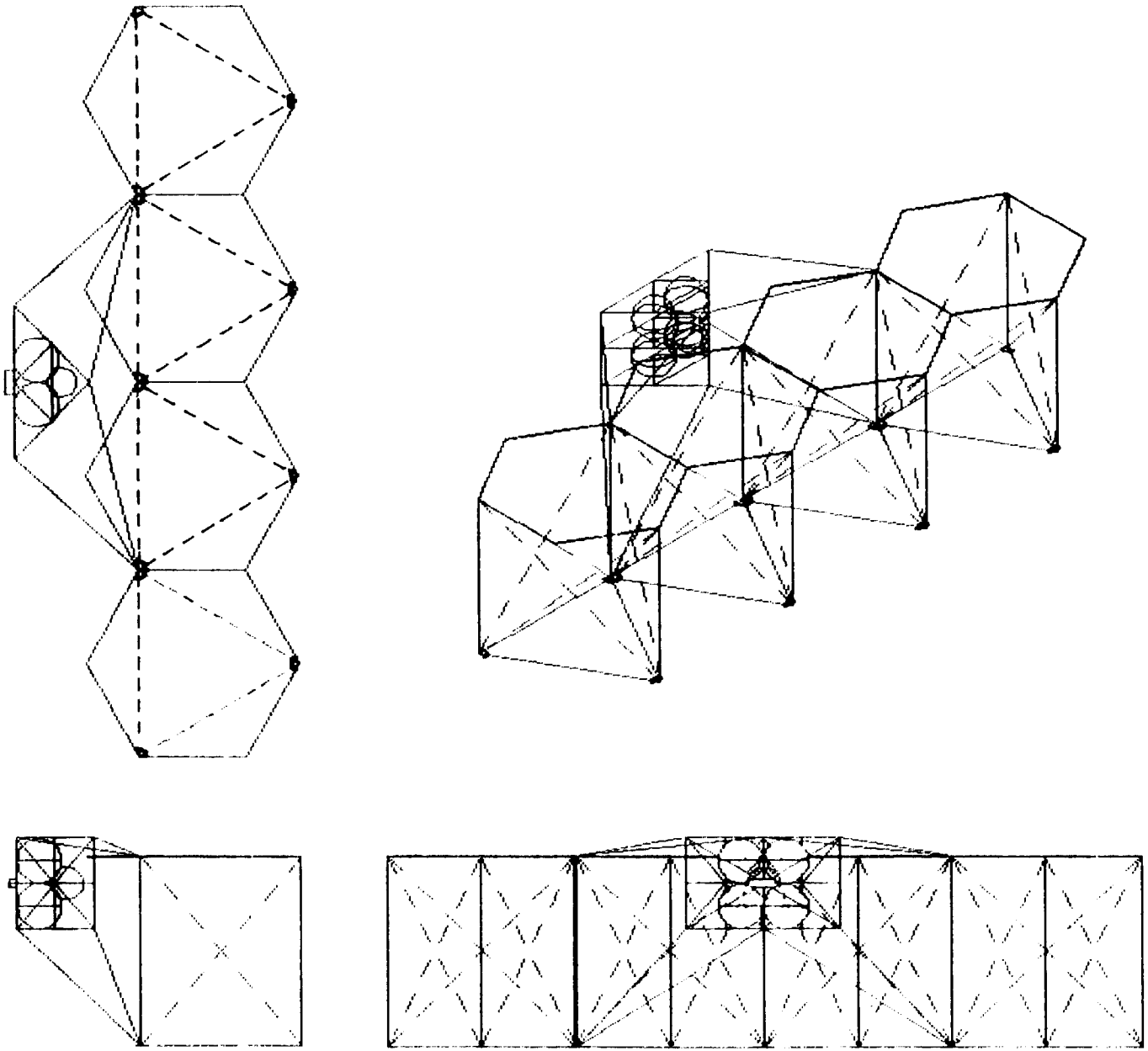

Figure 6-11 **West Thruster Configuration**

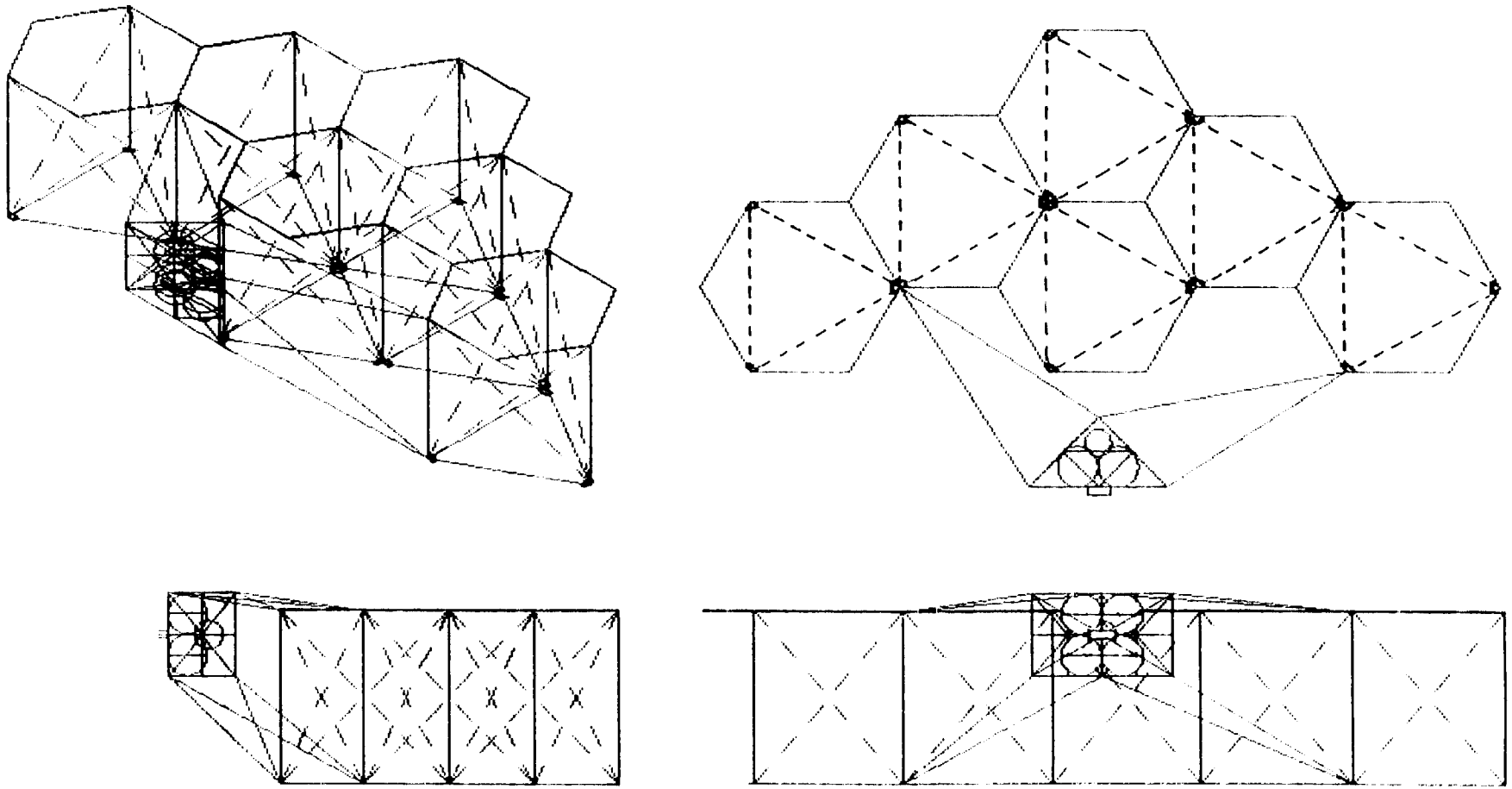

Figure 6-12 **South Thruster Configuration (North Similar)**

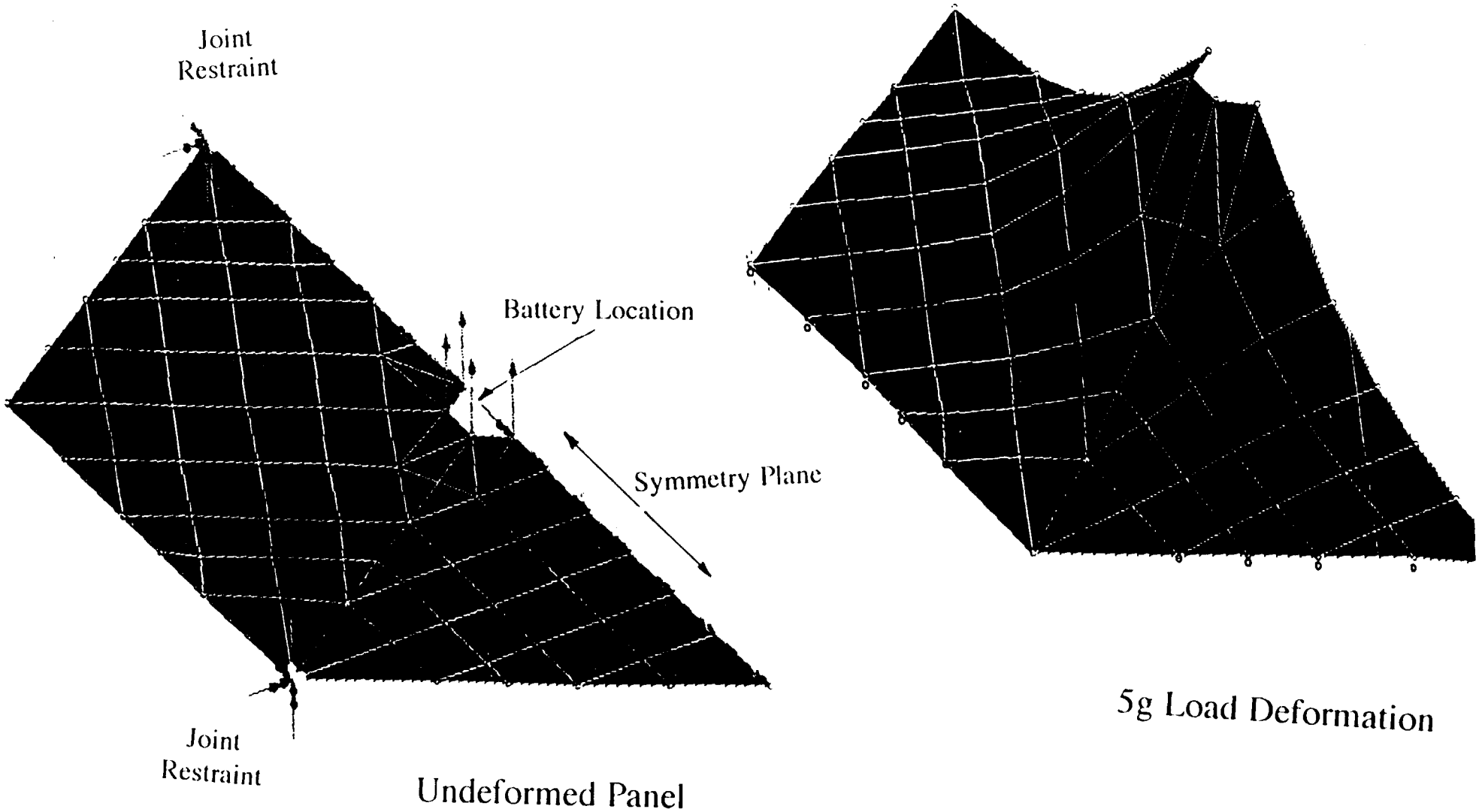

Figure 6-13 **Observatory Panel Under Launch Conditions**

7.0 POWER PRODUCTION

7.1 Requirements

The primary design goal for the electrical power system was to minimize the detrimental effects a power generating system might have on a observatory platform like PARAS. The addition of mass or motion to the spacecraft were to be avoided. The chosen power system must survive in its environment for ten years including its transfer through the Van Allen belts to GEO.

7.2 Power Generation Candidates

Figure 7-1 shows regions of optimum power generation methods for space missions. The long life of the observation platform would indicate investigation into the following power generation methods: photovoltaic, solar dynamic, radioisotope thermoelectric, and nuclear dynamic. Mass is the prime factor in determining a power system. Another major concern for this satellite is to limit moving parts and complexity. In GEO, even the simplest repair is unlikely, if not impossible.

7.2.1 Photovoltaic

Solar, static, power generation is accomplished by arrays of photovoltaic cells. To be most efficient, solar arrays need to be oriented to face the sun. This is accomplished by using a motor and bi-axial joint to position the solar panel. However, this creates an angular momentum

on the satellite. To counter balance this disturbing force large gimbaling system with counter-rotating masses would be required. Stationary solar panels affixed to the structure avoid this, but sacrifice their ability to receive constant, direct sunlight. A considerable increase in solar array area and battery mass would result.

7.2.2 Solar Dynamic

Solar dynamic power generation also has as a liability detrimental motions associated with its technology. It requires sensitive, precise aiming of its solar collectors to concentrate the incoming energy to power a dynamic cycle. In addition, vibrations from the machinery itself would undoubtedly be transmitted into the structure. The combination of this and its complex nature indicated that it was not a valid option for our geosynchronous orbiting platform.

7.2.3 Radioisotope Thermoelectric Generators

Radioisotope thermoelectric generators are an excellent source of nearly constant, low power. However as power requirements approach 10 kW, several RTGs are required. The largest RTGs currently in development are on the order of 1 kW. The major problem associated with high power RTGs is heat expulsion through large radiators.

7.2.4 Dynamic Nuclear

The radioisotope systems with greater constant power production consist of a Brayton or Stirling dynamic cycle. However, the ratio between electrical production and mass is about fifty percent lower than a solar, static system with secondary batteries. (Projected specific energy values for SP-100 in 2000 A.D. is 20-30 W/kg compared to 42.5 W/kg in current solar array technology). These also require large heat radiators for operation.

7.3 Selection of Photovoltaic System

The stationary photovoltaic system proves to be the best solution. The problems of disrupting motions and excess complexity are avoided. By placing the batteries along the central axis, stability of the whole configuration is improved, and a well designed array configuration provides a fairly constant energy supply.

Originally, the solar panels replace the observatory surface on a number of modules (determined by the required total area). On the underside of these modules is another solar panel. Eight modules converted to Silicon based solar arrays, only six for Gallium Arsenide, provide the required 11 kW of nominal power.

However, for a system to power a satellite the size of PARAS, a centralized power system is not very practical. Because of the danger of electrical arcing all voltages must be kept low. This in turn drives up the current required to

transmit power over a large distance, resulting in large heavy wires. Consequently, the power system had to be decentralized.

Along the lines of modular structural design, power production is also contained in each module. Each individual observatory module is fitted with stationary solar arrays, a battery, and supporting electronics. This eliminates the presence of an external wiring system on the satellite. There is no need to connect the power generation locations to the distribution and storage points. Other advantages to this configuration include reliability due to redundant systems and simplified construction in LEO.

7.4 Power Requirements and Profiles

A modular power system will be used to eliminate a complex and bulky power distribution system, so each type of module (thruster, observatory, and bus) is completely independent of the others in power production, storage, and usage. Figure 7-2 is the power profile over a one day period. The power required for an observation is in the range of 43.0 to 52.0 kW due to the use of receivers, amplifiers, phase shifters, and correlators. There are typically four five hour observational periods, each followed by 30 minutes of data transmission. This steps up the power requirement in the bus from a constant 600 W for the central computer, basic communications, and various control systems to 1 kW.

After every other data transmission period, the chemical thrusters, requiring at most 15 W for the heaters, fire for attitude control and station keeping for no longer than 30 minutes. This is followed by a one hour delay to allow vibrations to dampen out. The nominal power required for the entire radio astronomy platform is almost 53 kW.

7.4.1 Observatory Module Power Production Profile

The power production profiles in Figure 7-3 provide estimates that each module's double sided solar array face an equivalent maximum of 6.7 hours in darkness. During these hours the batteries are expected to provide the nominal power of 80.0 Watts. During a total eclipse from the Earth, the observatory surface is temporarily shut down to prevent overburdening the batteries.

7.4.2 Bus Power Production Profile

Figure 7-4 shows the power production profile for the solar arrays of the bus. The original configuration was similar to all the other modules resulting in an equivalent maximum darkness period is 7.29 hours including eclipse. This can be improved to 4.18 hours by arranging the lower solar arrays at nearly a 45 degrees angle. This maintains a near ideal solar incidence angle for longer periods. This change cut the battery mass by one third, from 189 kg to 126 kg.

7.5 Power Generation Configuration

7.5.1 Selection of Cell Type

The three most common types of solar cells for possible use in GEO are Silicon (Si), Gallium Arsenide (GaAs), and Indium Phosphide (InP). Gallium Arsenide cells have four major potential advantages for space application when compared with Silicon cells:

1) higher efficiency
2) higher temperature operation
3) higher radiation tolerance
4) lighter weight

The last advantage derives from the fact that the active region in a GaAs cell need to be only 4 or 5 μm thick to achieve complete absorption. A Silicon cell of a single crystal is tens of micrometers thick to achieve the same amount of light absorption.

The characteristics of the GaAs cells and the InP cells are projected to be similar, thus allowing the assumption that a photovoltaic array constructed from either InP or GaAs cells will be similar in size, mass and power output at the beginning of life (BOL). Table 7.1 shows the comparison of the three primary cells.

TABLE 7.1: Comparison of Types of Solar Cells

Solar Cell	Advantages	Disadvantages
Silicon	abundant 18% BOL efficiency	degradation
GaAs	abundant 21% BOL efficiency	degradation
InP	self-annealing 21% BOL efficiency (projected)	limited supply 14% (presently)

A primary problem associated with current photovoltaic cells is degradation induced by exposure to electron and proton radiation. Indium Phosphide and Gallium Arsenide cells have very different reactions to radiation exposure, each with definite advantages and disadvantages. With the state of present technology, GaAs cells would provide the best choice. Of the presently abundant cells, GaAs has the highest efficiency and is the most resistant to radiation. In order to contend with the degradation in power output, the size and mass of the entire photovoltaic array would need to be increased.

7.5.2 Solar Array Layout

In designing the solar array layout, the appropriate solar cell I-V curves need to be determined first. Figure 7-5 shows the I-V curve for a typical GaAs cell with an efficiency approaching 18% in the AMO spectrum. In the cases investigated, each cell is 4 cm x 6 cm with a voltage output of 0.819 V and a current output of 0.1 A. Excellent fill factors are routinely obtained, indicating both good junction quality and low series resistance.

The design of a solar cell array is an iterative process where the approximate array area is first determined by a solar array analysis as shown in Appendix 7.1. From this the mechanical designer determines the best method of obtaining the required area. A solar array is required for the top and bottom of each module and the bus.

Cross sections of the solar arrays are shown in Figure 7-6. A thin layer of Gallium Arsenide grown on a Germanium substrate absorbs the solar energy while a Ceria-doped glass covering provides protection from radiation effects. In GEO, 75μm for each layer is adequate. A thermal control layer is also required to direct heat away from the cells for maximum efficiency.

7.5.3 Observation Module Solar Array Configuration

The solar array provides a voltage of 24.6 ± 1.3 Volts with 30 GaAs cells in series. The cells are arranged into three circuits connected in series as shown in Figure 7-7.

Each circuit contains two 10 cell series connected in parallel. Therefore, there are two different networks on the panel for a total current of 0.2 ± 0.03 Amperes. For the top of the module, there are four 0.43 m x 0.37 m panels, and nine for the bottom. The module surface provides the structural support required for the solar array. Solar panel design calculations are found in Appendix 7.2.

7.5.4 Bus Solar Array Configuration

The computer and communications in the bus work most efficiently at high voltages such as 120 V. Each solar panel includes 152 GaAs cells in series to produce a voltage of 124.5 ± 7.0 V. The cells are arranged into four circuits connected in series. Each circuit contains 4 series of 38 cells connected in parallel resulting in a panel current of 0.4 ± 0.05 A. For each side of the bus, there are eight of these panels each of the size 1.62 m x 1.06 m as shown in Figure 7-8. Bus solar panel design calculations are found in Appendix 7.3.

7.6 Power Storage

The power storage system provides power when the earth eclipses the sun and when the solar incidence angle is too high for the solar cells to absorb the incoming energy. There are two eclipse seasons lasting 45 days every year around the vernal and autumnal equinoxes. The longest

possible eclipse is 70 minutes. Secondary batteries are the only source providing the required nominal power at these and other times.

The actual battery system consists of multiple cells of either Nickel Cadmium (NiCd) or Nickel Hydrogen (NiH_2). The Nickel Hydrogen batteries are a relatively recent development with successful tests in GEO. The major advantages of the NiH_2 battery over the NiCd include a higher energy per weight density (specific energy), a higher allowable temperature, and a longer cycle life. The disadvantages include a high internal pressure, a low energy per volume fraction, and a slightly lower recharge efficiency. Extensive research is underway to try to improve the specific energy and recharge efficiency for both NiCd and NiH_2 cells.

Each module and the bus contain a secondary battery and a subsystem, such as a coulometer and a shunt regulator, which oversee and control the processes of charging and discharging. The subsystem optimizes the charge rate and prevents dangerous overcharging by bleeding off excess power which is especially high at the beginning of life. A thermal control device is included to radiate excess heat.

7.6.1 Module Battery Configuration

The major constraint of the battery is for it to fit within the 5.0 cm thickness of a collapsed module. The

smallest NiH_2 cells are about 7.7 cm in diameter and could not be used. Eighteen Nickel Cadmium cells, connected in series, lie flat within the hollowed out center of an observation module as shown in Figure 7-9. The battery voltage is 23.9 ± 1.0 V with a current of 2.92 ± 0.32 A. Each cell has a rated capacity of 42.0 Ahr and a mass of 15.3 kg.

Because of the excessive mass of this design Sodium Sulfur batteries were chosen for the module power storage system. These batteries have an energy density of 200 Whrs/kg and a depth of discharge of 80%. Although many aspects of this technology are uncertain by the year 2010 this level of energy storage should be available. The use of these batteries reduces the observatory modules power storage mass to 2.47 kg. A similar configuration is to be used for the thruster modules.

7.6.2 Bus Battery Configuration

The power storage system for the bus is two 90 cell NiH_2 batteries connected in parallel. Each cell has a mass of 0.70 kg resulting in a total battery mass of 126 kg. Each cell, example shown in Figure 7-10 is connected in series and has a rated capacity of 38 Ahr and a diameter of 8.96 cm. With the large volume available in the bus, NiH_2 was chosen to reduce the mass. The two parallel batteries provide a nominal voltage of about 119.7 ± 4.0 V at a current of 15.0 ± 1.5 A to the bus as calculated in Appendix

7.4. With a depth of discharge not greater than 50 percent, this provides a constant 900 Watts of power for even the longest of eclipses.

7.7 System Summary

The power system for the radio telescope is divided among each individual module. The bus requires 16 solar panels totalling 9728 GaAs/Ge cells and 27.4 m^2 of area and two 90 cell NiH_2 batteries to provide 900 W of power. Each observation module consists of thirteen 43 cm x 37 cm solar panels totalling 780 GaAs/Ge cells and an eighteen cell NiCd battery which provide 80.0 W. The entire observatory surface requires 52.0 kW of power, 1336.0 m^2 of GaAs solar panels, and 1620 kg of NaS battery mass.

Figure 7-1 **Power Usage Profile**

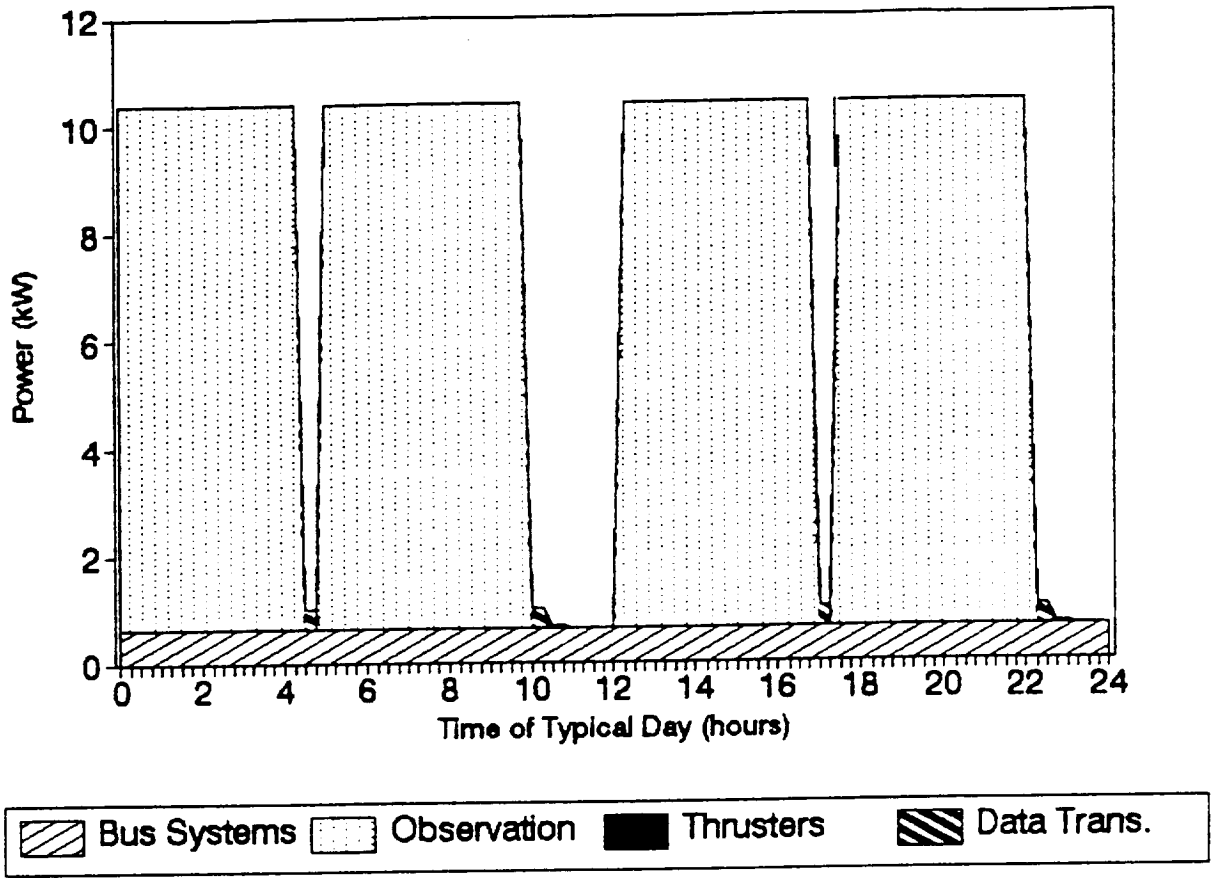

Figure 7-2 **Power Production Profile - Module**

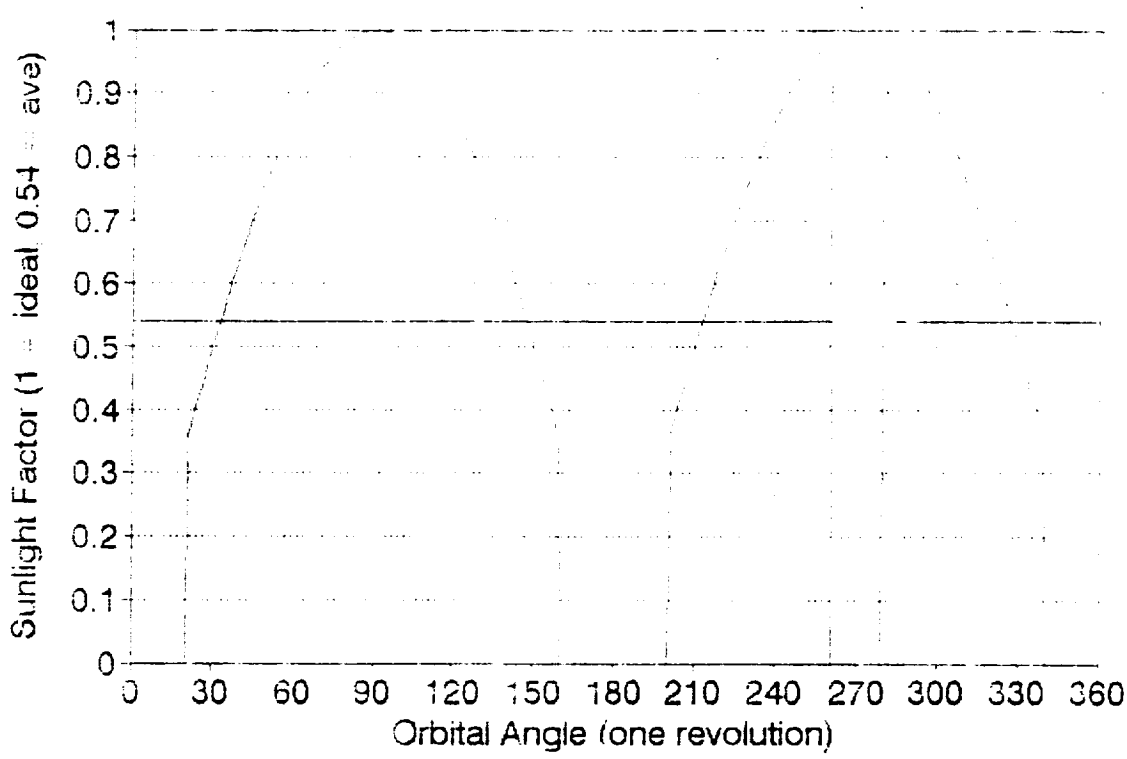

No Inclination: Maximum Eclipse

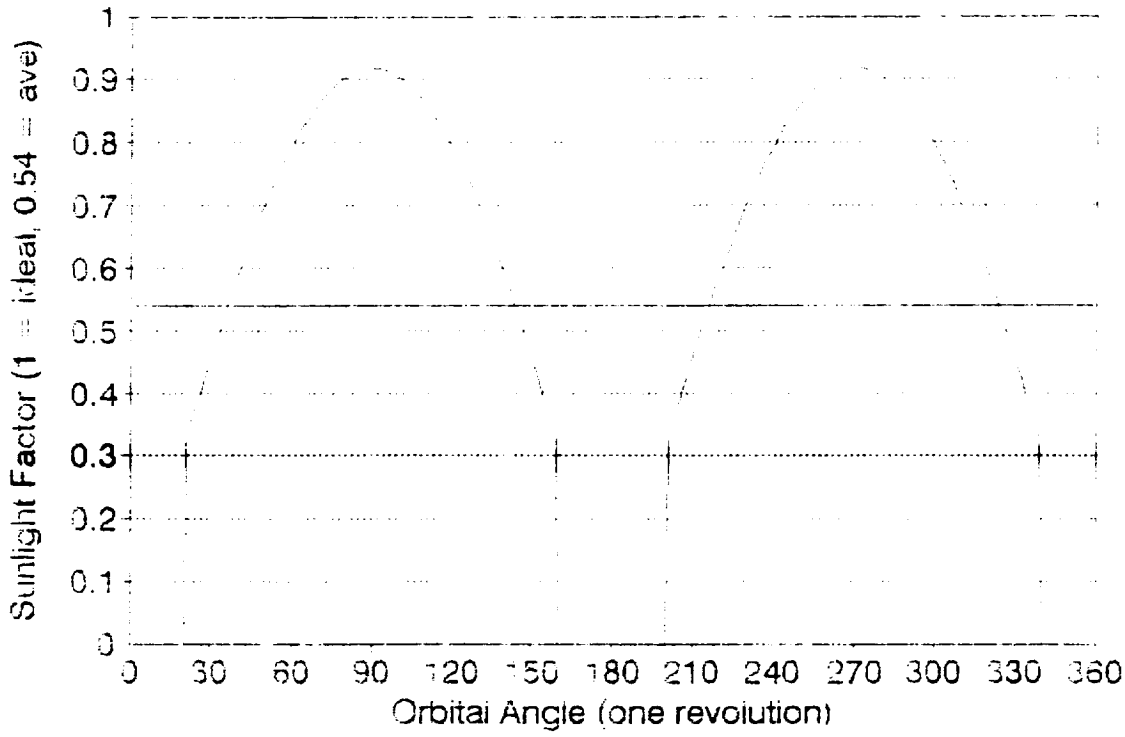

Maximum Inclination (23.4 degrees): No Eclipse

Figure 7-3 **Power Production Profile - Bus**

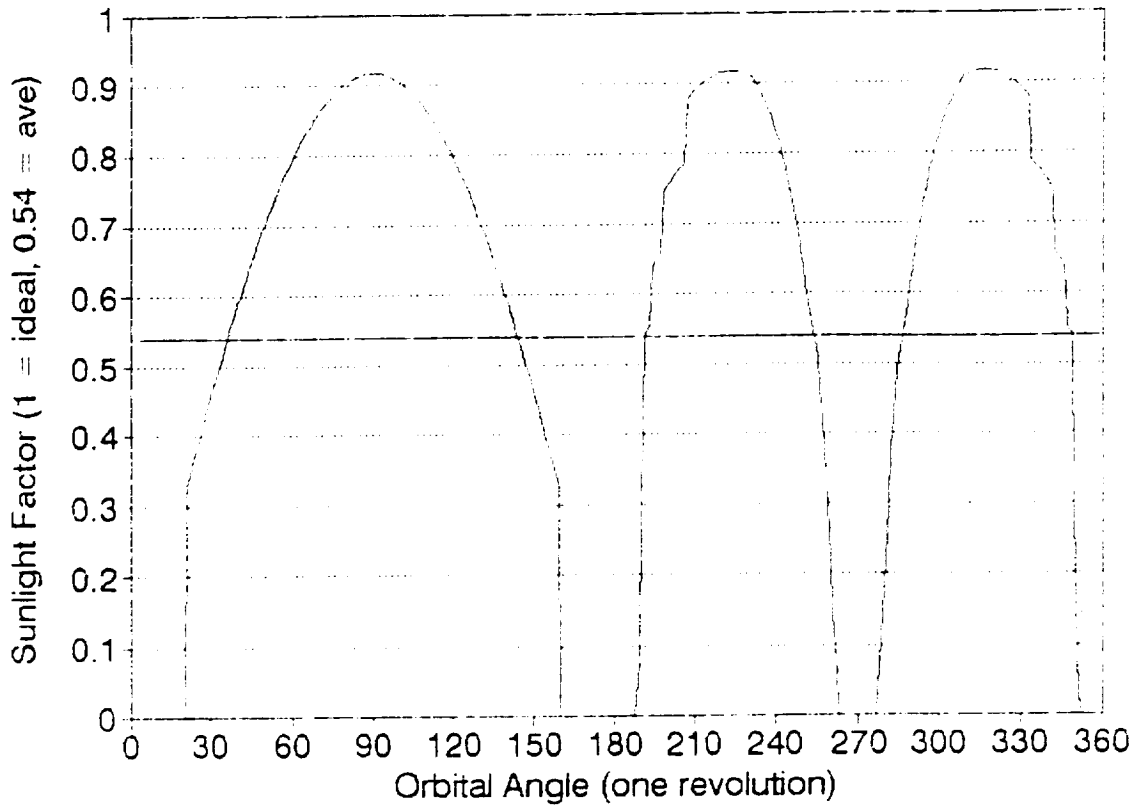

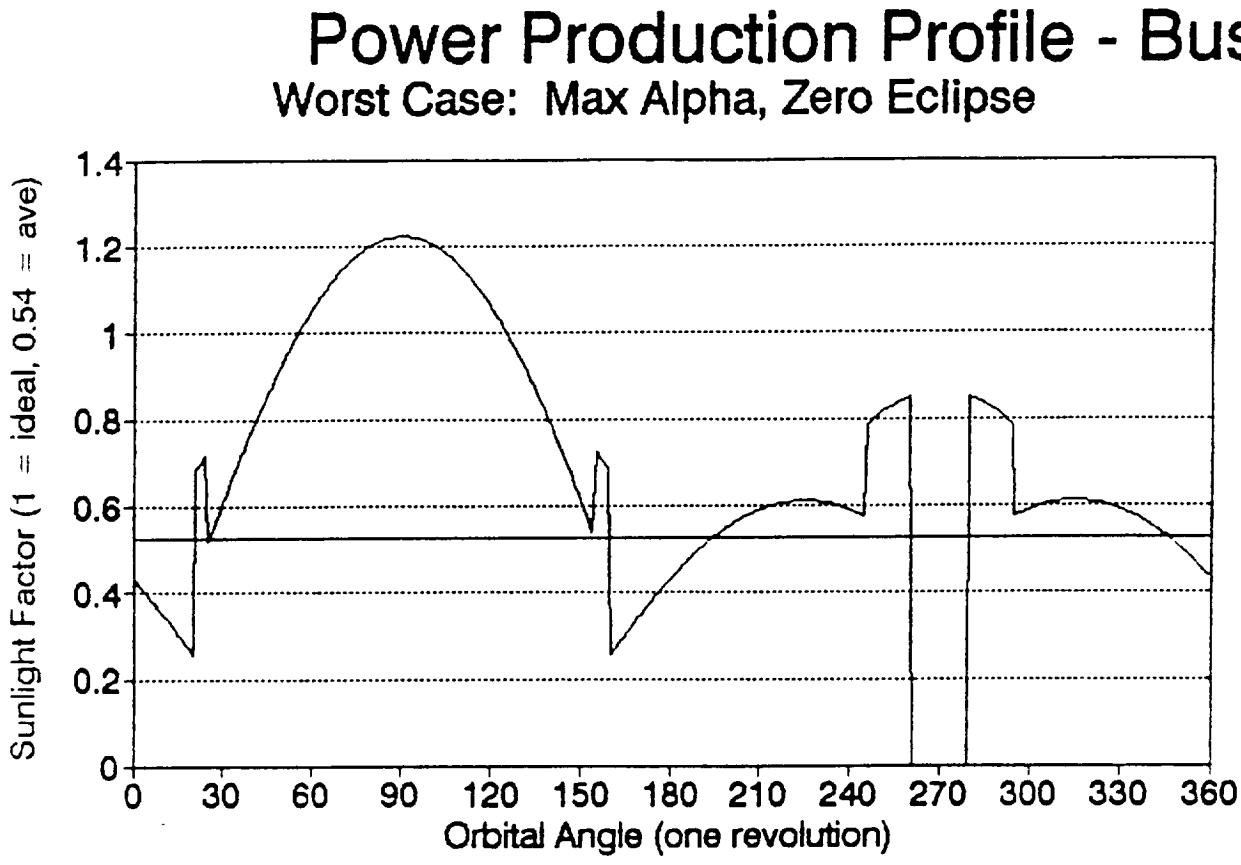

Figure 7-4 **Ranges of Application of Different Power Sources**

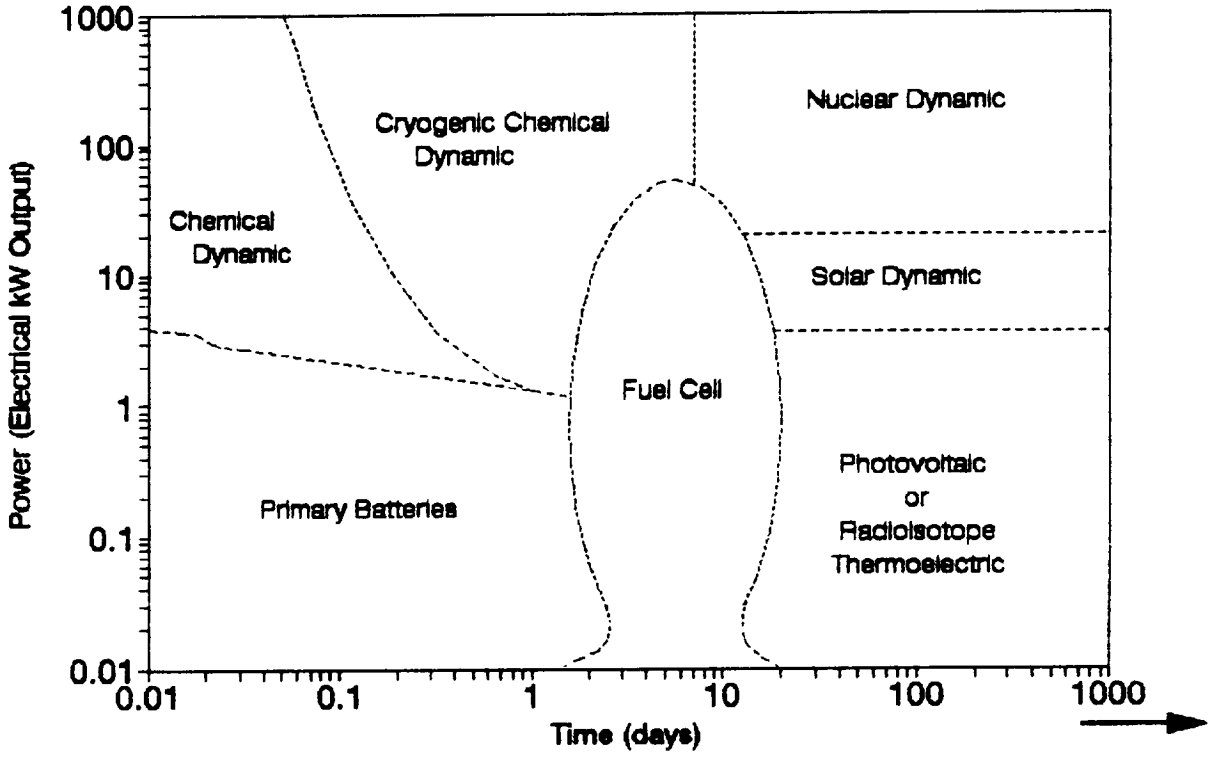

Figure 7-5 **Current-Voltage Curve for GaAs Cel**

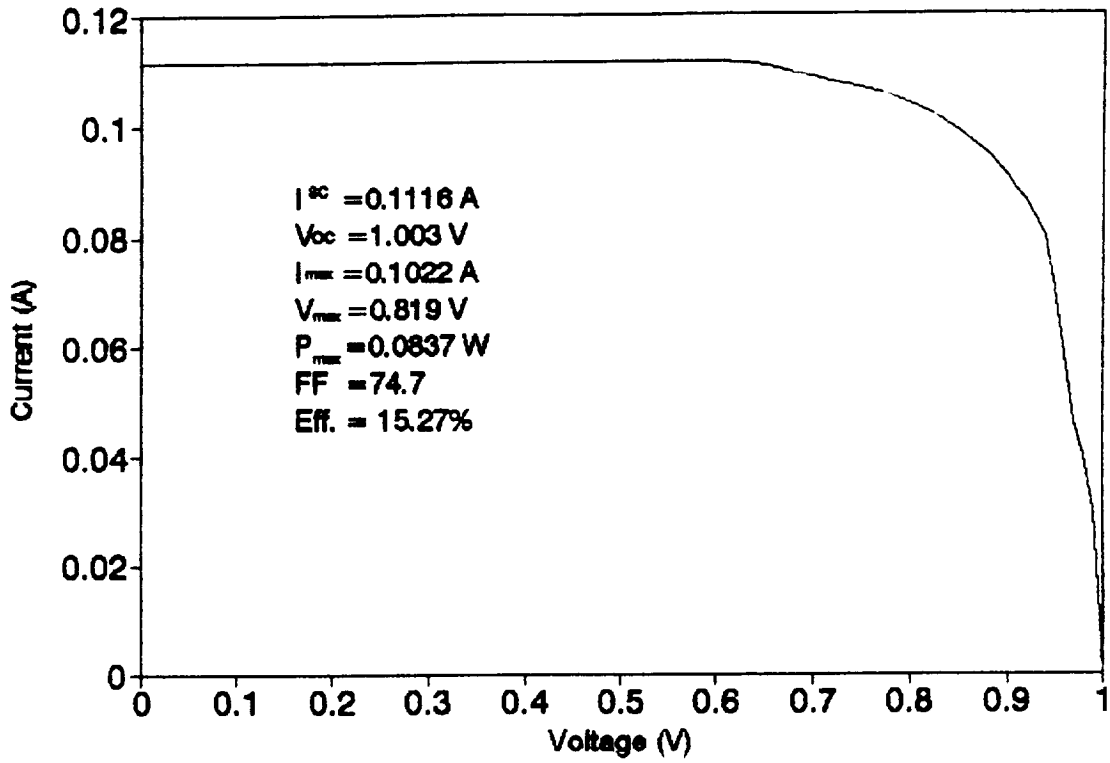

Figure 7-6 Solar Array Cross Sections

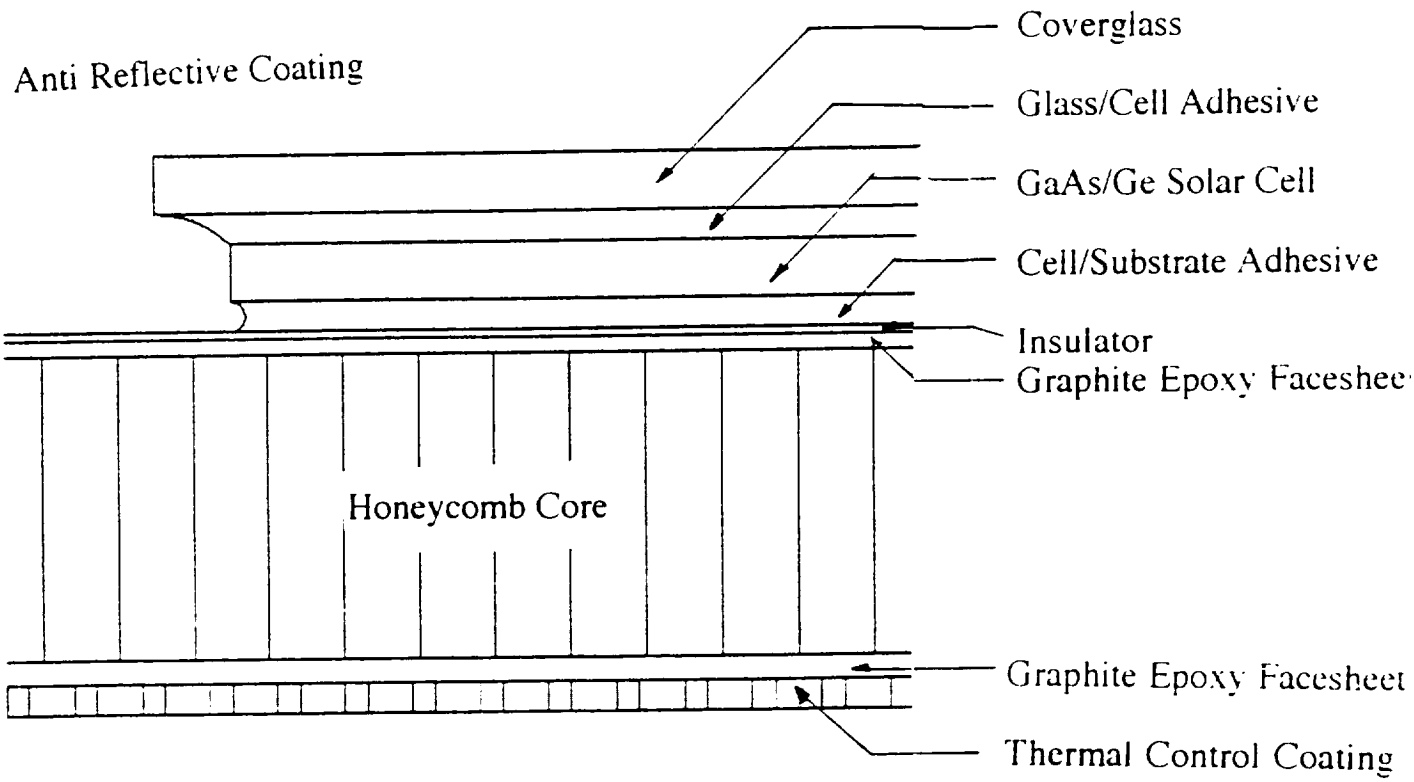

Bus Panel with Solar Array

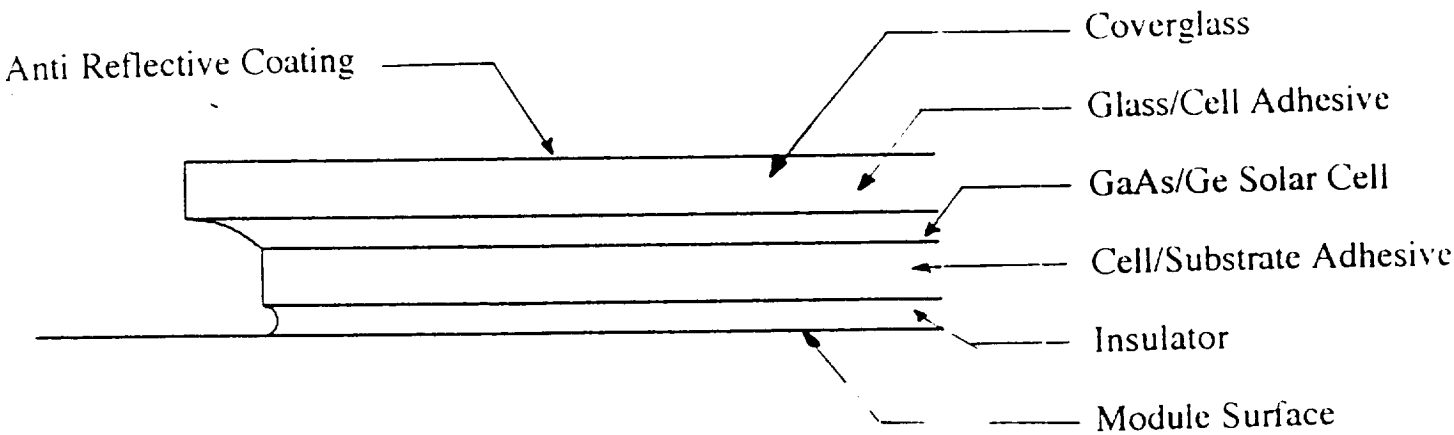

Module Solar Array

Figure 7-7 Configuration of Module Solar Array

60 GaAs Cells per 43x37 cm Panel
Four Panels on Top of each Module
Nine Panels on Bottom of each Module

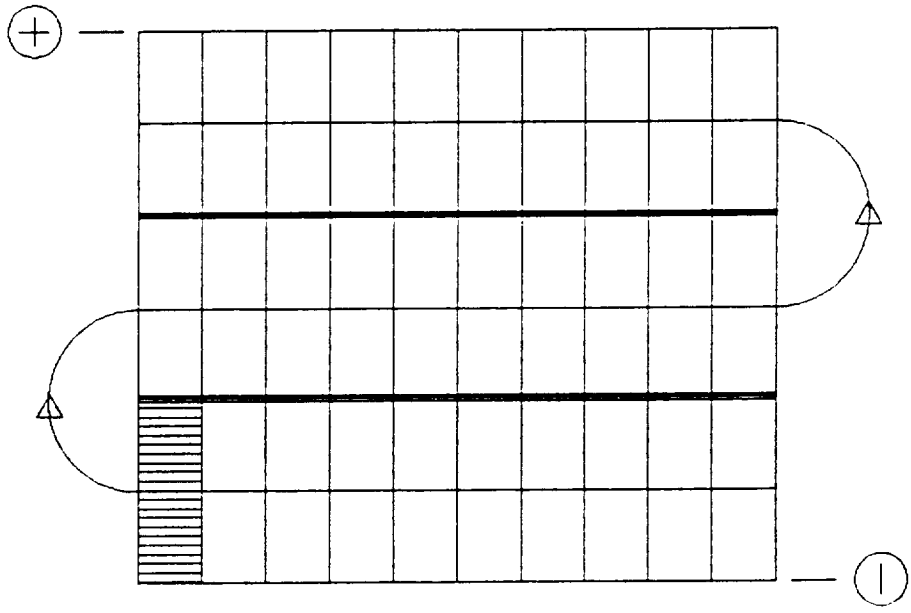

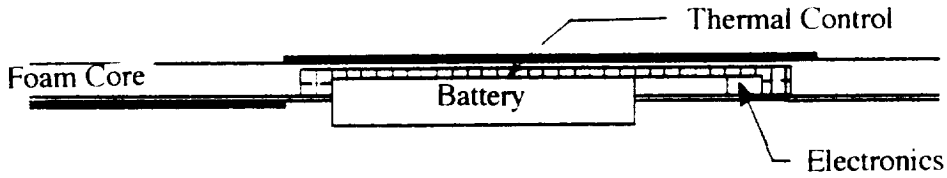

Figure 7-8 Configuration of Bus Solar Array

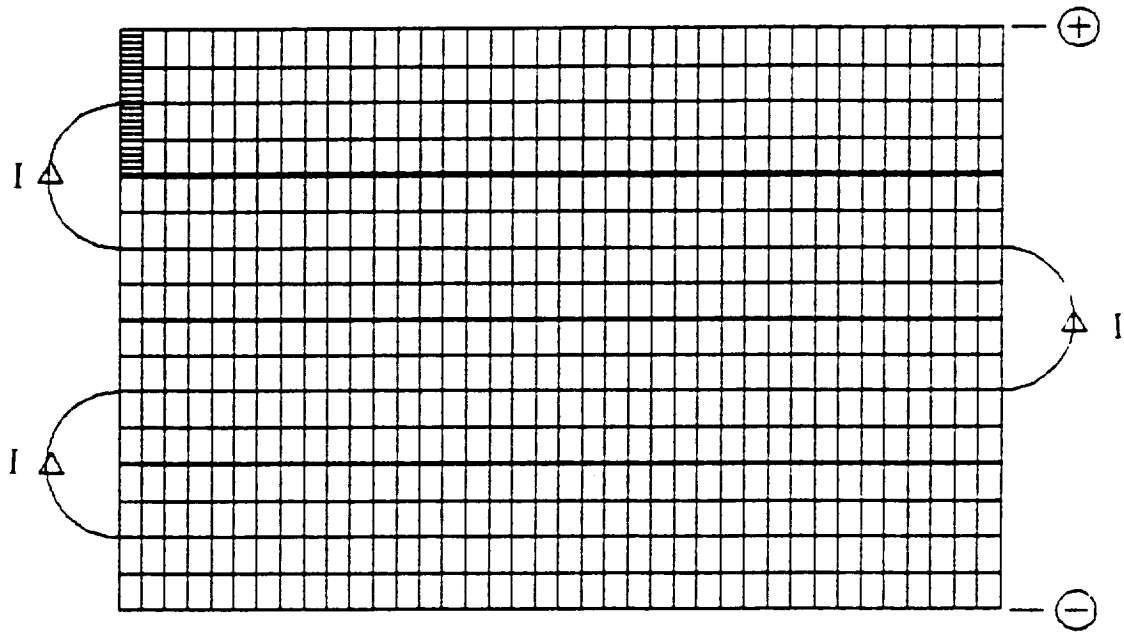

152 GaAs Cells per Panel
Eight 1.06 x 1.62 m Panels on Each Side of Bus

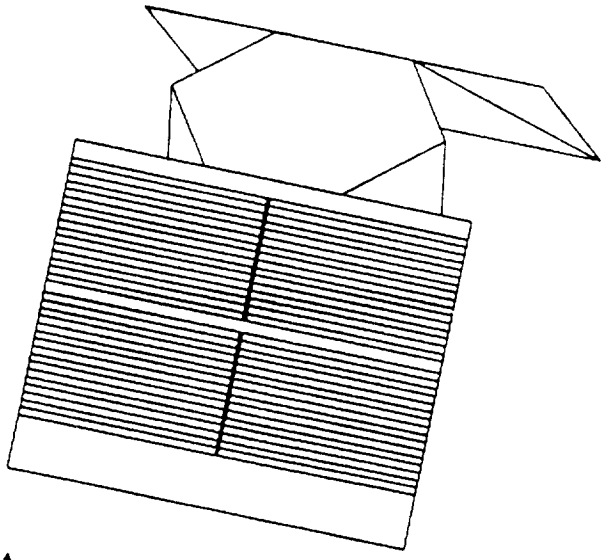

Bus Panel Arrangement

Figure 7-9 Configuration of Module NiCd Batter

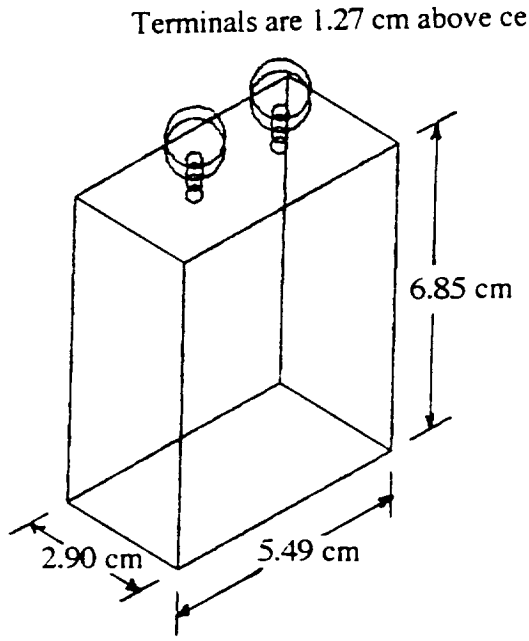

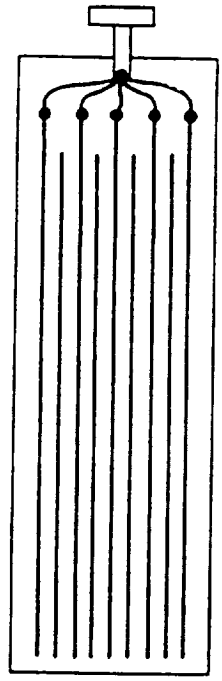

- Positive plate: Nickel-hydroxide electrode
- Negative plate: Cadmium-hydroxide electrode
- Separator: Nylon
- Electrolyte: Potassium hydroxide
- Container: Stainless steel

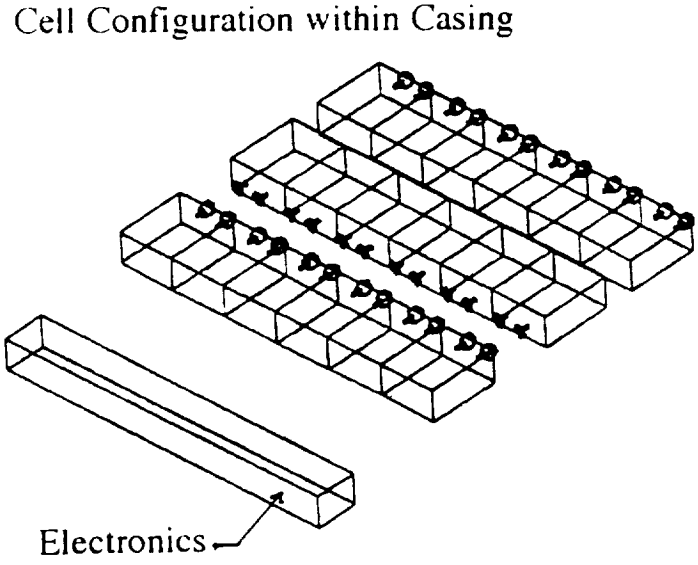

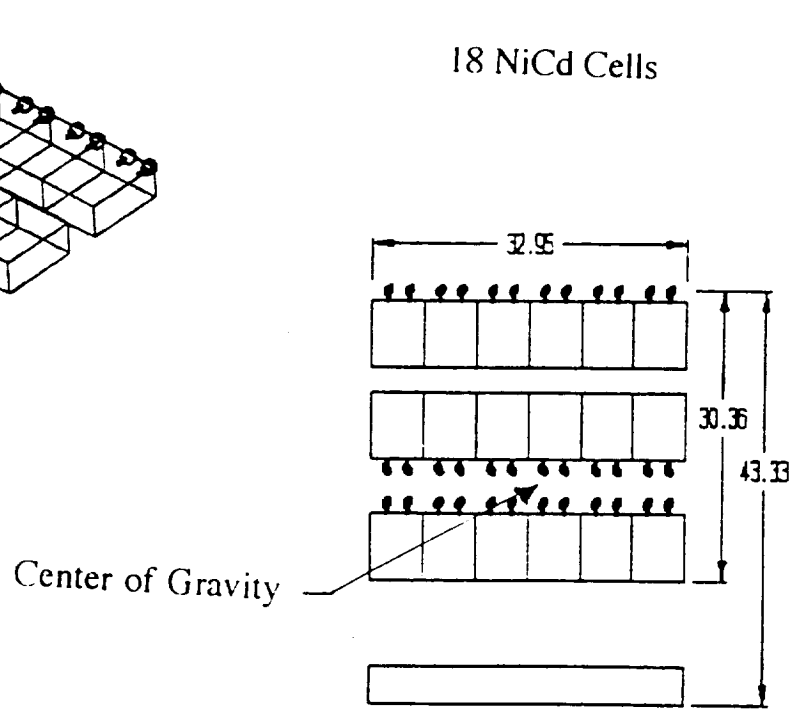

Figure 7-10 Configuration of Bus NiH_2 Battery

Two 90 Cell Series in Parallel

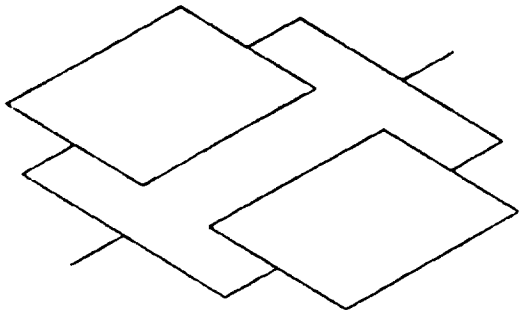

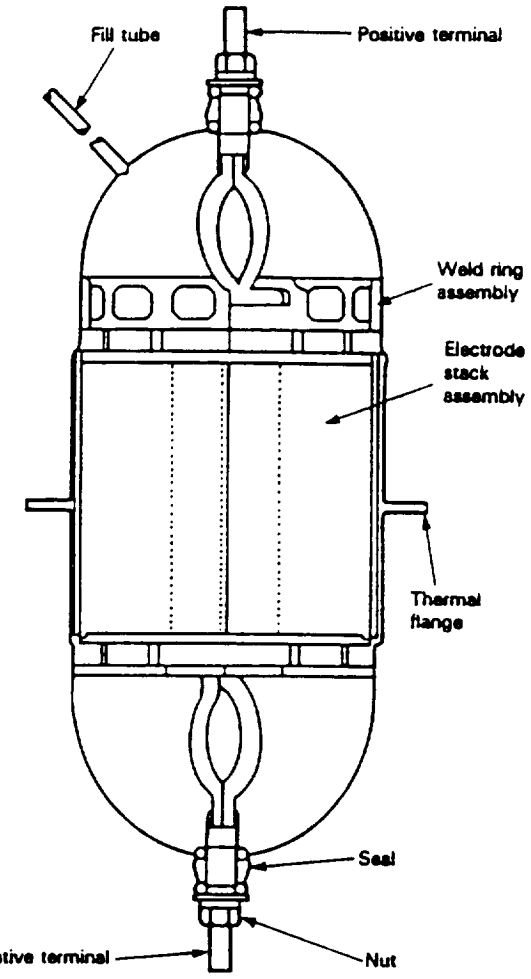

- Negative plate: Platinum black PtFe bonded, PtFe backed electrode
- Positive plate: Scintered nickel electrode
- Separator: Asbestos
- Electrolyte: Potassium hydroxide
- Case: Inconel

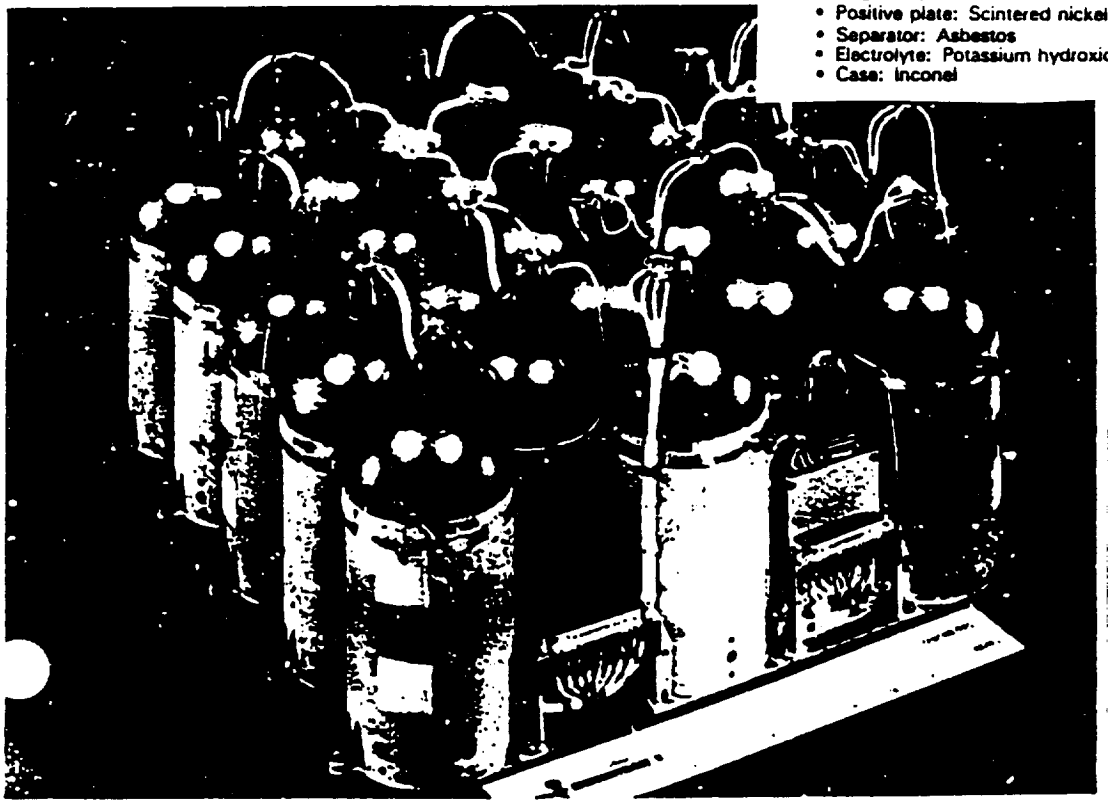

INTELSAT V NICKEL-HYDROGEN FLIGHT BATTERY

8.0 SPACECRAFT BUS SUBSYSTEMS AND STRUCTURE

8.1 Guidance, Navigation, and Control (GN&C) Subsystem

Attitude sensors, control gyroscopes, reaction wheels, and other stability and pointing devices are positioned in the bus. The largest torques which act on the platform as it orbits, are solar radiation pressure torques, and much smaller gravity gradient torques due to the Earth, Sun, and Moon. The required pointing accuracy was specified to be 0.1^0 with a stability of $< 0.01^0/s$.

The control system that was selected for the telescope was a set of four reaction wheels arranged in a tetrahedral configuration, three on axes and one skewed. For further discussion of these requirements, see Section 5 on Stability and Control. Table 8.1 lists attitude and control hardware selected and Figures 8-1 and 8-2 show positioning of the GN&C hardware.

Table 8.1
Attitude and Control Hardware

Sensors	Mass (kg)	Power (W)
1 Inertial Measurement Unit (IMU)	16	63
2 Star Trackers	16	36
2 Horizon Sensors	6	5
4 Sun Sensors	1.2	0
Subtotal	39.2 kg	104 W
Control	**Mass (kg)**	**Power (W)**
4 Momentum Wheels	100	600
Control Computer	25	75
Subtotal	125 kg	675 W
Total GN&C Package	164.2 kg	779 W

The IMU's consist of sensors that measure rotational motion using gyros and translational motion using accelerometers. The units will be strap down systems eliminating the need high for high-powered, gimbaling systems which were once popular. High-resolution software will be used to resolve the output of the fixed sensors. Four sun sensors will be placed on the bus, two on the top surface and two on the bottom for unobstructed views of the sun. On the underside of the bus will be two horizon sensors with rotating heads that will repeatedly scan the Earth's surface. Two star trackers are placed on the top of the bus to accurately track a group of stars within one arc second. The data is stored and used to determine the telescope's inertial position in space.

The momentum wheel package consists of three wheels, each on an axis, and one skewed; they are placed the center of mass, 0.83 m from the observing surface. See section 5 for more details on this system.

8.2 Command and Data Handling (C&DH) Subsystem

The primary responsibilities of the C&DH subsystem is to receive and store data from the phased array surfaces, distribute telemetry and commands to other subsystems. The system includes command encoders and decoders, an atomic clock for timing, data recorders, and a central computer for spacecraft operations. During each observation, vast amounts of data are stored for transmission to Earth at a

later time. The frequency of data transmission will be three to four times a day, depending on the number of observations scheduled for the day. Table 8.2 gives approximate C&DH system specifications that have been selected and Figure 8-3 details a block diagram of the subsystem.

Table 8.2
Command and Data Handling System

Unit	Mass (kg)	Power (W)	Size (cm)
Central Computer	200	100	--
Telemetry and Command Unit	2.5	8.75	12x22x14
Remote Unit	5.2	8.45	12x27x30
Remote Unit w/ μProcessor	7.2	27.0	12x27x39
Solid State Recorder $128*10^6$ bits	6.2	3.0	12x28x47
Power Conditioning Unit (PCU)	10.0	5.0	--
Power Control and Distribution (PCDU)	10.0	5.0	--
Totals	241.1	157.2	

This table specifies requirements for a typical C&DH system and would be subject to technological advances in the future. The telemetry and command unit receives demodulated uplink information and routes it to either the remotes or the central computer. It also formats downlink information which is sent to the transponders. The remote units receive and process commands and requests for data as well as correlate data from each of the modules.

8.3 Communications Subsystem

The communications package selected was a Ku band (12Ghz) system with two transponders for redundancy, each radiating 0.5 W rf output and each having solid state amplifiers. Two 1 meter high gain antennas were selected for data uplink and downlink and are to fixed on the bottom triangular truss. As an antenna's aperature size increases, its gain increases and the transmitter's rf output decreases, thus lowering the power requirements. Because the telescope will not deviate from its orbit more than $1/2^0$, small beamwidth antennas became feasible as well as fixed antennas with no gimballing. Feed arrays will leave the bus and be routed allong the Gr/Ep tubes where the eventually feed into the antennas. Table 8.3 summarizes mass and power requirements for the communications package and Figures 8-1 and 8-2 display locations of communication hardware.

Table 8.3

Communications Subsystem

Component	Mass (kg)	Power (W)
2 Transponders	8.9	
- receiver		4.3
- transmitter		20.0
Filters/switch diplexers/etc.	1.2	0
2 1m High gain antennas	6.5	0
2 Antenna Feed arrays	4.0	4.0
Total	20.6	28.3

8.4 Thermal Control Subsystem

The thermal control system is necessary to maintain the bus systems at operable temperatures. Most spacecraft electronics have temperature limits from 0 to 40^0C while the batteries must be kept between 5 and 20^0C.

The bus requirements dictate a semi-passive system incorporating thermal control coatings and a multilayer insulation (MLI) thermal blanket surrounding the exterior of the bus. The semi-passive system is expected to provide 95% of the temperature control. MLI is the primary insulating material used on spacecraft and consists of 20 to 30 layers of aluminized Mylar spaced by a coarse net material. The outer coating would SiO_2, similar to the Gr/Ep tube coating and also provides radiation protection.

Additional fixed conductance heat pipes will be housed in honeycomb floor to provide more accurate temperature

control to for the electronics. Esitmates of the positioning of such control pipes should be explored in a future detailed design of the bus. Thermal space radiators may be required to provide some cooling for the bus; one possible position would be on the bus wall behind the shield of the solar panels where the cold of space is most always present. Figure 8-1 depicts a possible position for the space radiators. The full requirements of the thermal system cannot be estimated without a thermal cycling profile. However, an estimated power consumption for thermal control based on past spacecraft averages is 20 W. Schematics of this system are presented in Figure 8-4.

8.5 Bus Power Subsystem

The maximum power required for bus subsystems in presented in Table 8.4.

Table 8.4
Subsystems Power

System	Power
GN&C	779 W
C&DH	157.2
Comm.	28.3
Thermal	20
Total	**984.5**

Gallium Arsenide solar cells will provide the necessary power for the bus. Figures 8-1 and 8-2 show the positioning of the solar arrays. Eight panels, each 0.1.62 x 1.06 m will be placed on top of the bus panel to provide power while the observing plane is facing the sun. Extending from the edge of the observing panel to the base of the bus are two rectangular solar panels, 1.9 x 3.34 m, angled down 46^0 from the observing plane. These panels are to provide power while the dish is on its side to the Sun's rays or the back side of the dish is facing the sun. Each has four solar collecting panels 1.62 x 1.06 m. More details of the bus power system can be found in Section 7. Two nickel hydrogen batteries, each 81x90x27 cm and 127 kg, will be housed within the bus to supply power when the telescope is eclipsed.

8.6 Bus Structure and Layout

The bus design must be able to house each subsystem in an efficient and structurally sound manner. The design of the bus requires much additional study, however, Figures 8-1, 8-2, 8-4 present preliminary drawings and layouts.

The design of the bus is primarily dictated by placement of the reaction wheels at the center of mass, 0.83 m from the observing surface. A smaller hexagonal cylinder, 2.3m diameter to the corners (2.0m to the flats), and 2m long, will house the components. This housing structure, as shown in Figure 8-4, consists of aluminum honeycomb panels

mounted to a longeron-stringer frame with three floor panels, one for the power module, one to mount the momentum wheels, and a bottom panel for the communications package. The outer walls would be insulated with MLI and heat pipes would be embedded in the honeycomb as shown.

Two rectangular solar panels, each 9.2 m^2, angle down 46^0, and are attached at the top to the 5.8 m observing panel and fastened at the bottom of the 2.0 m bus. They are supported by Gr/Ep tubes and are fixed rather than deployable. Eight solar panels are on top observatory plane as well as two star trackers and two sun sensors. Refer to figures 8-1 and 8-2 for layouts.

Extended down 5.8 m, are the two parabolic communications antennas, fixed to the graphite tubes. This truss will collapse to the base of the bus for stowing in the launch tube, Figure 8-2. The antenna feed lines will be routed along the Gr/Ep tubes to the central bus.

Floor plans for each level are also shown in Figure 8-2. The top 33 cm will house the nickel hydrogen batteries and the power processing and distribution units. The mid section for the CN&C module measures 84 cm, with the reaction wheels at the center of gravity. The last 33 cm will house the communications package. All of these measurements are preliminary and would require further study.

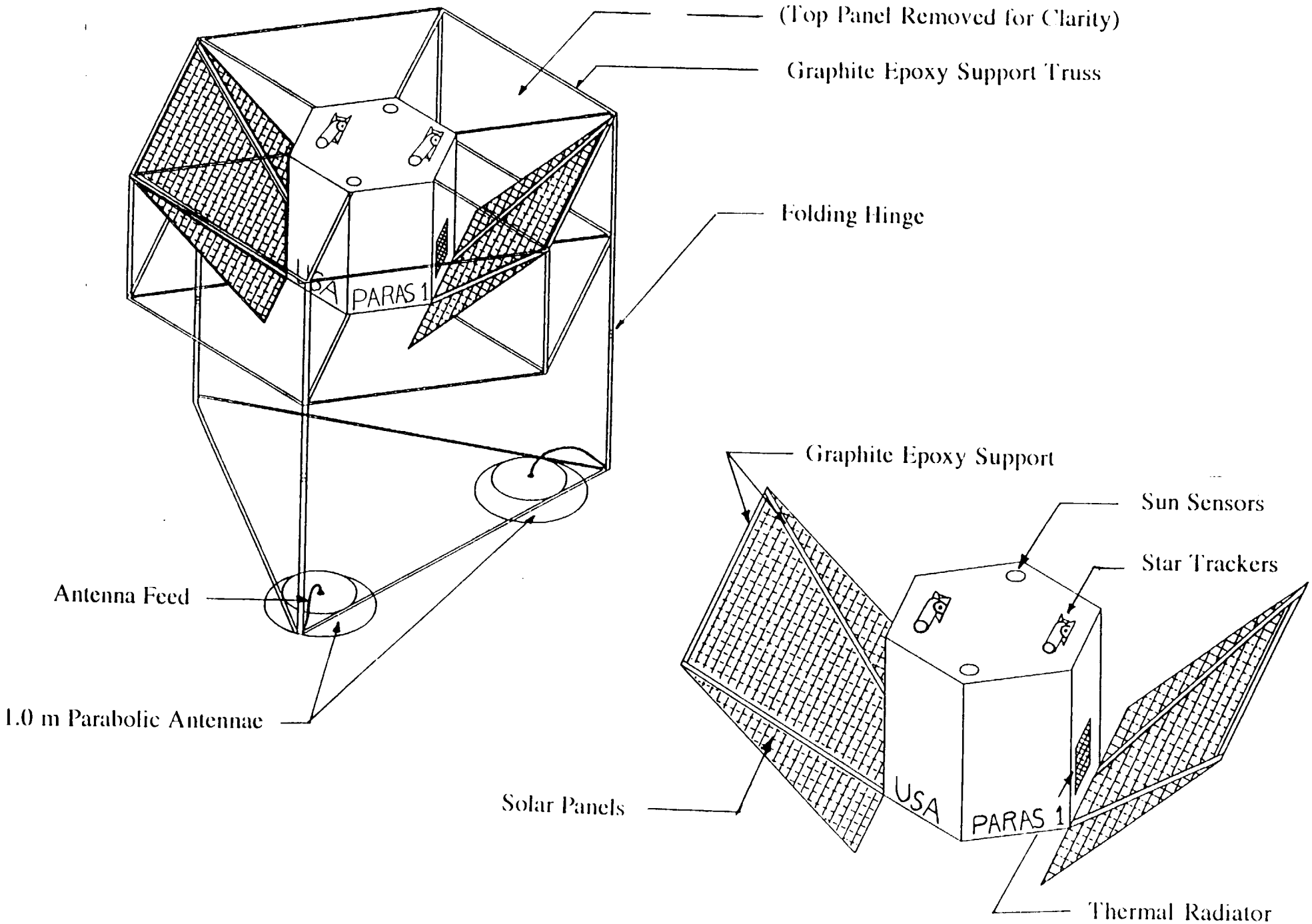

Figure 8-1 **Spacecraft Bus**

Figure 8-2 **Internal Layout**

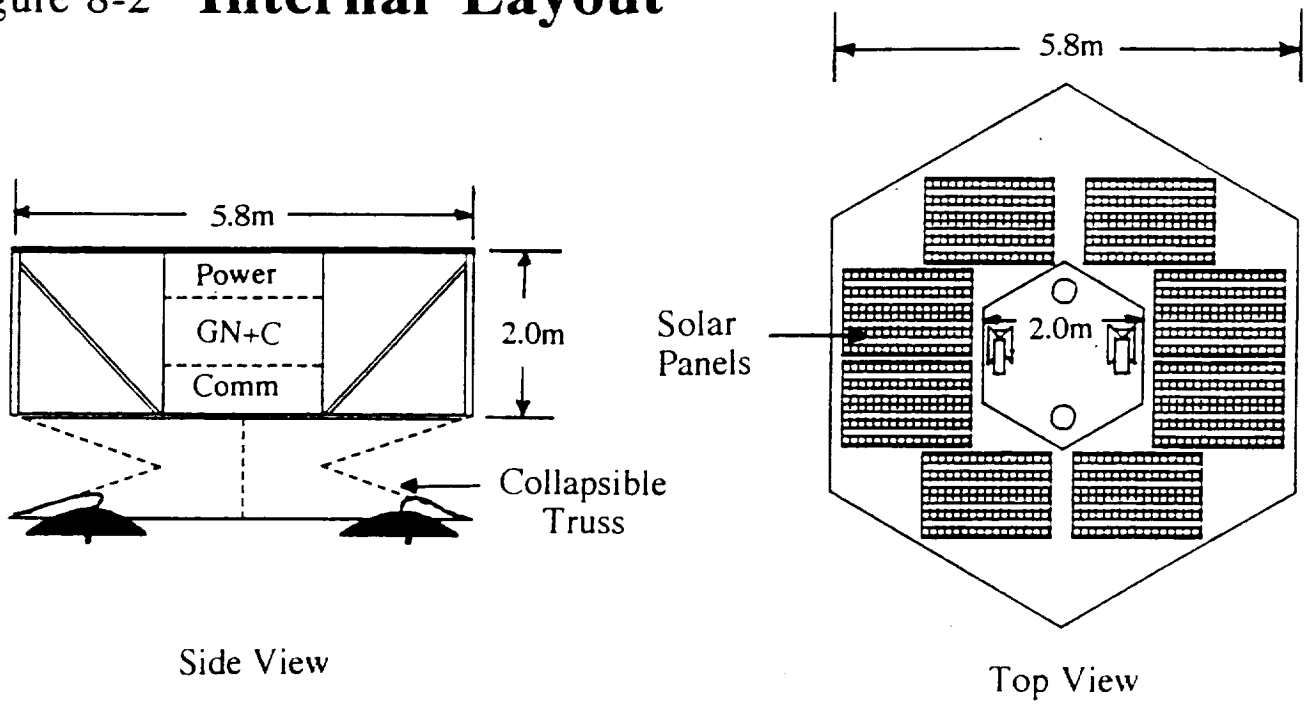

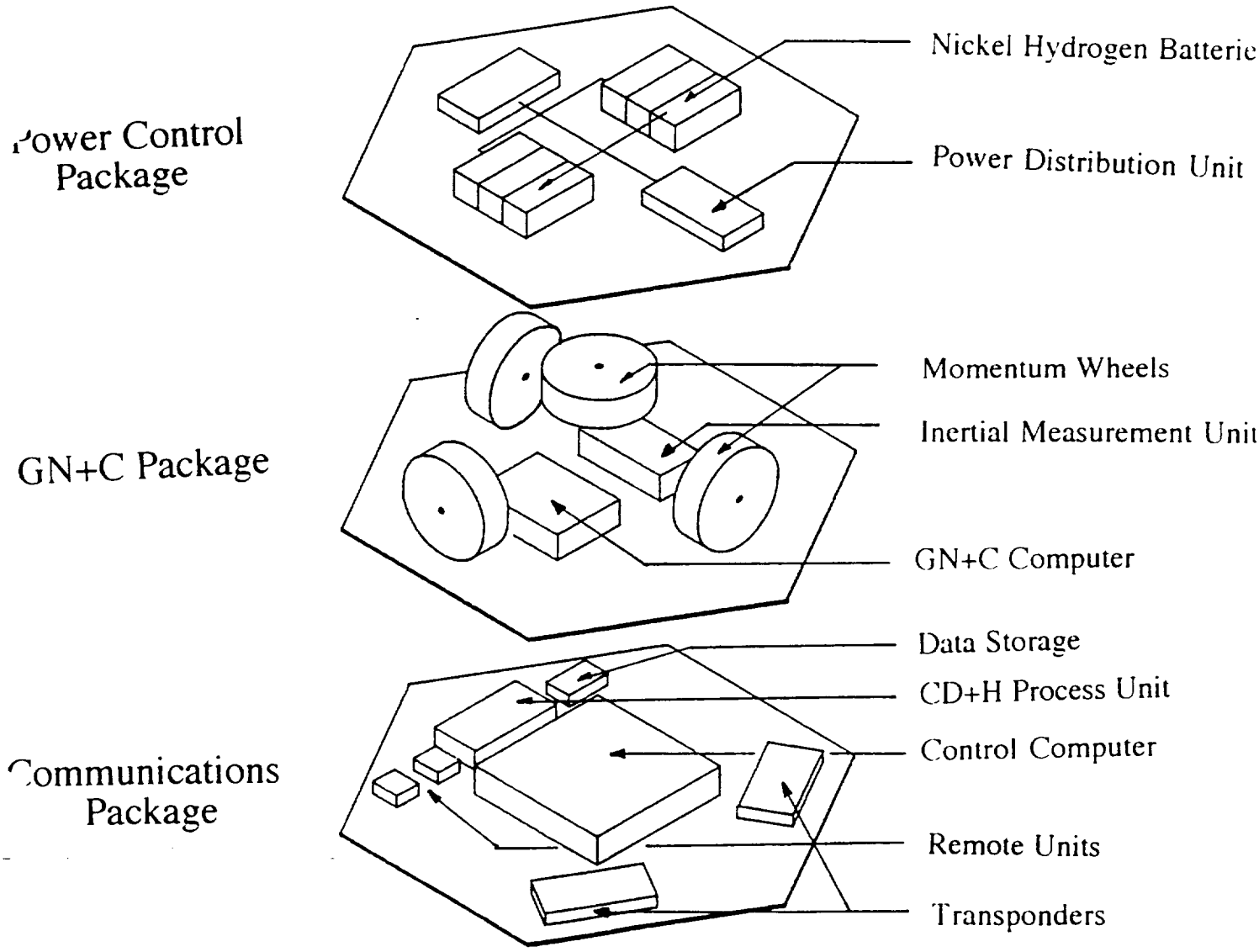

Figure 8-4

Bus Structure and Materials

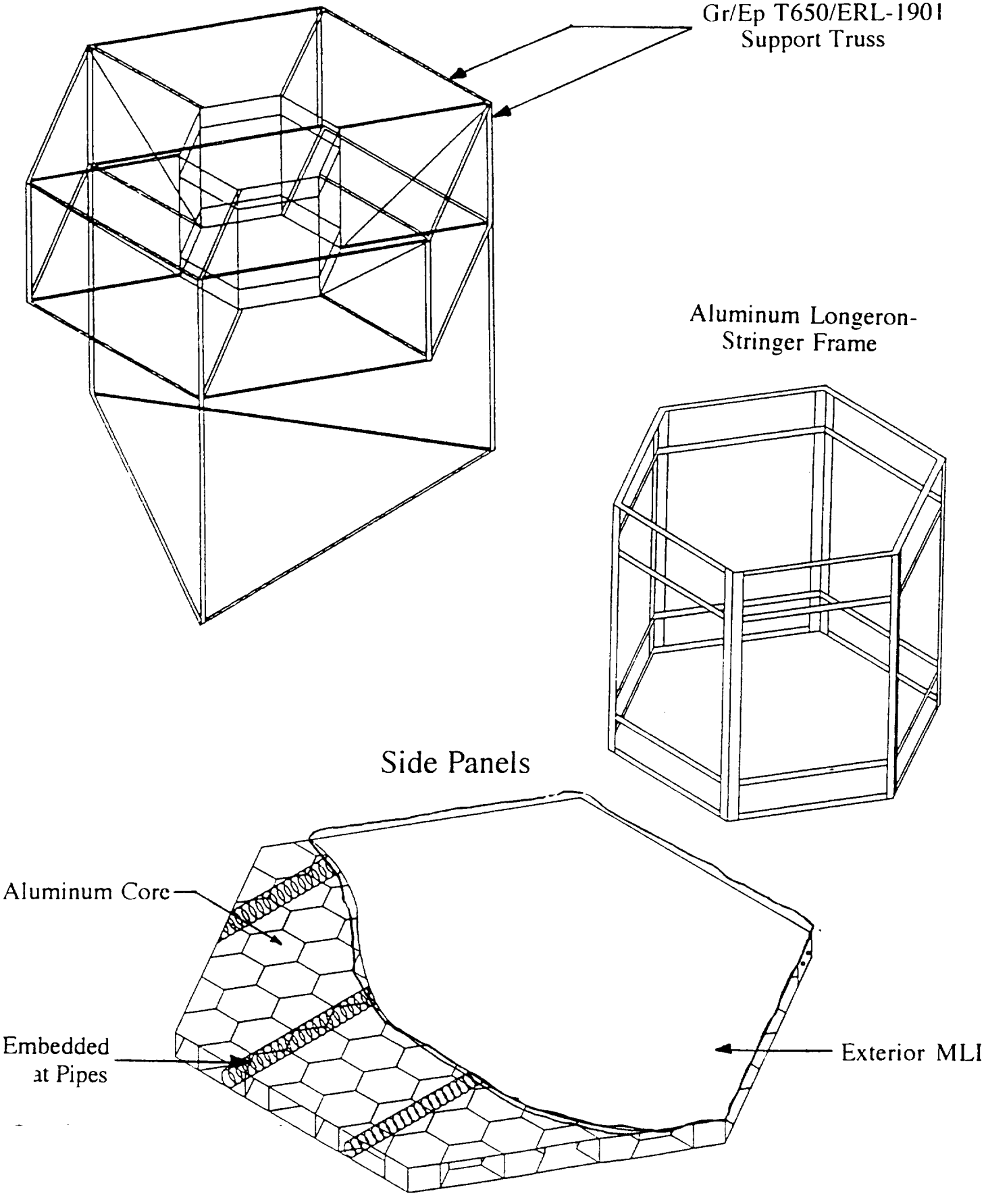

9.0 PARAS SUMMARY

9.1 Overview

Radio Astronomy will greatly benefit from the presence of an orbital radio telescope. The increase in aperture gained by using radio interferometry will clarify images and help solve mysteries faced by todays astronomers.

The PARAS system is an option for such a radio telescope. Previous studies have been done for orbital radio telescopes that use a conventional parabolic reflector. The PARAS study provides an analysis of a phased array system. Other options for space based radio astronomy include observations from telescopes on the far side of the moon.

9.2 Basic Design

The design of the PARAS system has simplicity as its primary emphasis. The construction of such a large structure in space is rife with difficulties and dangers. EVA must be minimized as must the possibility of mission failure due to complicated deployment schemes or lack of redundant systems. For these reasons a modular design was developed.

Every aspect of this design has been modulized. Not only are the observatory modules complete structures, they also have their own power source and electronics (Figure 4.1.) Each module can communicate with the central computer at the bus using the fiber optic connectors that are

incorporated into the structural connector joints (Figure 4.7.) Each of these modules are identical, simplifying the assembly of the structure. And by using discrete, structural modules it becomes easier for manipulator arms or robots to assemble the structure.

The thruster system has also been modulized. Four identical modules will be place on the four compass points of the observatory dish (Figure 5.7, 6.8, 6.9). It is only in the attachment of these four modules to the structure and in the running of the two 50A power cables that any EVA may be required. The complex mounting structure and the communication wire that must be run from each thruster module to the bus will also probably require the attention of a human assembler. However, these are minor tasks that would only require a days work.

As stated earlier, the modular design reduces the risk of system failure due to a structural component failing during deployment or the lack of redundant systems. If one of the modules fails to deploy properly it can simply be replaced by another, identical module. If one of the batteries, or electronics packages were to fail while in GEO that module would cease to operate but the spacecraft could still function normally with its remaining 655 modules. In addition the thruster modules have a set of redundant thrusters and a margin of safety built into the quantity of propellant.

These are very important considerations. A spacecraft of this size would be very expensive and it is very unlikely that the satellite could be repaired once it was placed in GEO. So the modular design is critical in insuring the viability of the mission despite the possibility of various system failures.

9.2.1 The Observatory Module (Section 4)

The observatory module (Figure 4-1) is composed of a large hexagonal panel 6.7 meters in diameter. This panel is composed of a rigid foam sheet 3.4 centimeter thick with a polyimide film sheet on each surface. The phased array surface is incorporated into the top of the panel. An electronics package, and battery are located in the center of the panel. A small collection of solar cells on the top and bottom of the panel will power the electronics and charge the battery. The electronics will operate the phased array surface and process the data for optical transfer to the bus.

At three of the corners of the panel are titanium connector joints. These joints, and the set beneath them, are the locking mechanisms by which the modules are joined together. Incorporated into the top joints are the fiber optic connectors. The joints also serve as attachment points for graphite tension wires and caps for the vertical inflatable members. The vertical inflatable members are 5.8 meters in length and link the top panel to a triangular

truss of Gr/Ep tubes. These tubes form a equilateral triangle, 5.8 meters for each side. At each of the corners of the triangle are connector joints similar to the ones found on the observatory panel (sans optic connector.) The mass for each module is given in Table 9.1.

Table 9.1
Mass of Observatory Module

Component	Mass (kg)
Battery	2.47
Solar Cells	4.44
Electronics and Optics	0.50
Top Connector Joint (3)	1.253
Foam Panel	9.279
Graphite Tension Wires (6)	0.148
Inflatable Tubes (3)	0.133
Graphite Epoxy Tubes (3)	4.023
Bottom Connector Joint (3)	1.32
Material Coatings	0.066
Total	23.632

9.2.2 The Thruster Module (Section 5)

The Thruster Module (Figures 5.6, 6.8) houses four carbon overwrapped stainless steel tanks 1.37 meters in diameter, and a carbon overwrapped titanium tank 0.777 meters in diameter. Two of the large tanks contain hydrazine and the other two contain NTO. The small tank contains high pressure helium used to pressurize the fuel tanks. Each module has a thruster package with 4 nozzles and engines for each direction and another 4 for redundancy. The fuel tanks and thrusters are mounted to a Gr/Ep frame that has structural attachments and connector joints to attach it to the observatory structure (Figures 6-9 to 6-12).

The monopropellant thrusters will be required to fire once a day to desaturate the momentum wheels responsible for attitude control. These operations will last less than 80 seconds. The arcjet thrusters will be needed for orbital corrections or stationkeeping. These firing will last no longer than six hours a day and will only have to be operated during a fraction of a year. These firings will be of a low thrust so will require a very short time for the structural vibrations to dampen out.

The subsequent mass for each module is given in table 9.2.

Table 9.2
Mass of Thruster Modules

Component	Mass (kg)
Thrusters & Associated Equipment (16)	713.6
Propellant	2685.2
Tankage	61.8
Pressurizing System	75.1
Tankage Structure	112.9
Module Frame and Connector Joints	302.8
Power Generation and Storage	1250.0
Total	5201.4
Mass for each module	1300.4

9.2.3 The Bus Module (Section 8)

The bus module contains the central data processing unit for the observatory, the command computer, the communications system, attitude sensors and the attitude control system (Figure 8-1 to 8-4). The bus itself is a hexagonaly shaped honeycomb panel box. This box is suspended within a graphite epoxy truss so that the entire

module is of the same size and has the same connection joints as a observatory module.

The power system consists of three solar panels. One on the top and two on the sides of the bus. A large array of nickle/hydrogen battery cells provides the energy storage capacity required for the systems in the bus. The attitude control is performed by a guidance, navigation and control computer that samples data from sensors and corrects and controls the attitude of the spacecraft with four momentum wheels.

A central computer receives data from the observatory modules processes it and stores the data for transmission down to earth. The computer is also responsible for processing and instructions from earth and distributing commands to the various modules. Two one meter high gain antenna will be used for communications with ground stations.

The subsequent mass for the bus module is given in Table 9.3.

Table 9.3
Mass of Bus Module

Component	Mass (kg)
Guidance, Navigation and Control System	164.2
Control and Data Handling System	241.1
Communication System	20.6
Gr/Ep Truss Members	21.2
Connection Joints (6)	3.66
Honeycomb Panel and Bus Structure	621.0
Solar Panels	32.3
Batteries	254.0
Total	1358.1

9.3 Launch and Assembly

The PARAS modules will be launched using two National Launch System vehicles. The estimated size of the launch container is 6.7 meters in diameter and 27 meters in length. The maximum lift capacity is 70 metric tons. The arrangement for the modules in the launch vehicle is shown in Figure 9-1.

When placed in LEO the bus will be removed and deployed. Remote manipulator arms or a robot will begin attaching the deployed modules onto the bus in a radial pattern. When completed the thruster modules will be attached and wires will be run to the bus. The satellite can then be system checked before its deployment into GEO. The entire satellite is shown in Figure 9-2.

The final mass for the entire spacecraft is shown in Table 9.4.

Table 9.4
PARAS Observatory Mass

Module	Mass (kg)
Observatory Module (656)	15502.6
Thruster Modules (4)	5201.4
Bus Module	1358.1
Total	22062.1

9.4 The Mission

It was discussed in the introduction how this satellite will increase the resolution of radio observations several fold. Assuming the wavelengths chosen for the observatory are 1.35 and 18 cm this will allow a 30 and 0.1 microsecond resolution respectively. This corresponds to the ability to

resolve objects 4 light days across when they are the distance of the galaxy M87. The sensitivity of the satellite will allow the dynamic range map of 100 to 1 to be achieved. This can be done when only 25-50 mJy sources are available at 1.35 cm or 5-10 mJy sources at 18 cm. This ability to detail the dynamic properties of the most distant of radio sources will allow significant advances in astronomy and cosmology.

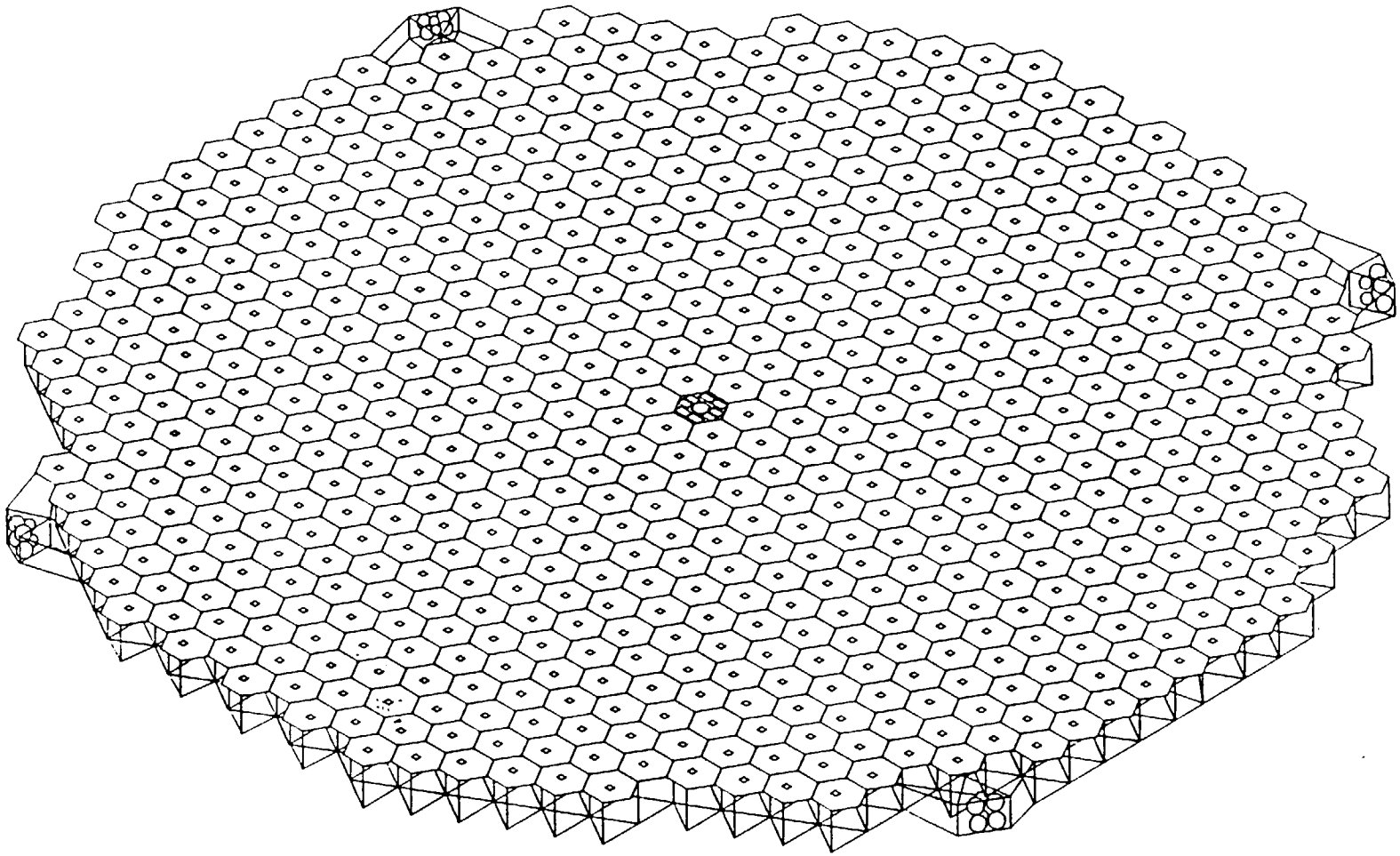

22,060 Kg

Figure 9-1 **Final Configuration and Mass**

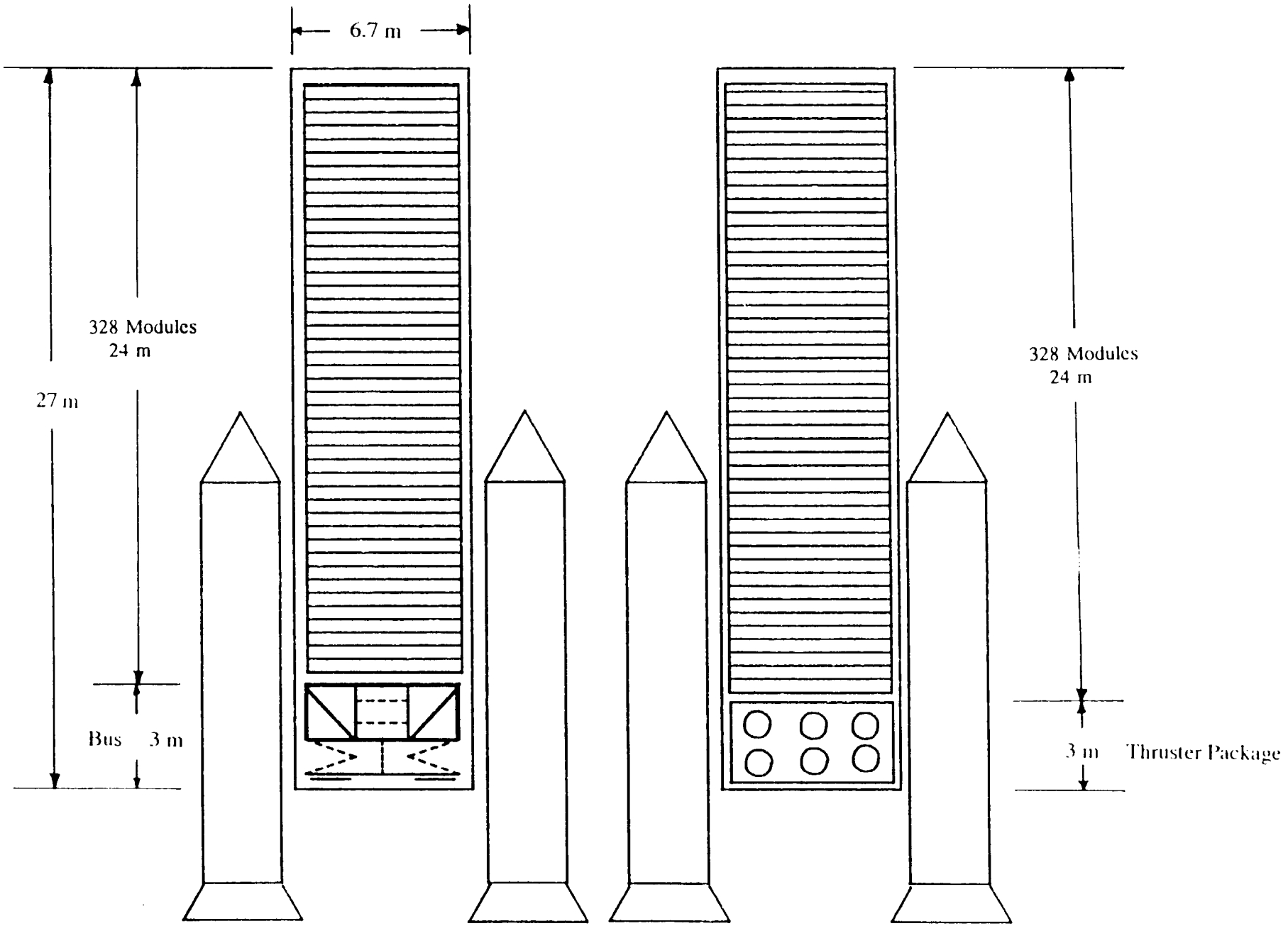

Figure 9-2 **Launch Manifest**

REFERENCES

Flood, B. and H. Brandhorst. Space Solar Cells.

Wertz, James R. and Wiley J. Larson. Space Mission Analysis and Design.

Morrow, G. and T. Yi (eds.). The 1986 Goddard Space Flight Center Battery Workshop. NASA Conference Publication 2468, November 18-19, 1986 at Greenbelt, Maryland.

Bate, Roger R., Donald D. Mueller, and Jerry E. White. Fundamentals of Astrodynamics. Dover Publications, Inc. New York, NY, 1971.

Scott, Willard R. and Douglas W. Rusta. Sealed-Cell Nickel-Cadmium Battery Applications Manual. NASA Reference Publication 1052. Greenbelt, MD, 1979.

The 1990 NASA Aerospace Battery Workshop. NASA Conference Publication 3119, December 4-6, 1990 at Huntsville, AL.

Sullivan, Ralph M. "Space Power Systems," Notes from Space Systems I, Johns Hopkins University Applied Physics Laboratory. Fall 1989.

Slifer, Luther W., Jr. "Performance, Size, Mass and Cost Estimates for Projected 1kW EOL Si, InP, and GaAs Arrays." N91-19199

Mills, Michael W. and Richard M. Kurland. "The Impact of Solar Cell Technology on Planar Solar Array Performance." N89-24715

Cataldo, Robert L. "Parametric and Cycle Tests of a 40-A-hr Bipolar Nickel-Hydrogen Battery." NASA Technical Memorandum 88793, 21st Intersociety Energy Conversion Engineering Conference, San Diego, CA, Aug 25-29, 1986.

El-Genk, Mohamed S. and Mark D. Hoover. Space Nuclear Power Systems. AIP Conference Proceedings 217. Vol. 2, Albuquerque, New Mexico, 1991.

Large Space Antenna Systems Technology - 1982. Nasa Conference Publication 2269, Parts 1 and 2, November 30 - December 3, 1982 at the Langley Research Center, Hampton, Virginia.

Sorbello, Robert M., "Advanced Satellite Antenna Developments for the 1990's." AIAA 12th International Communication Systems Conference, Arlington, Virginia. March 13-17, 1988.

Enviromental Effects on Materials for Space Applications. AGARAD Conference Proceedings No. 327. Totonto, Canada. September 19-24, 1982.

Fox, Derek J. Fox. Space Enviromental Effects on Graphite-Epoxy Compressive Properties and Epoxy Tensile Properties. Blacksburg, Virginia. June, 1987.

Large Space Antenna Systems Technology, 1984. Nasa Conference Publication 2368, Part 1. Langley Research Center, Hampton, Virginia. December 4-6, 1984.

Olstad, Walter B. Heat Transfer, Thermal Control, and Heat Pipes. AIAA Publication, New York, New York, 1980.

Piscane, Vincent L. Space Systems I and II. Notes fron the Johns Hopkins University Applied Physics Laboratory. June 1989.

Proceeding of the 18th International SAMPE Technical Conference. October 7-9, 1986.

Wertz, James R.; Larson, Wiley J. Space Mission Analysis and Design. Kluwer Academic Publishers: Dordrecht, 1991.

"The Basics on Bonded Sandwich Construction, TSB 124." Hexcel Corporation, Fall 1989.

"Mechanical Properties of Hexcel Honeycomb Materials, TSB 120." Hexcel Corporation, Fall 1989.

Amoco Performance Products, Inc. Manufacturer specifications, 1991.

CIBA-CEIGY Group Companies. Manufacturer specifications, 1991.

Rohm Tech, Inc. Malden, MA. Manufacturer specifications, 1991.

"Upilex Polyimide Films." ICI Films. Wilmington, Delaware. 1991.

Reibaldi, G. G. "QUASAT Program: The ESA Reflector." Pergamon Journals, Ltd. Great Britain, 1987.

Drusch, Harry W. and Carl L. Hendricks. "Protective Coatings for Composite Tubes in Space Applications." SAMPE Quarterly, 1987.

Knott, Tamara W. and Michael W. Hyer. "Thermally-Induced Stresses in Graphite-Epoxy Tubes Coated with Aluminum Foil." SAMPE Quarterly, 1987.

Wertz, James R.; Larson, Wiley J. Space Mission Analysis and Design. Kluwer Academic Publishers: Dordrecht, 1991.

Wertz, James R., ed. Spacecraft Attitude Determination and Control. Kluwer Academic Publishers: Dordrecht, 1978.

Sovey, James S.; Pidgeon, David J. "Advanced Propulsion for LEO and Geo Platforms," AIAA-90-2551, July 1990.

Rawlin, Vincent K.; Majcher, Gregory A. "Mass Comparisons of Electric Propulsion Systems for NSSK of Geosynchronous Spacecraft," AIAA-91-2347.

Byers, David C.; Terdan, Fred F.; Myers, Ira T. "Primary Electric Propulsion for Future Space Missions," AIAA-79-0881, May 1979.

Stone, James R.; Bennett, Gary L. "The NASA Low Thrust Propulsion Program," AIAA-89-2492, July 1989.

Bennett; Watkins; Byers; Barnett. "Enhancing Space Transportation: The NASA Low Thrust Propulsion Program," NASA-TM-4244, October 1990.

Sutton, George P., Rocket Propulsion Elements, John Wiley & Sons,New York, 1986.

Rosenberg and Schoenman, "A New Generation of High Performance Engines for Spacecraft Propulsion," AIAA-91-2039, June 1991.

Stechman, R.C.;and Smith, J.A., "Monomethyl-hydrazine Versus Hydrazine Fuels: Test Results Using Flight Qualified 100 lbf and 5 lbf Bipropellant Engine Configurations," AIAA-83 1257, June 1983.

Patterson, M.J.; Curran, F.M. "Electric Propulsion for 10 KW Class Earth-Space Missions," NASA-TM-102337, May 1989.

Gruber, R.P.; Gott, R.W.; Haag, T.W. "5 KW Arcjet Power Electronics," AIAA-89-2725.

Knowles, S.C.; Yano, S.E. "Design, Testing, and Integration of a Flight-Ready Hydrazine Arcjet System," AIAA-89-2720, July 1989.

Morren, W. E.; Curran, F. M. "Preliminary Performance and Life Evaluationsm of a 2-kW Arcjet," AIAA-91-2228, June 1991.

Goodfellow, K. D.; Polk, J. E. "Throttling Capabnility of a 30-kW Class Ammonia Arcjet," AIAA-91-2577, June 1991.

Beattie, J.R.; Penn, J.P. "Electric Propulsion - A National Capability," AIAA-89-2490, July 1989.

Manzella; Curran; Myers; Zube. "Preliminary Plume Characteristics of an Arcjet Thruster." AIAA-90-2645, July 1990.

Smith; Roberts; Davies; Vaz. "Development and Demonstration of a 1.8 kW Arcjet Thruster." AIAA-90-2547, July 1990.

Feconda, R.T.; Weizman, J.I. "Satellite Raction Control Subsystem with Augmented Catalytic Thrusters," AIAA-84-1235, June 1984.

Roberts, C.R. "Life Demonstration of an Uprated Augmented Catalytic Thruster," AIAA-87-0996, May 1987.

Zee, Chung-Hung. The Theory of Geosynchronous Satellites, Kluwer Academic Publishers, Dordrecht, 1989.

Bate; Mueller; and White. Fundamentals of Astrodynamics. Dover Publications: New York, 1971.

Battin, Richard H. An Introduction to the Mathematics and Methods of Astrodynamics. AIAA Education Series.

The Astronomical Almanac. US Government Printing Office: Washington, 1991.

Ruppe, H. O. Introduction to Astronautics. Academic Press Inc.New York: 1967.

"Star Tracker Users Guide." Ball Inc.

"Sun Sensors." Lockheed Missiles and Space Comapny Fact Sheet.

Tai; Kascak; McLaughlin; Ward. "An Innovative Design For Autonomous Backup Attitude Control of the Gamma Ray Observatory."

Jerkovsky; Keranen; Koehler; Ward. "GRO Attitude Control and Determination." AAS-86-032, Febuary 1986.

Balla, John; Petty, Paul. "A Survey of Electrically Propelled Rockets." Unpublished.

Hearn, H.C. "Evaluation of Bipropellant Pressurization Concepts for Spacecraft." Journal of Spacecraft and Rockets, Vol. 19, July 1982, pp. 320-325.

Vickers; Babel; Parechanian. "Materials and Design Selection for Minimum Weight Pressure Vessels." AIAA-90-2349, July 1990.

Haddock; Morris; Darms. "Safety of Filament Wrappped Graphite/Epoxy Composite Pressure Vessels for Aerospace Applications." AIAA-91-2409, June 1991.

Braun; Papanicolopoulos; Devy. "Advanced Composite Fiber/Metal Pressure Vessels for Space System Applications." AIAA-91 1976, June 1991.

Tiller; Khawand; Murrray; McClellan. "Design and Qualification of a Carbon Overwrapped, Aluminum Lined Pressurant Tank for the INTELSAT VII Satellite." AIAA-91-2092, June 1991.

Tiller; Murray; Veys. "Design and Development of a Carbon Overwrapped, Aluminum Lined Spherical Pressure Tank." AIAA-90 2225, July 1990.

Haddock; Darms. "Space System Appplications of Advanced Composite Fiber/Metal Pressure Vessels." AIAA-90-2227, July 1990.

Veys; Cederberg; Schimenti. "Design and Analysis Techniques For Composite Pressurant Tankage with Plastically Operating Aluminum Liners." AIAA-90-2345, July 1990.

Vickers; Babel; Parechanian. "Materials and Design Selection for Minimum Weight Pressure Vessels." AIAA-90-2349, July 1990.

Cardin, J. "A Standardized Spacecraft Resupply Interface." AIAA-91-1841, June 1991.

Heubush, Henry; Pugmire, Kent. "The Compatability of Stainless Steels with Nitrogen Tetroxide and Hydrazine." AIAA-90-2063, July 1990.

NASA Conference on Large Space Antenna Systems Technology, Large Space Antenna Systems Technology. NASA, Langely. Dec. 4-6, 1984.

NASA Conference on Large Space Antenna Systems Technology, Large Space Antenna Systems Technology. NASA, Langely. Nov. 30 - Dec. 3, 1982.

Fox, Derek J., "Space Environmental Effects on Gr/Ep Compressive Properties and Epoxy Tensile Properties." Diss. VPI&SU, 1987.

Forward, Robert L. "Solar Photon Thruster." Journal of Spacecraft and Rockets. July 1990.

Knott. Tamara W,; Hyer, M. W. "Thermally-Induced Stresses In Graphite-Epoxy Tubes Coated With Aluminum Foil." SAMPE Quarterly. April 1989.

Dursch, Harry W.; Hendricks, Carl L. "Protective Coatings For Composite Tubes in Space Applications." SAMPE Quarterly, Oct., 1987.

Bernasconi, M. C.; Rits, W. J. "Inflatable, Space-Rigidized Support Structures For Large Spaceborne Optical Interferometer Systems." Acta Astronautica. v 22 1990.

Ribaldi, G. G.; Bernasconi, M. C. "QUASAT Program: The ESA Reflector." Acta Astronautica. v 15 1987.

Agrawal, Brij N. Design of Geosynchronous Spacecraft. Englewood Cliffs, NJ: Prentice Hall, 1987.

Stuhlinger, Ernst. Ion Propulsion for Space Flight. McGraw-Hill Book Co., New York, 1964.

Jahn, Robert G. Physics of Electric Propulsion. McGraw-Hill Book Company, New York, 1968.

Oates, Gordon C. Aerothermodynamics of Gas Turbine and Rocket Propulsion. AIAA Publications, Washington, 1988.

Patterson, M. J.; Curran, F. M. "Electric Propulsion Options for Deep Space Missions". NASA-TM-102337, May 1989.

Garner; Brophy; and Pless. "Ion Propulsion System Design and Throttling Strategies for Planetary Missions". AIAA-88-2910, July 1988.

Kami, S.; Dulgeroff, C. "Status of the J-Series 30-cm Mercury Ion Thruster". AIAA-82-1904, November 1982.

Byers; Terdan; and Myers; "Primary Electric Propulsion for Future Space Missions". NASA TM-79141, May 1979.

Sovey, James S.; and Pidgeon, David J. "Advanced Propulsion for LEO and GEO Platforms". AIAA-90-2551, July 1990.

Sovey, James S. "Improved Ion Containment Using A Ring-Cusp Ion Thruster". AIAA-82-1928, November 1982.

Beattie, J. R.; and Kami, S. "Advanced-Technology 30 cm-Diameter Mercury Ion Thruster". AIAA-82-1910, November 1982.

Beattie; Matossian; and Poeschel. "Xenon Ion Propulsion Subsystem". AIAA-85-2012 September 1985.

Beattie; Matossian; and Robson. "Status of Xenon Ion sian; and Robson. "Status of Xenon Ion Propulsion". AIAA-87-1003, May 1987.

Rawlin, Vincent K. "Operation of the J-Series Thruster Using Inert Gas". AIAA-82-1929, November 1982.

Rawlin, Vincent K.; and Patterson, Michael J. "Performance of 10-Kw Class Xenon Ion Thrusters". AIAA-88-2914, July 1988.

Rawlin, Vincent K.; and Majcher, Gregory A. "Mass Comparisons of Electric Propulsion Systems for NSSK of Geosynchronous Spacecraft". AIAA-91-2347, 1991.

Brophy, J. R.; and Aston, G. "A Detailed Model of Ion Propulsion Systems". AIAA-89-2268, July 1988.

Patterson, Michael J.; and Foster, John E. "Performance and Optimization of a Derated Ion Thruster for Auxiliary Propulsion". AIAA-91-2350, June 1991.

Byers; Bennet; Watkins; and Barnet. "Enhancing Space Transportation: The NASA Program to Develop Electric Propulsion". NASA-TM-4244, October 1990.

Stone, James R.; and Bennet, Gary L. "The NASA Low Thrust Propulsion Program". AIAA-89-2492, July 1989.

Agrawal, Brij N. Design of Geosynchronous Spacecraft. Prentice Hall, Inc.: Englewood Cliffs, NJ. 1986.

Tinmat, Y. M. Advanced Chemical Rocket Propulsion. Academic Press: London. 1987.

Galecki and Patterson. "Nuclear Powered Mars Cargo Transport Mission Utilizing Advanced Ion Propulsion." AIAA-87-1903. June, 1987.

Hardy; Rawlin; and Patterson. "Electric Propulsion Options for the SP-100 Reference Mission." NASA-TM-88918. January, 1987.

Zafran and Jackson. "Electrothermal Thruster Diagnostics. Vol. II." NASA-CR-168174 Vol-2, 1983.

Collin, Robert E. Antennas and Radiowave Propagation, McGraw-Hill Book Company, 1985

Christiansen, W. N. and Hogbom, J. A., Radiotelescopes, 2nd ed., Cambridge University Press, 1985

Thompson, A. R., Moran, J. M., Sivenson, G. W. Jr., Interferometry Synthesis in Radio Astronomy, John Wiley & Sons, 1986

Fauti, R., Kellerman, K., and Setti, G., VLBI and Compact Radio Sources, D. Reidel Publishing Co, 1984

Zensus, J. A., Pearson, J. J., Parsec Scale Radio Jets, Cambridge University Press, 1990

Appendix 4 - Material Selection

List of Symbols

E	Tensile Modulus of Elasticity
G	Shear Modulus of Elasticity
v	Poisson's Ratio
a_t	Thermal expansion Coefficient
t	Nominal thickness
p	Material Density
Q	Reduced Material Stiffness Matrix
Q_{FM}	Q Matrix for Film
Q_{FO}	Q Matrix for Foam
A	In-Plane Stiffness Matrix

Observatory Panels

Comparison of Facesheets

	Upilex Poly. Film	Gr/Ep T300/934	Gr/Ep T650/ERL-1901	Kevlar 49
Density (g/cm^3)	1.47	1.60	1.59	1.38
Compr. (ksi)	--	250	250	--
Tension				
(ksi)	56.775	222	300	200
(MPa)	392	1530	2100	1378
E				
(Msi)	1.28	18.9	22.0	10.9
(GPa)	8.83	130	150	75.0
t				
(in)	9.84E-4	.005	.005	.005
(mm)	.025	.127	.127	.127
a_t				
($in/in/^0F$)		.75E-6	-.1E-6	
($cm/cm/^0C$)	9.0E-6			-4.0E-6
Specific Stiffness				
E/p (Nm/kg)	6000	8,130	94,300	54,300

The most attractive graphite-epoxy is the T650/ERL-1901 for proposed honeycomb facesheets and truss members due to overwhelming stiffness, high modulus of elasticity, E, and negative CTE.

The polyimide film, due to its low density and extremely thin, nominal ply thickness, make it an attractive candidate for the observatory panels.

Comparison of Cores

	Rohacell 31 IG	HRH-10 1/8"	HRH-10 1/16"	HRH 49 Kevlar
Density (kg/m^3)	32.0	28.8	54.5	69.0
Compr. (psi)	57	130	205	122
Tension (psi)	142	--	--	--
E (psi)	5120	15,000	20,000	125,000
G (psi)	1850	3700	6000	2500
v	.384	--	--	--

The most attractive core material is the 1/8" nomex core, HRH-10, due to low mass, high compression strength and high modulus, E. It is desirable to select a core with small hex size so that the Gr/Ep sheets do not warp, or bubble when the sandwich is cured at 350^0F.

Rohacell is similar in mass, and could be used withe Gr/Ep facesheets, however, it must be used with polyimide film. The foam is an isotropic material supplying both tensile and compressive properties where honeycomb cores only supply compressive properties. Poisson's ratio v, is therefore not applicable to honeycomb cores.

The following options were formulated: Option 1) Rohacell/Upilex film, 2) HRH-10-1/8" / Gr/Ep T650/ERL1901, 3) HRH 49 / Kevlar 49. To find the effective engineering material properties, E, G, and v, Option 1 can be analyzed using Composite Laminate Theory for isotropic materials. Analysis for both honeycomb options makes two assumptions: the compression member is the core, and the facesheets are the tensile member. A nominal thickness of cores was 2.5 cm was chosen for comparison of cores. The following properties are calculated below.

Option 1

$$Q_{FM} = \begin{bmatrix} 1.46 & .51 & 0 \\ .51 & 1.46 & 0 \\ 0 & 0 & .47 \end{bmatrix} *10^6 \text{ ps} \qquad Q_{FM} = \begin{bmatrix} 5.58 & 1.60 & 0 \\ 1.60 & 5.58 & 0 \\ 0 & 0 & 1.99 \end{bmatrix} *10^3 \text{ psi}$$

Where $Q11=Q22= E/(1-v^2)$ $Q33= E/2(1+v)$ $v = (E/2G) -1$

Assuming a laminate of 25um film / 2.5cm foam / 25um film, the complete laminate A matrix can be calculated.

$$A = \begin{bmatrix} 8.36 & 1.57 & 0 \\ 1.57 & 8.36 & 0 \\ 0 & 0 & 2.88 \end{bmatrix} *10^3 \text{ psi} \quad \text{where } A = \text{Sum}(Q_i * t_i) \; i=1,..,N$$

Effective engineering properties:

$$E = 1/h\ (A11*A22 - A12^2)/(A22) = 8{,}070 \text{ psi}$$

$$G = A33/h = 2{,}900 \text{ psi}$$

$$v = A12/A22 = .307$$

Option 2 and 3

For facesheet analysis, the ply orientation, $[0/90]_s$ was chosen to yield minimal thermal expansion. Calculations were similar to option 1, above.

2) Gr/Ep	$E = 22*10^6$ psi	$G = 8.37*10^6$ psi	v = .314
3) Kevlar 49	$E = 7.6*10^6$ psi	$G = 2.13*10^6$ psi	v = .314

The three options were then looked at in terms of total structural mass which is tabled below.

	Foam/film	Nomex/GrEp	HRH-49/Kevlar
mass/module (kg)	26.5	47.8	42.6
total structure x 656 modules (kg)	17,384	31,357	27,946

Based on reduced mass, the foam/film is by far the superior choice for our structure. Past designs of parabolic dishes, have selected honeycomb cores and graphite sheets as the optimum. However these dishes were 10-20 m in diameter and large masses do not accumulate due to the small number of panels. Because our array is planar, stringent reflecting requirements for parabolic dishes do not apply. For this decreased requirement, the

foam/film option is acceptable. Option 1, foam/film, is therefore selected as the observatory panel material.

APPENDIX 5.1: CALCULATION OF DELTA V REQUIREMENTS

5.1.1 Stationkeeping

The pole (angular momentum vector) of the radio telescopes orbit will experience an angular drift caused by the perturbing forces of the solar radiation pressure, lunar gravity, solar gravity, and (to a very small extent) the triaxiality of the earth. A change in the direction of the pole reflects an increase or decrease in the inclination of the orbit. A geosynchronous object moving in an inclined orbit traces a path over a point on the earth that fluctuates in latitude (or the North-South direction). These fluctuations contain periodic terms; the longest period follows the apparent year long orbit of the Sun about the Earth. Corrections need to cancel only the secular terms. Thus, the average yearly drift of the pole determines the delta-v for North South stationkeeping (NSSK).

The same forces that disturb the inclination of the satellite also cause the spacecraft to drift in longitude (i.e. the East-West direction over the Earth). These perturbing forces either accelerate or decelerate the spacecraft along its orbit. The accelerations contain terms that are periodic over an orbit (approximately one Julian Day). Therefore, the average daily secular acceleration defines the delta-v for East-West stationkeeping (EWSK). The equations used to convert the angular drift of the orbit pole and the longitudinal acceleration into stationkeeping delta v's are:

NSSK:

Delta-v per maneuver, V_m = 107.3*inc m/s

Time between maneuvers, T = 2*inc*365/i_d (days)

Delta-v per year = V_m*365/T

EWSK:

Delta-v per maneuver, $V_m = 11.32\ (3L_{avg}3*1)$ m/s

Time between maneuvers, $T = 4\ (1/3L_{avg}3)'$ (days)

Delta-v per year = V_m*365/T

To get the parameters required to calculate the delta v's, the following program, DELTAV, [illegible] the orbit of the spacecraft under the influence of perturbing forces. The scheme used was Cowell's method (direct numerical integration of the equations of motion) employing a fifth order Runga-Kutta-Nystrom mumerical integrating technique. The program contains the following fea

1) Apparent motions of the moon and sun in geocentric coordinates are calculated using low precision algebraic functions in time found in the Astronomical Almanac.

2) A fourth order model, the Goddard Earth Model (GEM 6), for the Earth's gravitational potential is used to calculate the disturbance from the earth's oblateness.

3) For purposes of the effects of solar radiation pressure, the radio telescope was modelled as a disk with the backside normal always pointing toward the earth's center. Also, the reflectivities on the front and back of the disk were considered to be different.

4) The program was run on the IBM 3090 using VS Fortran. The code runs faster in scalar mode than vector. It takes less than eight minutes using a one minute time step to execute one year of spaceflight.

```
      PROGRAM DELTAV
* This program numerically integrates the equations of motion (Cowell's
* method) to determine the perturbed orbit of the radio telescope. A
* 5th Order Runga-Kutta-Nystrom scheme is used for the integration.
* The calculated orbit is used to find the inclination drift rate and
* longitudinal acceleration which are required to determine the delta-v's
* for stationkeeping.
      IMPLICIT DOUBLE PRECISION (A-H,O-Z)
      DOUBLE PRECISION CEPSILON,COEF1,COEF1T,COEF2,COEF3,COEF3T,COEF4,
     $COEF5,COEF6,COEF7,COEF8,DAYCONV,DELTAD,DOT,EARTHMU,EPSILON,KO,K1,
     $K2,K3,LO,OMEGA,PI,PI2,R_GEO,RSAT,RTEMP,SEPSILON,THETA,TIME,TJD,
```

```
     $TJD2,VCIRC,VSAT,DTHETA,INCLIN,LAMACC,LAMDOT,LAMDOT2,H,RADCONV,
     $ABSAVG,ARITHAVG,MAG
* Notes on angles:  Any variable name formed from an angle name prefixed with
*  a 'C' or 'S' represents a value holding the cosine or sine of that angle
*  respectively.
* COEF?? = Variables that hold values [illegible] following loops.
* DAYCONV = Conversion from sid[illegible] day.
* DELTAD = Time step in units of days
* DOT = see function of same name
* EARTHMU = Gravitational coeficient for the Earth.
* EPSILON = Obliquity of ecliptic.
*           holding the value of the functions used in the RKN method
* L0 = Nominal longitude of the radio telescope in radians
* OMEGA = average angular rate of the Earth's rotation (rad/sec)
* PI? = constant values using the value of pi.
* R_GEO = radius of the geosynchronous orbit in meters
* RSAT = Vector holding the position of the satellite in geocentric coordinates
* RTEMP = Vector holding intermediate values of RSAT.
* THETA = Initial angular position (in radians) of the telescope on the XY
*         plane (geocentric coordinates)
* TIME = Date in Julian days
* TJD = Same as TIME
* TJD2 = Intermediate values of the date in Julian days
* VCIRC = Velocity of a geosynchronous spacecraft
* VSAT = Vector holding the velocity of the telescope
* DTHETA = Differential change in theta.
* INCLIN = Inclination of the radio telescope orbit
* LAMACC = Longitudinal acceleration
* LAMDOT = Longitudinal drift rate
* LAMDOT2 = Intermediate value of LAMDOT
* H = Angular momentum vector of the telescope orbit
* MAG = see function of the same name
* RADCONV = conversion factor for radians inot degrees
      REAL T,T2
* These real values hold the number of days of flight calculated by the
* program during execution.
      INTEGER DELTAT,I,ITERATIONS,J
* DELTAT = time step in seconds
* I,J = loop counters
* ITERATIONS = Number of iterations to be run based on the time step
* ABSAVG = absolute value average of the longitudinal acceleration
* ARITHAVG = arithmetic average of the longitudinal acceleration
      DIMENSION K0(3),K1(3),K2(3),K3(3),RSAT(3),RTEMP(3),VSAT(3),H(3)

      COMMON /ANGLES/PI,PI2,THETA,CEPSILON,SEPSILON,DTHETA
      COMMON /GEO/OMEGA,R_GEO,L0/STEP/DELTAT/GRAV/EARTHMU
      PARAMETER  (DAYCONV= 1.00273790935, EPSILON= 23.439)
      DATA LAMDOT2,LAMDOT,LAMACC,INCLIN,T,T2/4*0.0D0,0.0,0.0/
      DATA ABSAVG,ABSARITH/2*0.0D0/

* Initialize the variables dealing with pi, set the time step, and define
* the constants used in the RKN Method
      PI= DACOS(-1.0D0)
      PI2=
      RADCONV= 1.8D2/PI
```

```
      CEPSILON= DCOS(EPSILON*PI/1.8D2)
      SEPSILON= DSIN(EPSILON*PI/1.8D2)
      DELTAT= 60
      DELTAD= DBLE(DELTAT)/8.64D4
      COEF1= DELTAT/5.0D0
      COEF1T= DELTAD/5.0D0
      COEF2= DELTAT*DELTAT/50.0D0
      COEF3= DELTAT*2.0D0/3.0D0
      COEF3T= DELTAD*2.0D0/3.0D0
      COEF4= -DELTAT*DELTAT/27.0D0
      COEF5 = DELTAT
      COEF6= DELTAT*DELTAT/70.0D0
      COEF7= DELTAT*DELTAT/336.0D0
      COEF8= COEF7/DELTAT

*  Calculate the values that determine the initial geosynchronous orbit of
*  the telescope and the spacecrafts initial position in "inertial" space
      OMEGA= 2.0D0*PI*DAYCONV/8.64D4
      R_GEO= (EARTHMU/OMEGA/OMEGA)**(1.0/3.0)
      TJD= 2455357.0D0
      TIME= (TJD-2451545.0D0)/36525.0D0
      THETA= 4.894838296D0+2.0D0*PI*(8.640184812866D6*TIME+9.3104D-2*
     $TIME*TIME-6.2D-6*TIME**3)/8.64D4+L0-2.4381774D-2*TIME-
     $1.079311609D0*TIME*TIME
      RSAT(1)= R_GEO*DCOS(THETA)
      RSAT(2)= R_GEO*DSIN(THETA)
      RSAT(3)= 0.0D0
      VCIRC= R_GEO*OMEGA
      VSAT(1)= VCIRC*DCOS(THETA+PI2)
      VSAT(2)= VCIRC*DSIN(THETA+PI2)
      VSAT(3)= 0.0D0

*  Set up the output files which contain the daily position, velocity,
*  inclination, and longitudinal drift, acceleration, and deviation.
      OPEN (UNIT=1,FILE='ORBITR')
      OPEN (UNIT=2,FILE='ORBITV')
      OPEN (UNIT=3,FILE='DANGLE')
      OPEN (UNIT=4,FILE='LONGIT')
      WRITE(1,10)
      WRITE(2,20)
      WRITE(6,25)
      WRITE(3,25)
      WRITE(4,35)
      WRITE(1,70) T,RSAT
      WRITE(2,70) T,VSAT
      WRITE(6,75) T2,DTHETA,INCLIN
      WRITE(3,75) T2,DTHETA,INCLIN
      WRITE(4,75) T2,LAMACC,LAMDOT
   10 FORMAT(5X,'TIME',19X,'POSITION (X,Y,Z)'/4X,'(days)',25X,'(m)')
   20 FORMAT(5X,'TIME',19X,'VELOCITY (X,Y,Z)'/4X,'(days)',24X,'(m/s)')
   25 FORMAT(5X,'TIME',6X,'DELTA LAMBDA',5X,'INCLINATION'/4X,'(days)',
     $8X,'(deg.)',10X,'(deg.)')
   35 FORMAT(5X,'TIME',6X,'LONGITUDINAL',4X,'LONGITUDINAL'/15X,
     $'ACCELERATION',6X,'DRIFT RATE'/4X,'(days)',4X,'(deg./sq. sec.)',
     $3X,'(deg./sec.)')
```

```
* Find the number of iterations required for the two year loop.
           TIONS= 2*86400*365/DELTAT-1
      TJD= TJD-DELTAD
* Begin the loop.  Each pass uses the RKN Method to find the velocity
* and position of the spacecraft at the end of each time step.
      DO 80 I=0,ITERATIONS,1
       TJD= TJD+DELTAD
       CALL GETK(K0,RSAT,TJD,0.0D0,I)
       TJD2= TJD+COEF1T
       RTEMP(1)= RSAT(1)+COEF1*VSAT(1)+COEF2*K0(1)
       RTEMP(2)= RSAT(2)+COEF1*VSAT(2)+COEF2*K0(2)
       RTEMP(3)= RSAT(3)+COEF1*VSAT(3)+COEF2*K0(3)
       CALL GETK(K1,RTEMP,TJD2,COEF1,I)
       TJD2= TJD+COEF3T
       RTEMP(1)= RSAT(1)+COEF3*VSAT(1)+COEF4*(K0(1)-7.0D0*K1(1))
       RTEMP(2)= RSAT(2)+COEF3*VSAT(2)+COEF4*(K0(2)-7.0D0*K1(2))
       RTEMP(3)= RSAT(3)+COEF3*VSAT(3)+COEF4*(K0(3)-7.0D0*K1(3))
       CALL GETK(K2,RTEMP,TJD2,COEF3,I)
       TJD2= TJD+DELTAD
       RTEMP(1)= RSAT(1)+COEF5*VSAT(1)+COEF6*(2.1D1*K0(1)-4.0D0*K1(1)+
     $1.8D1*K2(1))
       RTEMP(2)= RSAT(2)+COEF5*VSAT(2)+COEF6*(2.1D1*K0(2)-4.0D0*K1(2)+
     $1.8D1*K2(2))
       RTEMP(3)= RSAT(3)+COEF5*VSAT(3)+COEF6*(2.1D1*K0(3)-4.0D0*K1(3)+
     $1.8D1*K2(3))
       CALL GETK(K3,RTEMP,TJD2,COEF5,I)
       RSAT(1)= RSAT(1)+DELTAT*VSAT(1)+COEF7*(1.4D1*K0(1)+1.0D2*K1(1)+
     $5.4D1*K2(1))
       RSAT(2)= RSAT(2)+DELTAT*VSAT(2)+COEF7*(1.4D1*K0(2)+1.0D2*K1(2)+
     $5.4D1*K2(2))
       RSAT(3)= RSAT(3)+DELTAT*VSAT(3)+COEF7*(1.4D1*K0(3)+1.0D2*K1(3)+
     $5.4D1*K2(3))
       VSAT(1)= VSAT(1)+COEF8*(1.4D1*K0(1)+1.25D2*K1(1)+1.62D2*K2(1)+
     $3.5D1*K3(1))
       VSAT(2)= VSAT(2)+COEF8*(1.4D1*K0(2)+1.25D2*K1(2)+1.62D2*K2(2)+
     $3.5D1*K3(2))
       VSAT(3)= VSAT(3)+COEF8*(1.4D1*K0(3)+1.25D2*K1(3)+1.62D2*K2(3)+
     $3.5D1*K3(3))
* At the end of the day and at the last iteration, output the satellite
* positon and velocity, the orbit inclination, and the longitudinal drift,
* acceleration, and deviation.
       IF ((MOD(((I+1)*DELTAT),86400).EQ.0).OR.(I.EQ.ITERATIONS)) THEN
         T= (I+1)*DELTAT/8.64D4
         WRITE(1,70) T,RSAT
         WRITE(2,70) T,VSAT
   70 FORMAT(2X,F8.3,2X,3D16.8)
         T2= (I+1)*DELTAT/8.64D4
         LAMDOT=(DSQRT((VSAT(1)*VSAT(1)+VSAT(2)*VSAT(2))/(RSAT(1)*
     $RSAT(1)+RSAT(2)*RSAT(2)))-OMEGA
         LAMACC= (LAMDOT-LAMDOT2)/8.64D4
         LAMDOT2= LAMDOT
         ABSAVG= ABSAVG+DABS(LAMACC)
         ARITHAVG= ARITHAVG+LAMACC
         H(1)= RSAT(2)*VSAT(3)-RSAT(3)*VSAT(2)
         H(2)= RSAT(3)*VSAT(1)-RSAT(1)*VSAT(3)
```

```
            H(3)= RSAT(1)*VSAT(2)-RSAT(2)*VSAT(1)
            INCLIN= DACOS(H(3)/MAG(H))*RADCONV
            DTHETA= DTHETA*RADCONV
            WRITE(6,75) T2,DTHETA,INCLIN
            WRITE(3,75) T2,DTHETA,INCLIN
            WRITE(4,75) T2,LAMACC,LAMDOT
   75 FORMAT(2X,F8.3,2X,2D16.7)
          ENDIF
   80 CONTINUE
*  Calculate and output the absolute and arithmetic averages of the
*  longitudinal accelerations.
         ABSAVG=ABSAVG/((ITERATIONS*DELTAT)/86400)
         ARITHAVG=ARITHAVG/((ITERATIONS*DELTAT)/86400)
         WRITE(4,79) ARITHAVG,ABSAVG
   79 FORMAT(1X,'THE ARITHMETIC AVERAGE OF THE LONGITUDINAL ACCELERA',
        $'TION IS:',D16.7/1X,'THE AVERAGE OF THE ABSOLUTE VALUE OF THE',
        $' LONGITUDINAL ACCELERATION IS:'/1X,D16.7)
         END


         SUBROUTINE GETK(K,RSAT,TJD,DELTIME,I)
*  This procdure calculates the K vectors for the Runga-Kutta algorithm.
         DOUBLE PRECISION ANGLE,AREA,AU,BETA,COEF1,COEF2,COEF3,COEF4,
        $CEPSILON,CPHI,CTHETA,DELTIME,DOT,DTHETA,DVV1,DVV2,DVV3,EARTHMU,
        $EARTHEQ,F,FRAD,G_EARTH,J2,J21,J22,J3,J31,J32,J33,J4,J41,J42,
        $J43,J44,K,L0,L21,L22,L31,L32,L33,L41,L42,L43,L44,LAMBDA,LCRAFT,
        $LIGHT,LSUN,LUNAR,MAG,MASS,MOONMU,MOONR,MSUN,NORM,OMEGA,P,PHI,PI,
        $PI2,PILUNA,PNM,R_GEO,RCRAFT,RE_R,REFLECT,RHO,RIDEAL,RLUNA,RMOON,
        $RSOL,RSAT,RSATXY,RSUN,SEPSILON,SOLAR,SPHI,STHETA,SUNEQ,SUNMU,SUNR,
        $THETA,THETA3,TIME,TJD,TPHI,TRIAX,DTHETA2
*  ANGLE = angular position of an ideal geosynchronous spacecraft on the XY
*          plane
*  AREA = cross-sectional area of spacecraft
*  AU = astronomical unit
*  BETA, LAMBDA, PILUNA= angles used in determining the position of the moon
*  COEF?? = same as main program
*  DELTIME = increment of time over time zero used to evaluate K's in RKN method
*  DOT = see function
*  DTHETA = same as main program
*  Find the number of iterations required for the loop.
*  EARTHMU = same as main program
*  EARTHEQ = Equatorial radius of the Earth
*  F =                .ie triaxiality of the earth in spherical coordinates
*  FRAD = solar radiation force (a vector)
*  G_EARTH = gravitational acceleration due to the Earth
*  J?? = J harmonic coeficients of the Earth's gravitaional potetial
*  K = same as main program
*  L?? = Lambda harmonic coefficients of the Earth's gravitational potential
*  LCRAFT = longitude of spacecraft
*  LIGHT = Solar radiation constant
*  LSUN, MSUN,  = parameters used to define the position of the sun in
*    geocentirc coordinates
*  LUNAR = position of the moon relative to the spacecraft (vector)
*  MAG = see function
*  MASS = Mass of spacecraft
```

```
* MOONMU = Gravitational constant for the moon
* MOONR = position of moon relative to the center of the Earth (vector)
* NORM = Normal of spacecraft dish
* P= Solar radiation flux
* PHI = angle between spacecraft position and equatiorial (XY) plane
* PI, PI2 = same as main program
* PNM = Legendre polynomials
* R_GEO = same as main program
* RCRAFT = radius of spacecraft orbit
* RE_R = ratio of earth radius to orbit radius
* REFLECT =  vector holds reflectivities for front and back side
* RHO = angles that determine when spacraft is in eclipse
* RIDEAL = postion of ideal geosynchronous spacecraft
* RLUNA = distance of moon from satellite
* RMOON = distance of moon from earth
* RSOL = distance of sun from satellite
* RSAT = position of satellite in geocentric coordinates
* RSATXY = X,Y value of sateliite position (a vector)
* RSUN = position of sun relative to Earth
* RSOLAR = Position of sun relative to the spacecraft
* SUNEQ = Solar equatiorial radius
* SUNMU = Solar gravitational constant
* SUNR = distance of sun from earth
* THETA = angular position of spacecraft on XY plane
* THETA3 - unused
* TIME, TJD - same main program
* TPHI = tangent of PHI
* TRIAX = triaxial forces in geocentric coordinates
* DTHETA2 = unused
      INTEGER I,J,DELTAT,FACE,L
* I,J,L = Counters
* DELTAT = time
* FACE = face of observatory in light of the sun
      DIMENSION DVV1(9),DVV2(9),F(3),FRAD(3),K(3),LUNAR(3),NORM(3),
     $PNM(12),REFLECT(2,2),RHO(3),RIDEAL(3),RMOON(3),RSAT(3),RSATXY(3),
     $RSUN(3),SOLAR(3),TRIAX(3)
      COMMON /ANGLES/PI,PI2,THETA3,CEPSILON,SEPSILON,DTHETA2
      COMMON /GEO/OMEGA,R_GEO,LO/STEP/DELTAT/GRAV/EARTHMU

* Initialive constant variables.
      PARAMETER (AU= 1.49597870D11)
      PARAMETER (MOONMU= 4.902794D12, SUNMU= 1.32712438D20,
     $EARTHEQ= 6378140, SUNEQ= 6.96D8, LIGHT= 1.013747712D17)
      PARAMETER (J2=1082.6283D-6, J21=-4.2915D-9, J22=-1.8083D-6,
     $J3=-2.5418D-6, J31=2.1791D-6, J32=-3.8480D-7, J33=-2.2132D-7,
     $J4=-1.6086D-6, J41=-6.7614D-7, J42=-1.6853D-7, J43=-5.9015D-8,
     $J44=-7.3147D-9)
      PARAMETER (L21= 4.43822219, L22=-.259965046, L31=0.123340672,
     $L32=-.297313347, L33=0.372074525, L41=3.852014963,
     $L42=0.546839579, L43=-.075211473, L44=0.515748284)
      DATA MASS/25000/,RSATXY(3)/0.0D0/,RIDEAL(3)/0.0D0/,AREA/17700.0/
      DATA ((REFLECT(L,J),L=1,2),J=1,2)/0.5D0,0.3D0,0.35D0,0.45D0/

* Determine the position of the moon in geocentric coordinates relative
* to both the earth and the spacecraft
```

```
      TIME= (TJD-2.451545D6)/3.6525D4
      LAMBDA= 3.810402823D0+8.399709142D3*TIME+0.10978121D0*
     $DSIN(2.354449161D0+8.328691119D3*TIME)-2.2165681D-2*
     $DSIN(4.523893421D0-7.214063296D3*TIME)+3.665191429D-3*
     $DSIN(4.710643651D0+1.665738224D4*TIME)-3.316125579D-3*
     $DSIN(6.239552076D0+6.283019501D2*TIME)-1.919862177D-3*
     $DSIN(3.256784384D0+1.686693258D4*TIME)
      BETA= 8.953539D-2*DSIN(1.628392192D0+8.433466376D3*TIME)+
     $4.886921906D-3*(DSIN(3.982841353D0+1.676215732D4*TIME)-
     $DSIN(5.555383009D0+1.047752566D2*TIME))-2.967059728D-3*
     $DSIN(3.797836452D0-7.109288039D3*TIME)
      PILUNA= 1.659459D-2+9.040805525D-4*DCOS(2.354449161D0+
     $8.328691119D3*TIME)+1.658062789D-4*DCOS(4.523893421D0-
     $7.214063296D3*TIME)+1.361356817D-4*DCOS(4.113741047D0+
     $1.554275442D4*TIME)+4.886921906D-5*DCOS(4.710643651D0+
     $1.665738224D4*TIME)
      RLUNA = EARTHEQ/DSIN(PILUNA)
      RMOON(1)  RLUN*DCOS(BETA)*(          DA)
      RMOON(2) = RLUNA*(CEPSILON*DCOS(BETA)*DSIN(LAMBDA) SEPSILON*
     $DSIN(BETA))
      RMOON(3)= RLUNA*(SEPSILON*DCOS(BETA)*DSIN(LAMBDA)+CEPSILON*
     $DSIN(BETA))
      LUNAR(1)= RMOON(1)-RSAT(1)
      LUNAR(2)= RMOON(2)-RSAT(2)
                RMOON(3)-RSAT(3)
      MOONR= MAG(LUNAR)

*  Use the spacecraft position to determine its spherical coordinates and
*  the current deviation inlongitude
      RCRAFT= MAG(RSAT)
      G_EARTH= EARTHMU/RCRAFT**3
      RE_R= EARTHEQ/RCRAFT
      PHI= DASIN(RSAT(3)/RCRAFT)
      ANGLE= OMEGA*(I*DELTAT+DELTIME)+THETA3
      RSATXY(1)=RSAT(1)
      RSATXY(2)=RSAT(2)
      RIDEAL(1)= R_GEO*DCOS(ANGLE)
      RIDEAL(2)= R_GEO*DSIN(ANGLE)
      DTHETA= DACOS(DOT(RSATXY,RIDEAL)/(MAG(RSATXY)+1.0D-4)/MAG(RIDEAL))
      COEF1= RSATXY(2)*RIDEAL(1)-RSATXY(1)*RIDEAL(2)
      IF (DELTIME.LT.(DELTAT/5.1D0)) DTHETA2= DSIGN(DTHETA,COEF1)
      LCRAFT= L0+DSIGN(DTHETA,COEF1)
      CPHI=DCOS(PHI)
      SPHI=DSIN(PHI)
*  Prepare frequently used values in the functions for the triaxial forces
      DVV1(1)= LCRAFT-L21
      DVV1(2)= 2.0D0*(LCRAFT-L22)
      DVV1(3)= LCRAFT-L31
      DVV1(4)= 2.0D0*(LCRAFT-L32)
      DVV1(5)= 3.0D0*(LCRAFT-L33)
      DVV1(6)= LCRAFT-L41
      DVV1(7)= 2.0D0*(LCRAFT-L42)
      DVV1(8)= 3.0D0*(LCRAFT-L43)
      DVV1(9)= 4.0D0*(LCRAFT-L44)
      DVV2(1)= DCOS(DVV1(1))
```

```
      DVV2(2)= DCOS(DVV1(2))
      DVV2(3)= DCOS(DVV1(3))
      DVV2(4)= DCOS(DVV1(4))
      DVV2(5)= DCOS(DVV1(5))
      DVV2(6)= DCOS(DVV1(6))
      DVV2(7)= DCOS(DVV1(7))
      DVV2(8)= DCOS(DVV1(8))
      DVV2(9)= DCOS(DVV1(9))
      COEF1= G_EARTH*Re_R*Re_R*RCRAFT
      COEF2= SPHI*SPHI
      COEF3= CPHI*SPHI
      COEF4= CPHI*CPHI
      TPHI= SPHI/CPHI
*  Calculate the Legendre polynomials
      PNM(1)= 0.5D0*(3.0D0*COEF2-1.0D0)
      PNM(2)= 3.0D0*COEF3
      PNM(3)= 3.0D0*COEF4
      PNM(4)= 0.5D0*SPHI*(5.0D0*COEF2-3.0D0)
      PNM(5)= 0.5D0*CPHI*(1.5D1*COEF2-3.0D0)
      PNM(6)= 1.5D1*COEF4*SPHI
      PNM(7)= 1.5D1*COEF4*CPHI
      PNM(8)= 0.125D0*(COEF2*(3.5D1*COEF2-3.0D1)+3.0D0)
      PNM(9)= 0.25D0*COEF3*(7.0D1*COEF2-3.0D1)
      PNM(10)= 0.25D0*COEF4*(2.1D2*COEF2-3.0D1)
      PNM(11)= 1.05D2*COEF4*COEF3
      PNM(12)= 1.05D2*COEF4*COEF4
* Calculate the triaxial forces in spherical coordinates
      F(1)= COEF1*(3.0D0*(J2*PNM(1)+J21*PNM(2)*DVV2(1)+J22*PNM(3)*
     $DVV2(2))+RE_R*(4.0D0*(J3*PNM(4)+J31*PNM(5)*DVV2(3)+J32*PNM(6)*
     $DVV2(4)+J33*PNM(7)*DVV2(5))+5.0D0*RE_R*(J4*PNM(
     $DVV2(6)+J42*PNM(10)*DVV2(7)+J43*PNM(11)*DVV2(8)+J44*PNM(12)*
     $DVV2(9))))
      F(2)= COEF1*(J21*PNM(2)*DSIN(DVV1(1))+2.0D0*J22*DSIN(DVV1(2))*
     $PNM(3)+RE_R*(J31*PNM(5)*DSIN(DVV1(3))+2.0D0*J32*DSIN(DVV1(4))*
     $PNM(6)+3.0D0*J33*PNM(7)*DSIN(DVV1(5))+RE_R*(J41*DSIN(DVV1(6))*
     $PNM(9)+2.0D0*J42*PNM(10)*DSIN(DVV1(7))+3.0D0*J43*DSIN(DVV1(8))*
     $PNM(11)+4.0D0*J44*PNM(12)*DSIN(DVV1(9)))))/CPHI
      F(3)= COEF1*(-J2*PNM(2)+J21*DVV2(1)*(TPHI*PNM(2)-PNM(3))+2.0D0*
     $J22*PNM(2)*DVV2(2)+RE_R*(-J3*PNM(5)+J31*(TPHI*PNM(5)-PNM(6))*
     $DVV2(3)+J32*(2.0D0*TPHI*PNM(6)-PNM(7))*DVV2(4)+3.0D0*J33*PNM(7)*
     $DVV2(5)+RE_R*(-J4*PNM(9)+J41*DVV2(6)*(TPHI*PNM(10)-PNM(9))+J42*
     $DVV2(7)*(2.0D0*TPHI*PNM(11)-PNM(10))+J43*DVV2(8)*(3.0D0*TPHI*
     $PNM(11)-PNM(12))+4.0D0*J44*DVV2(9)*PNM(12))))
      THETA= DATAN2(RSATXY(2),RSATXY(1))
      CTHETA= DCOS(THETA)
      STHETA= DSIN(THETA)
* Transfoem the triaxial forces into geocentric coordinates
      TRIAX(1)= CTHETA*(F(1)*CPHI-F(3)*SPHI)-F(2)*STHETA
      TRIAX(2)= F(2)*CTHETA+STHETA*(F(1)*CPHI-F(3)*SPHI)
      TRIAX(3)= SPHI*F(1)+CPHI*F(3)

* Calculate the position of the sun in geocentric coordinates relative to both
* the spacecraft and the Earth
      TIME= TIME*3.6525D4
      LSUN= 4.89495042D0+.017202792D0*TIME
```

```
      MSUN= 6.240040768D0+.01720197D0*TIME
      LAMBDA= LSUN+.033423055D0*DSIN(MSUN)+3.490658504D-4*DSIN(2*MSUN)
      RSOL= AU*(1.00014D0-1.671D-2*DCOS(MSUN)-1.4D-4*DCOS(MSUN))
      RSUN(1)= RSOL*DCOS(LAMBDA)
      RSUN(2)= RSOL*CEPSILON*DSIN(LAMBDA)
      RSUN(3)= RSOL*SEPSILON*DSIN(LAMBDA)
      SOLAR(1)= RSUN(1)-RSAT(1)
      SOLAR(2)= RSUN(2)-RSAT(2)
      SOLAR(3)= RSUN(3)-RSAT(3)
      SUNR= MAG(SOLAR)

* Set up the angular vector that determines whether the spacecraft is in
* eclipse
      RHO(1)= DASIN(SUNEQ/SUNR)
      RHO(2)= DASIN(Re_R)
      RHO(3)= DACOS(-1.0D0*DOT(SOLAR,RSAT)/(SUNR+1.0D-3)/RCRAFT)
* Check for immersion in total eclipse
      IF ((SUNR.GT.RSOL).AND.((RHO(2)-RHO(1)).GT.RHO(3))) THEN
       FRAD(1)= 0.0D0
       FRAD(2)= 0.0D0
       FRAD(3)= 0.0D0
      ELSE
       P= LIGHT/SUNR/SUNR
* Check for immersion in partial eclipse
       IF ((SUNR.GT.RSOL).AND.((RHO(2)+RHO(1)).GT.RHO(3)).AND.(RHO(3)
     $.GT.(RHO(2)-RHO(1)))) THEN
* Calculate reduction of solar flux in partial eclipse
      DVV1(1)= DCOS(RHO(1))
      DVV1(2)= DSIN(RHO(1))
      DVV1(3)= DCOS(RHO(2))
      DVV1(4)= DSIN(RHO(2))
      DVV1(5)= DCOS(RHO(3))
      DVV1(6)= DSIN(RHO(3))
      P= P/PI/(1-DVV1(1))*(PI-DVV1(1)*DACOS((DVV1(3)-DVV1(1)*DVV1(5))/
     $DVV1(2)/DVV1(6))-DVV1(3)*DACOS((DVV1(1)-DVV1(5)*DVV1(3))/DVV1(6)/
     $DVV1(4))-DACOS((DVV1(5)-DVV1(1)*DVV1(3))/DVV1(2)/DVV1(4)))
       ENDIF
* Calculate the normal of the spacecraft dish in geocentric coordinates
      NORM(1)= CTHETA*CPHI
      NORM(2)= STHETA*CPHI
      NORM(3)= SPHI
* Determine which side is illuminated and setup the correct constants for it
      IF (RHO(3).GE.PI2) THEN
        FACE=1
      ELSE
        FACE=2
        NORM(1)= -NORM(1)
        NORM(2)= -NORM(2)
        NORM(3)= -NORM(3)
      ENDIF
* Calculate the solar radiation pressure force
      DVV1(1)= DOT(SOLAR,NORM)/SUNR
      DVV1(2)= -P*AREA*DVV1(1)
      DVV1(3)= (1.0D0-REFLECT(1,FACE))/SUNR
      DVV1(4)= 2.0D0*(REFLECT(1,FACE)*DVV1(1)+REFLECT(2,FACE)/3.0D0)
```

```
        FRAD(1)= DVV1(2)*(DVV1(3)*SOLAR(1)+DVV1(4)*NORM(1))
        FRAD(2)= DVV1(2)*(DVV1(3)*SOLAR(2)+DVV1(4)*NORM(2))
        FRAD(3)= DVV1(2)*(DVV1(3)*SOLAR(3)+DVV1(4)*NORM(3))
        ENDIF

* Calculate the functions that define K.
      DVV1(1)= SUNMU/SUNR**3
      DVV1(2)= SUNMU/RSOL**3
      DVV1(3)= MOONMU/MOONR**3
      DVV1(4)= MOONMU/RLUNA**3
      K(1)= DVV1(1)*SOLAR(1)-DVV1(2)*RSUN(1)+DVV1(3)*LUNAR(1)-RMOON(1)*
     $DVV1(4)+FRAD(1)/MASS-G_EARTH*RSAT(1)+TRIAX(1)
      K(2)= DVV1(1)*SOLAR(2)-DVV1(2)*RSUN(2)+DVV1(3)*LUNAR(2)-RMOON(2)*
     $DVV1(4)+FRAD(2)/MASS-G_EARTH*RSAT(2)+TRIAX(2)
      K(3)= DVV1(1)*SOLAR(3)-DVV1(2)*RSUN(3)+DVV1(3)*LUNAR(3)-RMOON(3)*
     $DVV1(4)+FRAD(3)/MASS-G_EARTH*RSAT(3)+TRIAX(3)
      RETURN
      END


      DOUBLE PRECISION FUNCTION MAG(A)
      DOUBLE PRECISION A(3)
* This function calculates ... ...gn... of a vector.
      MAG= DSQRT(A(1)*A(1)+A(2)*A(2)+A(3)*A(3))
      RETURN
      END


      DOUBLE PRECISION FUNCTION DOT(A,B)
      DOUBLE PRECISION A(3), B(3)
* This function produces the dot product of two vectors.
      DOT= A(1)*B(1)+A(2)*B(2)+A(3)*B(3)
      RETURN
      END


      BLOCK DATA
      DOUBLE PRECISION EARTHMU,OMEGA,R_GEO,LO,PI,PI2,THETA,CEPSILON,
     $SEPSILON,DTHETA
      COMMON /GRAV/EARTHMU/GEO/OMEGA,R_GEO,LO
      COMMON /ANGLES/PI,PI2,THETA,CEPSILON,SEPSILON,DTHETA
      DATA EARTHMU/3.986005D14/, LO/-1.8326248034D0/, DTHETA/0.0D0/
      END
```

The results of the last run of this program were: 1) The inclination of the orbit changes by an average of 0.9x/yr. 2) The average longitudinal acceleration is 5.535192×10^{-12} deg./sec.

5.1.2 Momentum Dumping and Attitude Maneuvers

The large distance of the thrusters from the center of mass, ~75 m, proves advantageous for delta-v's associated with desaturation of momen-

tum wheels and high rate maneuvering. The engines supply a 3.75 N-m moment to each axis (roll, pitch, and yaw). This power leads to small thrusting times and, thus, very small delta-v's when compared to those of stationkeeping. It will be assumed that the delta-v contribution will be that for maximum continuous attitude correction. One calculates the delta-v associated with each moment (roll, yaw, and pitch) as follows:

$$v(\text{year}) = I_{avg}/M/L/DI*366.25$$

At geosynchronous orbit, only solar radiation and gravity gradient torques have meaningful effects.

A program design to do the numerical integration of the solar radiation torque in reaction with the gravity gradient torques gives the value of I_{avg}. Unlike the stationkeeping problem where one must numerically integrate the equations of motion to find the delta-v. The delta-v's associated with environmental torques are relatively insensitive to orbit perturbations. Thus one can find the angular moment impulse of the observatory in an ideal geosynchronous orbit and the error incurred from this simplification will be very [illegible]. The following program GEOTORQ performs this analysis.

The numerical models for the environmental torques are:

Solar Radiation Pressure

$$F = -P\ A\ \cos(i)\ [(1-C_s)S+2(C_s\cos(i)+C_d)N]$$

$$T_{SR} = F \times r_{OC}$$

Gravity Gradients

$$T_{GG} = 3f/R_r^3\ [R \times (IyR)]$$

Tables 5.A to 5.C list selected data from the output. The results (not fully contained in the tables) demonstrated the following:

1) When comparing Table 5.A with Table 5.C one can see the solar

radiation torque does dominate the roll and pitch perturbations.

2) The yaw torque impulse fluctuates with a period of about 28 days indicating a strong lunar influence. The roll impulse moment oscillates with a period of about 183 days, again demonstrating the strong solar radiation contribution. The pitch moment impulse only mildly changes. The gravity gradient torque for the earth is zero; this occurs because it is assumed that the spacecraft maintains a perfect orientation toward earth. These expected effects varifies the validity of the data.

4) The upper limit of moment impulse (calculated from the square root of the sum of the squares of the individual maximums of roll, yaw, and pitch) is approximately 540 Nms for half an orbit. Both the yaw and roll torques continue to add to their impulse over many orbits; however, the pitch torque impulse over one half orbit tends to counter the impulse accumulated over the previous half orbit. Errors in the pointing of the spacecraft will cause random changes in the momentum impulse because of the earth gravity gradient torque. But the effect of the earth's gravity gradient torque will be small (being a random occurrence). It will be assumed that these will only cause an increase in the number of desaturations needed for the pitch. The final delta-v's for momentum dumping and maneuvering are:

Pitch = 0.09 m/s/yr

Roll = 1.26 m/s/yr

Yaw = ~0 m/s/yr (>

```
      PROGRAM GEOTOR
* The program calculates the environmental torques on the radio tele-
*scope assuming that it maintains ideal geosynchronous orbit (i= 0) and
*that the moments of inertial remain constant.  It does account for
*the apparent movements of the Sun and Moon.
      IMPLICIT DOUBLE PRECISION (A-H,O-Z)
      DOUBLE PRECISION EARTH,AMOON,AREA,ASUN,BETA,CD,COEF1,COEF2,
     $COEF3,COEF4,COEF5,COEF6,CS,CTHETA,DELTAD,DELTAT,DOT,EARTHMU,
```

```
      $EPSILON,G_EARTH,G_MOON,G_SUN,HPI,LAMBDA,LSUN,MAG,MOONMU,MSUN,
      $NORM,OMEGA,P,PI,P_PER_M,R,RCG,R_EARTH,Re_R,RHOP,RHOS,RM,RMOON,
      $RS,RSAT,R_SUN,RSUN,RSUNS,STHETA,SUNMU,SUNR,TEMP,THETA,THETA0
      $THETA3,TIME,TJD,TJD0,TORQUE1,TORQUE2,TORQUE3,TORQUE4,TORSR,FRAD

* EARTH = Gravity Gradient Torque imposed by the Earth
* AMOON = Gravity Gradient Torque imposed by the Moon
* AREA = Effecitive optical area of the observatory
* ASUN = Gravity Gradient Torque imposed by the Sun
* BETA, LAMBDA, HPI = Angles that determine the geocentric position and
*      distance of the Moon
* CD = Coefficient of diffuse reflection
* COEF's = "Coefficients", these are variables used to hold the value of
*      a repeated expression.  Thus reducing the number of calculations.
* CS = Coefficient of specular reflection
* CTHETA,STHETA = The cosine and sine respectively of the angular position
*      of the observatory with respect to the Earth.
* DELTAD, DELTAT = The time step in Julian days and seconds respectively
* DOT, MAG = User Defined Functions (see the subroutines for more info)
* EARTHMU, MOONMU, SUNMU = Gravitational Constants of the Earth, Moon and
*      Sun.
* EPSILON, LAMBDA, MSUN, LSUN = Angles that determine the position of the
*      Sun in geocentric coordinates.
* G_EARTH, G_SUN, G_MOON = Instantaneous gravitational acceleration of the
*      Earth, Sun, and Moon.
* NORM = The dish outward normal in spacecraft centered coordinates.
* OMEGA = Rotation rate of the earth and thus of the spacecraft.
* P = Solar Radiation Flux
* PI = pi
* P_PER_M = The average solar radiation flux at zero distance
*      of Sun from Earth
* R_EARTH, R_SUN = Equatorial Radii of the Earth and Sun
* Re_R = Ratio of the Earth's Equator to the observatories orbital radius
* RHOP, RHOS = Angles used to determine points of partial and total eclipse
* RM, RMOON = Distance of Moon from Satellite and position in geocentric
*      coordinates (and spacecraft centered coordinates after
*      transfromation.)
* RS, RSAT = Orbital distance and position of Satellite from Earth.
* SUNR, RSUN, RSUNS = Distance of Sun from Satellite and corresponding
*      position in geocentric and spacecraft centered coordinates.
* TEMP = Similar to COEF's but is a vector
* THETA = Anomaly (angle) along spacecraft orbit (defined by vernal equinox)
* THETA0 = X-Y plane angle of the Sun (defined by vernal equinox) at TIME = 0
* THETA3 = Angle between lines connecting the observatory to Earth and the
*       Sun to the observatory
* TIME,TJD,TJD0 = Time for calculating the positions of the Moon and Sun,
*       the instantaneous Julian Date and the initial Julian Date.
* TORQUE's = Angular momentum impulses: 1) Sums over the absolute value of the
*       instantaneous torques, 2) Sums over the instantaneous torques (to
*       find secular growth over the orbit), 3) Same as 1 for the Solar
*       Radiation Torque, 4) Same as 2 for the Solar Radiation Pressure
*       Torque.
* FRAD = Instantaneous Solar Radiation Pressure Force (in spacecraft-centered
*      coordinates)
* TORSR = Instantaneous Solar Radiation Pressure Torque
```

```
* Integer Variables are only counters

      INTEGER I,J,ITERATIONS
      DIMENSION EARTH(3),AMOON(3),ASUN(3),FRAD(3),TORQUE1(3),
     $NORM(3),RMOON(3),RSAT(3),RSUN(3),TORQUE2(3),TORQUE4(3),
     $TEMP(3),TORQUE3(3),TORSR(3),RSUNS(3)

      PARAMETER  (OMEGA= 7.292115855D-5)
      PARAMETER (EARTHMU= 3.986005D14, MOONMU= 4.902794D12,
     $SUNMU= 1.32712438D20, R_EARTH= 6378140, R_SUN= 6.96D8,
     $EPSILON= .409087723, P_PER_M= 1.013747712D17)
      DATA AREA/17700/,RS/42318200.00/
      DATA (TORQUE1(I),I=1,3)/3*0.0D0/,(TORQUE2(I),I=1,3)/3*0.0D0/,
     @(TORQUE3(I),I=1,3)/3*0.0D0/,(TORQUE4(I),I=1,3)/3*0.0D0/

* PI, Initial times, time steps, and # of iterations initialized
      PI= DACOS(-1.0D0)
      TJD0= 2452545.0
      TIME= (TJD0-2451545.0)
      DELTAT= 78.331
      DELTAD= 1.1574074D-05*DELTAT
      ITERATIONS= 1100*366.25

* THETA0 is calculated
      LSUN= 4.89495042+.017202792*TIME
      MSUN= 6.240040768+.01720197*TIME
      LAMBDA= LSUN+.033423055*DSIN(MSUN)+3.490658504D-4*DSIN(2*MSUN)
      THETA0 = DATAN2((DCOS(EPSILON)*DSIN(LAMBDA)),DCOS(LAMBDA))

* Initialization of zero value variables
      NORM(3)= 0.0D0
      T= 0.0D0
      TORSR(1)=0.0D0

* Open files to hold data and print the table heading for each
      OPEN (UNIT=1,FILE='TORQUE1.OUT')
      OPEN (UNIT=2,FILE='TORQUE2.OUT')
      OPEN (UNIT=3,FILE='TORQUE3.OUT')
      OPEN (UNIT=4,FILE='TORQUE4.OUT')
      WRITE(*,10)
      WRITE(1,10)
      WRITE(2,10)
      WRITE(3,10)
      WRITE(4,10)
      WRITE(*,100) T,TORQUE4
      WRITE(4,100) T,TORQUE4
   10 FORMAT(8X,'TIME',23X,'IMPULSE (r,theta,phi)'/7X,'(days)',31X,
     @'Ns')


* Calculate the Earth Gravity Gradient Torque which is a constant for a
* an ideal geosynchronous spacecraft.  Calculate RHOP which is also constant
      RSAT(1)= RS
      RSAT(2)= 0.0D0
      RSAT(3)= 0.0D0
```

```
      G_EARTH= EARTHMU/RS**3
      Re_R= R_EARTH/RS
      CALL G_GRAD(G_EARTH,RSAT,EARTH)
      RHOP= DASIN(Re_R)

      DO 20 I=0,ITERATIONS,1
* The observatory moves through its orbit.  Instantaneous orbit position is
* calculated
       TJD= TJD0+DELTAD*I
       THETA= THETA0+I*DELTAT*OMEGA
       CTHETA= DCOS(THETA)
       STHETA= DSIN(THETA)
       RSAT(1)= RS*CTHETA
       RSAT(2)= RS*STHETA

* The position of the Moon relative to the spacecraft is calculated in
* geocentric coordinates, transformed into spacecraft specific coordinates,
* and finally used to get the gravity gradient torque
       TIME= (TJD-2451545.0)/36525
       LAMBDA= 3.810402823+8399.709142*TIME+0.10978121*DSIN(2.354449161
     $+8328.691119*TIME)-2.2165681D-2*DSIN(4.523893421-7214.063296*
     $TIME)+3.665191429D-3*DSIN(4.710643651+16657.38224*TIME)-
     $3.316125579D-3*DSIN(6.239552076+628.3019501*TIME)-2.1177D-3
     $*DSIN(3.256784384+16866.93258*TIME)
       BETA= 0.08953539*DSIN(1.628392192+8433.466376*TIME)+
     $4.886921906D-3*(DSIN(3.982841353+16762.15732*TIME)-
     $DSIN(5.555383009+104.7752566*TIME))-2.967059728D-3*
     $DSIN(3.797836452-7109.288039*TIME)
       HPI= .01659459+9.040805525D-4*DCOS(2.354449161+8328.691119*TIME)
     $+1.658062789D-4*DCOS(4.523893421-7214.063296*TIME)+1.361356817D-4
     $*DCOS(4.113741047+15542.75442*TIME)+4.886921906D-5*
     $DCOS(4.710643651+16657.38224*TIME)
       RM= R_EARTH/DSIN(HPI)
       RMOON(1)= RM*DCOS(BETA)*DCOS(LAMBDA)-RSAT(1)
       RMOON(2)= RM*(.917484083*DCOS(BETA)*DSIN(LAMBDA)-.397772494*
     $DSIN(BETA))-RSAT(2)
       RMOON(3)= RM*(.397772494*DCOS(BETA)*DSIN(LAMBDA)+.917484083*
     $DSIN(BETA))
       G_MOON= MOONMU/MAG(RMOON)**3
       CALL TRANS(RMOON,RMOON,CTHETA,STHETA)
       CALL G_GRAD(G_MOON,RMOON,AMOON)



* The position of the Sun relative to the spacecraft is calculated in
* geocentric coordinates, transformed into spacecraft specific coordinates,
* and finally used to get the gravity gradient torque
       TIME= TIME*36525
       LSUN= 4.89495042+.017202792*TIME
       MSUN= 6.240040768+.01720197*TIME
       LAMBDA= LSUN+.033423055*DSIN(MSUN)+3.490658504D-4*DSIN(2*MSUN)
       R= 1.49597870D11*(1.00014-.01671*DCOS(MSUN)-.00014*DCOS(MSUN))
       RSUN(1)= R*DCOS(LAMBDA)-RSAT(1)
       RSUN(2)= R*DCOS(EPSILON)*DSIN(LAMBDA)-RSAT(2)
       RSUN(3)= R*DSIN(EPSILON)*DSIN(LAMBDA)
```

```
      SUNR= MAG(RSUN)
      G_SUN= SUNMU/SUNR**3
      CALL TRANS(RSUN,RSUNS,CTHETA,STHETA)
      CALL G_GRAD(G_SUN,RSUNS,ASUN)

* The positions of the Sun and observatory are used to determine the
* Solar Radiation Force.
      RHOS= DASIN(R_SUN/SUNR)
      THETA3= DACOS(-1*DOT(RSUN,RSAT)/SUNR/RS)
      IF ((SUNR.GT.R).AND.((RHOP-RHOS).GT.THETA3)) THEN
* Total eclipse condition
     DO 50 J=1,3
   50         FRAD(J)= 0.0
      ELSE
     P= P_PER_M/SUNR/SUNR
     IF ((SUNR.GT.R).AND.((RHOP+RHOS).GT.THETA3).AND.(THETA3.GT.
    $(RHOP-RHOS)))) THEN
* Partial eclipse condition
      COEF1=DCOS(RHOS)
      COEF2= DSIN(RHOS)
      COEF3= DCOS(THETA3)
      COEF4= DSIN(THETA3)
      COEF5= DCOS(RHOP)
      COEF6= DSIN(RHOP)
      P= P/PI/(1-COEF1)*(PI-COEF1*DACOS((COEF5-COEF1*COEF3)/COEF2/
    $COEF4)-COEF5*DACOS((COEF1-COEF5*COEF3)/COEF6/COEF4)-
    $DACOS((COEF3-COEF1*COEF5)/COEF2/COEF6))
      ENDIF
      NORM(1)= 1.0D0
      NORM(2)= 0.0D0
      IF (THETA3.GE.(PI/2)) THEN
* Front face of observatory faces the Sun.
      CS= 0.4
      CD= 0.2
      RCG= 0.83
     ELSE
* Back face of observatory faces the Sun.
      CS= 0.35
      CD= 0.15
      RCG= 0.805
      DO 60 J=1,2
   60         NORM(J)= -NORM(J)
     ENDIF
     COEF1= DOT(RSUNS,NORM)/SUNR
     COEF2= -P*AREA*COEF1
     COEF3= (1-CS)/SUNR
     COEF4= 2*(CS*COEF1+CD/3)
* The Solar Radiation Pressure Force is calculated in spacecraft-centered
* coordinates
     DO 70 J=1,3
   70         FRAD(J)= COEF2*(COEF3*RSUNS(J)+COEF4*NORM(J))
      ENDIF
* The Solar Radiation Torque is calculated.  TORSR(1) = 0.0D0
     TORSR(2)= FRAD(3)*RCG
     TORSR(3)= FRAD(2)*RCG
```

```
* The Angular Momentum Impulses are calculated using the Trapizoidal Rule.
      COEF1= 1.0D0
      COEF2= 1.0D0
      IF (MOD(I,1100).EQ.0) COEF1=0.5D0
      IF (MOD(I,550).EQ.0) COEF2=0.5
      DO 80 J=1,3
   80       TEMP(J)= DELTAT*(ASUN(J)+AMOON(J)+TORSR(J)+EARTH(3))*COEF1
      DO 90 J=1,3
      TORQUE1(J)= TORQUE1(J)+DABS(TEMP(J))
      TORQUE3(J)= TORQUE3(J)+DABS(TORSR(J)*DELTAT*COEF1)
      TORQUE4(J)= TORQUE4(J)+TORSR(J)*DELTAT*COEF2
   90       TORQUE2(J)= TORQUE2(J)+TEMP(J)
      IF ((COEF2.LT.0.8).AND.(I.NE.0)) THEN
* Every half orbit display TORQUE4 (see variables) values. Restart
* Integration.
      T= TJD-TJD0
      WRITE(*,100) T,TORQUE4
      WRITE(4,100) T,TORQUE4
      DO 95 J=1,3
   95       TORQUE4(J)= 0.5*DELTAT*TORSR(J)
      ENDIF
      IF ((COEF1.LT.0.8).AND.(I.NE.0)) THEN
* Every Orbit.
      T= TJD-TJD0
      WRITE(1,100) T,TORQUE1
      WRITE(2,100) T,TORQUE2
      WRITE(3,100) T,TORQUE3
  100       FORMAT(4X,D11.5,5X,3D16.7)
      DO 110 J=1,3
      TORQUE1(J)= 0.5*DABS(TEMP(J))
      TORQUE2(J)= 0.5*TEMP(J)
  110       TORQUE3(J)= 0.5*DELTAT*TORSR(J)
      ENDIF
   20 CONTINUE
      END


      SUBROUTINE G_GRAD(GRAV,R1,TORQUE)
*  This subroutine calculates gravity gradient torque.
      DOUBLE PRECISION GRAV,R,R1,I,TORQUE,IDOTR,MAG
      DIMENSION R(3),I(3,3),TORQUE(3),IDOTR(3),R1(3)
* I: The moment of inertia tensor.
      INTEGER J,K
      DATA ((I(K,J),J=1,3),K=1,3)/77.69D6,3*0.0D0,77.69D6,3*0.0D0,
     $1055.2D6/

      DO 500 J=1,3
  500  R(J)= R1(J)/MAG(R1)
      DO 510 J=1,3
  510  IDOTR(J)= I(J,1)*R(1)+I(J,2)*R(2)+I(J,3)*R(3)
      TORQUE(1)= GRAV*(R(2)*IDOTR(3)-R(3)*IDOTR(2))
      TORQUE(2)= GRAV*(R(3)*IDOTR(1)-R(1)*IDOTR(3))
      TORQUE(3)= GRAV*(R(1)*IDOTR(2)-R(2)*IDOTR(1))
      RETURN
```

```
      END

      SUBROUTINE TRANS(XYI,XYSAT,CTHETA,STHETA)
* This subroutine transforms vectors from geocentric coordinates to
* spacecraft-centered coordinates.
      DOUBLE PRECISION XYI,XYSAT,CTHETA,STHETA
      DIMENSION XYI(3),XYSAT(3)

      XYSAT(1)= XYI(1)*CTHETA+XYI(2)*STHETA
      XYSAT(2)= XYI(2)*CTHETA-XYI(1)*STHETA
      XYSAT(3)= XYI(3)
      RETURN
      END

      DOUBLE PRECISION FUNCTION MAG(A)
      DOUBLE PRECISION A(3)
* This function calculates the magnitude of a vector.
      MAG= DSQRT(A(1)*A(1)+A(2)*A(2)+A(3)*A(3))
      RETURN
      END


      DOUBLE PRECISION FUNCTION DOT(A,B)
      DOUBLE PRECISION A(3), B(3)
* This function produces the dot product of two vectors.
      DOT= A(1)*B(1)+A(2)*B(2)+A(3)*B(3)
      RETURN
      END
```

TABLE 5.A The Absolute Value Build-up of Angular Impulse From Environmental Torques (Selected Values)

TIME (days)	IMPULSE (Yaw,Roll,Pitch) Nms		
0.99727D+00	**0.1688602D+01**	**0.6694035D+02**	**0.1107307D+04**
0.19945D+01	0.1821113D+01	0.8102481D+02	0.1107966D+04
0.29918D+01	0.1935980D+01	0.9490198D+02	0.1107443D+04
0.39891D+01	0.2021173D+01	0.1091144D+03	0.1107753D+04
0.49863D+01	**0.2051208D+01**	**0.1235382D+03**	**0.1108374D+04**
0.59836D+01	0.1969232D+01	0.1377156D+03	0.1108323D+04
0.69809D+01	0.1606906D+01	0.1514746D+03	0.1107637D+04
0.79782D+01	0.8876129D+00	0.1659796D+03	0.1108124D+04
0.89754D+01	0.3931748D+00	0.1803224D+03	[illegible]
0.99727D+01	0.8766874D+00	0.1952046D+03	0.1107631D+04
0.10970D+02	0.1551389D+01	0.2100937D+03	0.1107825D+04
0.79782D+02	0.1775501D+01	0.8434535D+03	0.9792877D+03
0.80779D+02	0.2032214D+01	0.8448303D+03	0.9789815D+03
0.81776D+02	0.2219314D+01	0.8460437D+03	0.9787904D+03
0.82773D+02	**0.2367631D+01**	**0.8470731D+03**	**0.9786927D+03**
0.83771D+02	0.2485900D+01	0.8479145D+03	0.9787144D+03
0.84768D+02	0.2573847D+01	0.8485562D+03	0.9788367D+03
0.85765D+02	0.2625553D+01	0.8489894D+03	0.9790637D+03
0.86762D+02	**0.2627482D+01**	**0.8491968D+03**	**0.9794100D+03**

0.87760D+02	0.2545593D+01	0.8491362D+03	0.9798497D+03
0.88757D+02	0.2270727D+01	0.8487382D+03	0.9804060D+03
0.89754D+02	0.1593299D+01	0.8480294D+03	0.9809607D+03
0.90752D+02	0.1013034D+01	0.8472493D+03	0.9813520D+03

TABLE 5.B The Secular Build-up of Angular Impulse From Environmental Torques (Selected Values)

TIME (days)	IMPULSE (Yaw,Roll,Pitch) Nms		
0.99727D+00	-0.5298244D+00	0.6685732D+02	0.2993995D+00
0.19945D+01	-0.5945099D+00	0.8099517D+02	-0.5095704D-01
0.29918D+01	-0.6833807D+00	0.9489331D+02	0.6015925D+00
0.39891D+01	-0.7968372D+00	0.1091060D+03	0.2570825D+00
0.49863D+01	-0.9279102D+00	0.1235301D+03	0.4315059D+00
0.59836D+01	-0.1034793D+01	0.1377076D+03	0.1028318D+01
0.69809D+01	-0.9349952D+00	0.1514667D+03	0.1153282D+01
0.79782D+01	-0.3207135D+00	0.1659669D+03	0.1703471D+01
0.89754D+01	0.8452652D-01	0.1803150D+03	0.1391326D+01
0.99727D+01	-0.4415482D+00	0.1951445D+03	0.1904155D+01
0.10970D+02	-0.7088572D+00	0.2100005D+03	0.2003188D+01
0.79782D+02	-0.3836507D+00	0.8434535D+03	0.1827672D+01
0.80779D+02	-0.4464884D+00	0.8448303D+03	0.1651530D+01
0.81776D+02	-0.4849998D+00	0.8460437D+03	0.1467022D+01
0.82773D+02	-0.5290829D+00	0.8470731D+03	0.1280316D+01
0.83771D+02	-0.5880384D+00	0.8479145D+03	0.1097966D+01
0.84768D+02	-0.6643082D+00	0.8485562D+03	0.9078378D+00
0.85765D+02	-0.7574110D+00	0.8489875D+03	0.7208340D+00
[illegible]762D+02	-0.8614754D+00	0.8491968D+03	0.5299940D+00
0.87760D+02	-0.9469660D+00	0.8491348D+03	0.3366352D+00
0.88757D+02	-0.8909175D+00	0.8487353D+03	0.1488704D+00
0.89754D+02	-0.4345643D+00	0.8480294D+03	0.5932713D-01
0.90752D+02	0.1279096D+00	0.8472493D+03	0.2353557D+00

TABLE 5.C The Absolute Value Build-up of Angular Impulse From Solar Radiation Torque (Selected Values)

TIME (days)	IMPULSE (Yaw,Roll,Pitch) Nms		
0.99727D+00	0.0000000D+00	0.6722081D+02	0.1107307D+04
0.19945D+01	0.0000000D+00	0.8137545D+02	0.1107930D+04
0.29918D+01	0.0000000D+00	0.9524092D+02	0.1107370D+04
0.39891D+01	0.0000000D+00	0.1093998D+03	0.1107644D+04
0.49863D+01	0.0000000D+00	0.1237657D+03	0.1108227D+04
0.59836D+01	0.0000000D+00	0.1379326D+03	0.1108140D+04
0.69809D+01	0.0000000D+00	0.1518204D+03	0.1107418D+04
0.79782D+01	0.0000000D+00	0.1664264D+03	0.1107869D+04
0.89754D+01	0.0000000D+00	0.1804662D+03	0.1107266D+04
0.99727D+01	0.0000000D+00	0.1950418D+03	0.1107305D+04
0.10970D+02	0.0000000D+00	0.2099076D+03	0.1107463D+04
0.79782D+02	0.0000000D+00	0.8436843D+03	0.9788934D+03

0.80779D+02	0.0000000D+00	0.8451738D+03	0.9786241D+03
0.81776D+02	0.0000000D+00	0.8464420D+03	0.9784703D+03
0.82773D+02	0.0000000D+00	0.8474809D+03	0.9784103D+03
0.83771D+02	0.0000000D+00	0.8482972D+03	0.9784701D+03
0.84768D+02	0.0000000D+00	0.8488872D+03	0.9786309D+03
0.85765D+02	0.0000000D+00	0.8492490D+03	0.9788966D+03
0.86762D+02	0.0000000D+00	0.8493883D+03	0.9792819D+03
0.87760D+02	0.0000000D+00	0.8492973D+03	0.9797608D+03
0.88757D+02	0.0000000D+00	0.8489810D+03	0.9803564D+03
0.89754D+02	0.0000000D+00	0.8483921D+03	0.9809505D+03
0.90752D+02	0.0000000D+00	0.8474678D+03	0.9813212D+03

APPENDIX 5.2: NOTES ON MASS ESTIMATES

Relevant Equations: Except where noted all equations can be found in Hardy Rawlin and Patterson (1987) or Byers, et. al. (1979).

Thruster Masses (see Tables 5.3 thru 5.7 for sources):
- Monopropellant - 0.375 kg/thruster
- Bipropellant - 0.700 kg/thruster
- Arcjet - 1.750 kg/thruster
- Xenon Ion - 11.30 kg/thruster

Gimbals:
- 0.3 Thruster mass (in kg)

Thruster Support Structure:
- 0.31 (Thruster+Gimbal Mass)

Power Processing Units (Arcjet and Xenon Ion Engines Only):
- Discharge Supply -
  - $MD = 2.5\ PD^{3/4}+1.8\ PD^{1/2}+0.1\ PD+3.0$
- Beam Supply (Xenon Ion System Only) -
  - $MB = 2.5\ PB^{3/4}+1.8\ PB^{1/2}+0.1\ PB+7.6$
- Low Voltage Supply (Xenon Ion Engine Only) - MLow = 0.8 kg
- Total PPU Mass = (MD+MB+MLow)*Number of Engines

Thermal Control (Arcjet and Xenon Ion Engines Only):
- 27*PPU Efficiency*Power Input into the PPU (in kg).

Interface Module (Xenon Ion Engines and Arcjets Only):
- Converter -
  - $MC = PC^{3/4}+PC^{1/2}+0.1\ PC+0.9$
  - PC = 0.08 Number of Engines
- Controller:
  - MCon = 4.0
- Reconfiguration Unit -
  - MRU = 0.15 PRU
  - PLB (Xenon Ion Only) = 7/93 PB = beam supply dissipated power
  - PLD = discharge supply dissipated power = 3/22 PD
  - PRU = Number of Engines (PD+PLD+PB+PLB) = Total reconfiguration unit power
- Thermal Control -
  - MTherm = 27 (PLRU+PC+PLCon)
  - PLRU = reconfiguration unit power loss = 0.005 PRU

PLC = converter unit power loss = 1/9 PC

PLCon = controller power loss = 0.015

Interface Module Mass = 2 MRU + 2 MC + 2 MCon + Mtherm

Propellant Feed System (from Brophy and Aston, 1989):

Xenon Ion Engine - 4.45 + 2.26*Number of Engines

Bipropellant Thruster - approximately same as Xenon Ion system

Arcjet and Monopropellant - approximately 3/4 Xenon Ion System

Housing Structure -

0.4 * All items above (in kg).

Propellant Masses:

$\text{delta-v} = -I_{sp}\, g_0 \ln[(M-M_p)/M]$

Propellant Reserve: 0.06*Propellant Mass

Helium mass for pressurization:

$M_{He} = P_p\, V_p\, k/T_p/R_{He}/(1-P_p/P_{He})$

$k = 1.67$

$R = 2077.3$ J/kg xK

Tanks:

Several steps were taken to determine tank masses. The tank-to-propellant mass ratio equation (from Byers) for non-cryogenic storage is:

$$M_t/M_p = (3/2)(RHO_t X/RHO_p Y)[P_p + G(M_p/2/c)_{1/3(4\ RHO_p/3)^{2/3}}]$$

This equation was used to get the propellant-to-mass ratio of helium to titanium at a safety factor of 1.5. Propellant-to-mass ratios of N_2H_4 to stainless steel were taken from Bovey and Pidgeon (1990). The propellant-to-mass ratio of NTO to stainless steel was sized from the hydrazine ratio. The final ratios were formed from data given by Vickers, et. al.(1990) which gave the mass ratios of stainless steel and titanium to graphite/epoxy tanks fabricated for the same loads. The ratios were 2.8 and 2.5 respectively.

Tank Housing Structure:

0.4*(Tanks+Propellant+Helium)

```
**************************************************************
Eureka: The Solver, Version 1.0
Tuesday April 14, 1992, 10:50 am.
Name of input file: C:\EUREKA\DISH
**************************************************************


a=75
b=3
v=0.33
r0=3
E=200e9
ya=-.02

D=E*t^3/12/(1-v^2)
M=-1*q*a^2/C8*(C9/(2*a*b)*(a^2-r0^2)-L17)
QB=q/2/b*(a^2-r0^2)
ya=M*a^2/D*C2+QB*a^3/D*C3-q*a^4/D*L11
THET=M*a/D*C5+QB*a^2/D*C6-q*a^3/D*L14
C2=.25*(1-(b/a)^2*(1+2*LN(a/b)))
C3=b/4/a*(((b/a)^2+1)*LN(a/b)+(b/a)^2-1.0)
C5=.5*(1-(b/a)^2)
C6=b/4/a*((b/a)^2-1+2*ln(a/b))
C8=0.5*(1+v+(1-v)*(b/a)^2)
C9=b/a*((1+v)/2*ln(a/b)+(1-v)/4*(1-(b/a)^2))
L11=1/64*(1+4*(r0/a)^2-5*(r0/a)^4-4*(r0/a)^2*(2+(r0/a)^2)*ln(a/r0))
L14=1/16*(1-(r0/a)^4-4*(r0/a)^2*ln(a/r0))
L17=0.25*(1-(1-v)/4*(1-(r0/a)^4)-(r0/a)^2*(1+(1+v)*ln(a/r0)))

**************************************************************

S    ion:

 Variables    Values

 a          =     75.000000

 b          =     3.0000000

 C2         =     .24702490

 C3         =    .022256260

 C5         =     .49920000

 C6         =    .054393516

 C8         =     .66553600

 C9         =    .092311377

 D          = 1.7068438e+08

 E          = 2.0000000e+11

 L11        =    .015080510

 .          =    .061212290

 L17        =     .20601267

 M          =    -9751.7181

 q          =     1.2196177
```

```
r0          =      3.0000000
t           =      .20897315
[illegible] = -.00027725592
v           =      .33000000
ya          =    -.020000000

Maximum error is 6.8983106e-07

*********************************************************************
```

MASS DISTRIBUTION

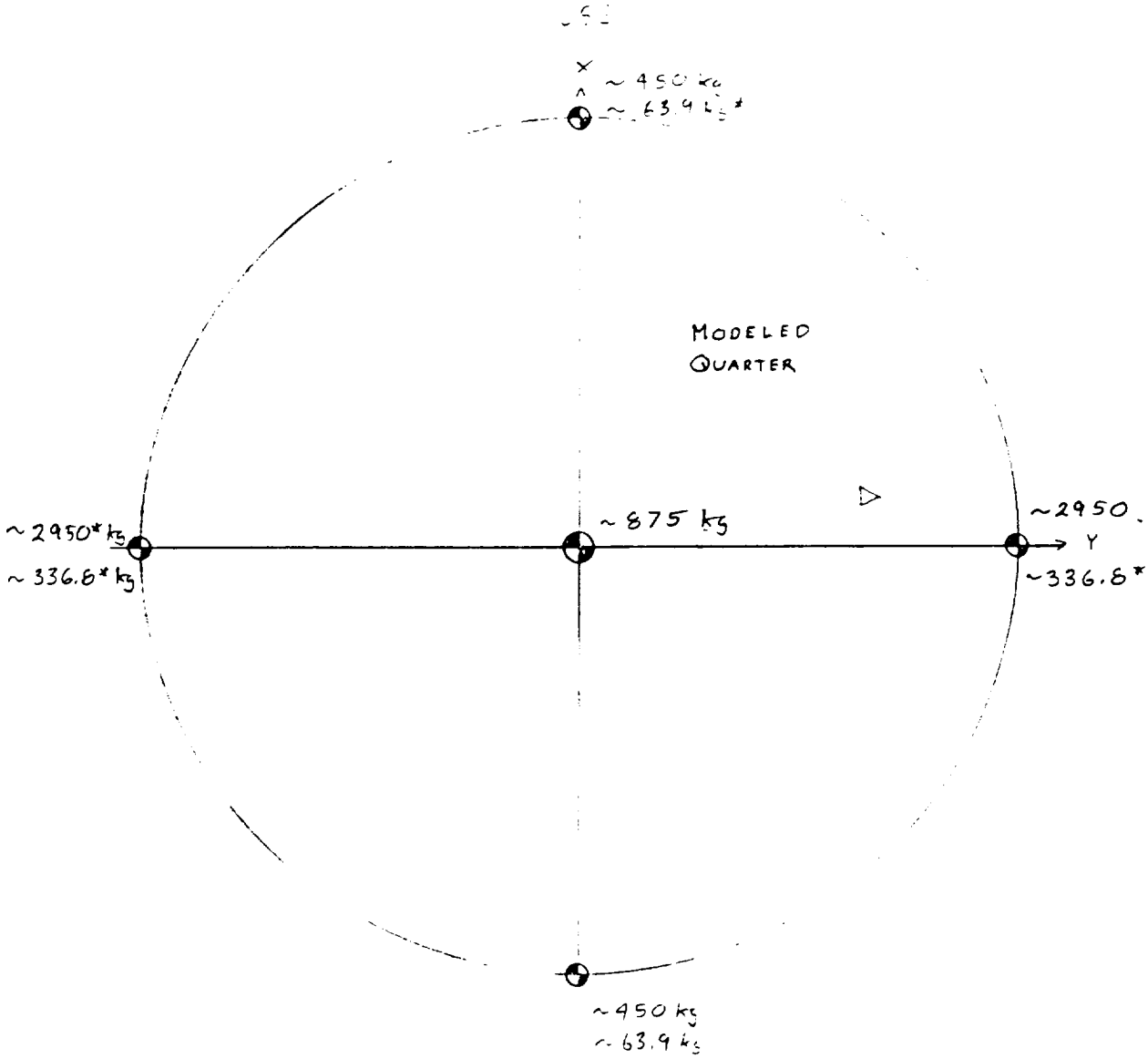

TOTAL MASS ~ 35,739 kg

TOTAL MASS (NO FUEL) ~ 29,740 kg

* DRY WEIGHT

FINITE ELEMENT MODEL LOADCASES

① SOLAR PRESSURE $P = 9.6 \times 10^{-6}\ N m^{-2}$ (80% REFLECTIVITY)

1 EACH PLATE ON MODULE = $29.16\ m^2$

EACH PLATE ON MODEL = $14.57\ m^2$

~ 50% OF AREA

∴ FOR SOLAR PRESSURE DISTRIBUTED LOAD USE:

$P = 9.6 \times 10^{-6}\ N m^{-2} \cdot 1.8 \cdot 2 = 3.456 \times 10^{-5}\ N m^{-2}$

CALCULATE INERTIAL LOAD - WORST CASE : NO FUEL

TOTAL SOLAR FORCE (ASSUME 80% REFL.)

$F = (9.6 \times 10^{-6} + 0.8 \cdot 9.6 \times 10^{-6})\ N m^{-2} \cdot 29.16\ m^2 \cdot 657$

$= 0.3311\ N$

$a = \frac{F}{m} = \frac{0.3311\ N}{29,790\ kg} = 1.113 \times 10^{-5}\ m s^{-2}$

∴ INERTIAL LOADS

MODULE $F = ma = 42.78\ kg \cdot 1.113 \times 10^{-5}\ m s^{-2}$
$= 4.763 \times 10^{-4}\ N$

TRANSFORM TO DISTRIBUTED LOAD
$= 4.763 \times 10^{-4}\ N / 14.57\ m^2$
$= 3.269 \times 10^{-5}\ N m^{-2}$

N-S THRUSTER $F = 63.9\ kg \cdot 1.113 \times 10^{-5}\ m s^{-2}$
$= 7.112 \times 10^{-4}\ N$

E-W THRUSTER $F = 336.8\ kg \cdot$ [illegible] $m s^{-2}$
$= 3.749 \times 10^{-3}\ N$

∴ LOAD SUMMARY

DISTRIBUTED PLATE LOAD $Z = -3.440 \times 10^{-5} + 2.720 \times 10^{-5}$
$= -3.259 \times 10^{-5}\ N m^{-2}$

POINT LOAD AT N-S THRUSTER $Z = 7.112 \times 10^{-4}\ N$ 393

POINT LOAD AT E-W THRUSTER $Z = 3.749 \times 10^{-3}\ N$ 39

④ THRUSTER FIRING IN Z DIRECTION
WORST CASE - TWO THRUSTERS FIRING AT EACH STATION. - NO FUEL LOAD

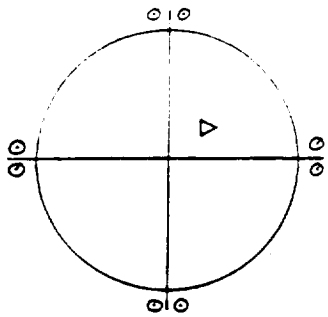

8 THRUSTERS

$F = 8 \cdot 22\ N = 176\ N$

$$a = \frac{F}{m} = \frac{176\ N}{29,790} = 5.917 \times 10^{-3}\ m\,s^{-2}$$

∴ INERTIAL LOADS

MODULE $F = ma = 42.78 \cdot 5.917 \times 10^{-3}\ m\,s^{-2}$
$= 0.2107$
DISTRIBUTED LOAD
$= 0.2107 / 14.57\ m^2$
$= 1.738 \times 10^{-2}$

N-S THRUSTER $F = 63.9\ kg \cdot 5.917 \times 10^{-3}\ m\,s^{-2}$
$= 0.3782\ N$

E-W THRUSTER $F = 336.8 \cdot 5.917 \times 10^{-3}\ m\,s^{-2}$
$= 1.993$

∴ LOAD SUMMARY

DISTRIBUTED PLATE LOAD $z = -1.738 \times 10^{-2}\ N\,m^{-2}$

POINT LOAD AT N-S THRUSTER $z = \frac{1}{2}(44 - 0.3782)$
$= 21.81\ N$ 353

POINT LOAD AT E-W THRUSTER $z = \frac{1}{2}(44 - 1.993)$
$= 21.00\ N$ 5[illegible]

Appendix 7.1 Power Requirements: Solar Array Calculations

Determination of ideal solar array area required (Wertz).

$$\frac{\text{Area}}{\text{Power}} = \frac{1}{X_d\ P_o\ I_d\ L_d\ \cos(\tilde{O})}$$

c	= solar energy intensity (1 A.U.)	1358 W/m^2
n	= efficiency of solar cells	0.21
P_o	= cn = output performance	285.18 W/m^2
X_d	= Power regulation efficiency	0.9

Inherent degredation components:

Design and Assembly (pf)	0.9
Shadowing of Cells	1.00
Temperature degradation $\frac{0.35\%}{(^oC - 28^oC)}$ @ 56^o	0.902

I_d	= Inherent degredation	0.812
L_d	= Life degredation (2.0% per year)	0.80
$\cos(\tilde{O})$	= cosine loss due to incidence	1.00 (ideal)

$\frac{A}{P}$ = Area required to produce 1 kW = 5.999 m^2/kW (for ideal case)

This factor takes into consideration the following:

- Eclipses during the two 45 day eclipse seasons
- A stationary, two sided solar panel and incidence problems due to orbit revolution and inclination

TABLE of Solar Array Characteristics

	Modules	Bus
Nominal Power	80.0 W cont. during operation	900 W cont. for life of system
Daily Nominal Energy Req'd.	1.92 kWh	21.6 kWh
Equivalent Maximum Eclipse Period	6.7 hours$_1$	4.2 hours$_2$
Panel Dimensions	0.43 x 0.37 m^2	1.06 x 1.62 m^2
Number of Panels	thirteen	sixteen
Area of GaAs Solar Array	2.055 m^2	27.4 m^2
Total Array Area 1363 m^2	1336 m^2	27.4 m^2

1 - Considers module operation shutdown during earth eclipse

2 - For a tent configuration on the lower side of bus

Appendix 7.2 Solar Array Design for Observation Modules

The following values are arrived at using formulas found in the references of Wertz and Sullivan.

Power of Solar Array:	P_{sa} = 94.1 W at 24.6 V
Current Supply of Array:	I_{sa} = 2.44 A to 5.49 A
Solar Array Area:	A_{sa} = 2.050 m^2
Total Solar Cell Area:	A = 1.872 m^2
(packing efficiency:	pf = 0.90)

The characteristics of each Gallium Arsenide cell.

cell area = 24 x 10^{-4} m^2 (6 cm x 4 cm)

cell output voltage = 0.819 V

cell output current = 0.1022 A

Layout for each panel.

Number of cells on solar panel = 60

Number of panel circuit modules = 2

Number of series cells to provide voltage = 30

Number of Parallel Series:	P = 6
Number of Cells in Series:	S = 10
Number of Top Panels:	N_p= 4
Number of Bottom Panels:	N_p= 9

Panel Voltage Output = 24.6 V

Panel Current Output = 0.1022 A x P = 0.61 A

Appendix 7.3 Solar Array Design for the Bus

The following values (for each side of the bus) are arrived at using formulas found in the references of Wertz and Sullivan.

Power of Solar Array:	P_{sa} = 1058.8 W at 124.5 V
Current Supply of Array:	I_{sa} = 13.08 A
Solar Array Area:	Asa = 13.7 m^2
Total Solar Cell Area:	A = 11.645 m^2
(packing efficiency:	pf = 0.85)

The characteristics of each Gallium Arsenide cell.

cell area = 24 x 10^{-4} m^2 (6 cm x 4 cm)

cell output voltage = 0.819 V

cell output current = 0.1022 A

Layout for each panel.

Number of cells on solar panel = 4864

Number of Panels = 8

Number of panel circuit modules = 4

Number of series cells to provide voltage = 152

Number of Parallel Series:	P = 16
Number of Cells in Series:	S = 38
Number of Panels:	N_p= 8

Panel Voltage Output = 124.5 V

Panel Current Output = 0.1022 A x P

$$= 13.1 \text{ A} / N_p = 1.635 \text{ A}$$

Appendix 7.4 Power Requirements: Battery Calculations

This appendix will run through the battery calcultation process.

TABLE of Battery Characteristics

	Modules	Bus
Nominal Power	80.0 W cont. during operation	900 W cont. for life of system
Number of Cells	18	90
Nominal (1.33 V)	23.94 V	119.7 V
Maximum (1.55 V)	27.90 V	139.5 V
TypicalC (1.45 V)	26.10 V	130.5 V
TypicalDC (1.25 V)	22.50 V	112.5 V
Minimum (1.10 V)	19.80 V	99.0 V
Load Current	3.34 A	7.52 A
Maximum Discharge Period per Day	6.7 hours$_1$	4.2 hours$_2$
Maximum Discharge (Te x Discharge I)	22.49 Ahr	31.4 Ahr
Required Capacity DoD = 50 %	44.98 Ahr	62.9 Ahr
Battery Capacity	1 x 48.0 Ahr	2 x 38.0 Ahr (parallel)
Dimensions (in cm)	35.5x30.4x2.9	81x90x27
Cell Mass	0.85 kg	0.70 kg
Total Mass	15.3 kg (x650)	126 kg

1 - Considers module operation shutdown during earth eclipse

2 - For an angled, two panel configuration beneath bus